universität wien

DIPLOMARBEIT

Titel der Diplomarbeit

The impact of ATGL deficiency on DHA biosynthesis.

angestrebter akademischer Grad

Magistra der Naturwissenschaften (Mag. rer.nat)

Verfasserin:	Teresa Sara Lindinger
Studienrichtung:	Molekulare Biologie
Betreuerin / Betreuer:	Prof. Dr. Johannes Nimpf

Wien, am

Danksagung

Ganz besonders möchte ich bei Prof. Dr. Johannes Nimpf bedanken, der sich sofort dazu bereit erklärt hat, meine Diplomarbeit zu betreuen und mich bei allen auftretenden Fragen und Problemen unterstützt hat. Weiters gilt mein aufrichtiger Dank Prof. Dr. Rudolf Zechner, der mir ermöglicht hat, den praktischen Teil meiner Arbeit in seinem Labor am Institut für molekulare Biowissenschaften an der Karl-Franzens-Universität in Graz zu absolvieren.

Ich möchte außerdem meinen Kollegen in Graz danken, die mir im Labor hilfreich zur Seite standen, mit denen ich aber auch nach der Arbeit viele lustige Stunden verbracht habe.
Einen großen Beitrag zum erfolgreichen Studium haben auch meine Studienkollegen in Wien, ganz besonders Babsi, Fabian, Isa, Gini und Martin geleistet, in denen ich sehr gute Freunde gefunden habe und mit denen auch anstrengende Lernphasen mit viel Spaß verbunden waren.

Mein allergrößter Dank gilt jedoch meiner Familie und meinem Freund Michael, die mich während der Studienjahre mit aller Kraft unterstützt haben und immer für mich da waren.
Meinen Eltern, die mir ohne Druck eine universitäre Ausbildung ermöglicht haben und auch meinen Erklärungen zu den Inhalten des Studiums stets großes Interesse entgegen gebracht haben.
Meiner Schwester, die mich jederzeit getröstet, wieder aufgebaut und beschützt hat und mir eine sehr gute Freundin war.
Meinem Freund Michael, der stets hinter mir stand, obwohl er die stressbedingten Launen in Prüfungszeiten und besonders während der Diplomarbeit sehr stark zu spüren bekommen hat.

Affidavit

I hereby declare that the following master thesis "The effect of ATGL deficiency on DHA biosynthesis" has been written only by the undersigned and without any assistance from third parties.

Furthermore, I confirm that no sources have been used in the preparation of this thesis other than those indicated in the thesis itself.

---------- ----------

Place, Date Signature

Abstract

The adipose triglyceride lipase (ATGL) is the main enzyme to catalyze the first and rate-limiting step in stimulated lipolysis in white adipose tissue. This 3-step-process is required to release free fatty acids from cytosolic triglyceride stores, called lipid droplets. The fatty acids are transported to various parts of the body, mainly muscles and liver. Given their high energy density, fatty acids are the most important substrates for ATP production but they are also needed as second messengers, regulators of gene expression and components of biological membranes.

Mice deficient for a functional ATGL display a severe phenotype of massive TG accumulation throughout the body which causes multiple metabolic disorders. The first mice die from cardiac insufficiency at the age of 12 weeks. In the human *ATGL* gene several autosomal recessive mutations have been described that cause neutral lipid storage disease with myopathy (NLSDM) which is characterized by a similar phenotype as in *Atgl*$^{-/-}$ mice.

Lipid profiling analysis in *Atgl*$^{-/-}$ mice revealed a reduction in C22:6n-3 (DHA)-containing phospholipids and triglycerides in the cardiac muscle whereas C18:0/C18:1/C18:2-containing lipids were increased. Docosahexaenoic acid (DHA) is a ω3-polyunsaturated fatty acid (PUFA) which is concentrated mainly in brain and retina and is needed for neural and retinal development. DHA itself and its derivatives (docosatrienes, resolvins) have many anti-inflammatory functions. DHA either has to be taken up with the diet or is synthesized from its precursor α-linolenic acid (C18:3n-3) which is an essential fatty acid that is enriched in vegetable oils. The liver is the main organ for DHA biosynthesis; the brain can also synthesize minor amounts whereas the quantities produced in the heart are marginal.

The aim of this study was to find the missing link between ATGL deficiency and reduced levels of DHA-containing lipids. By real-time PCR measurements, ATGL was identified as regulator of DHA (or PUFA) synthesis. In the liver of mice, the expression of selected enzymes involved in DHA-biosynthesis was induced by fasting but failed to be upregulated when ATGL was missing. Expression in the heart was independent of the nutritional status as relative expression levels were downregulated in both, fed and fasted mice, when ATGL was missing. Real-time PCR as well as Northern blotting analysis showed that (most of the) selected enzymes are PPARα target genes, in liver as well as in the heart. Thus, ATGL deficiency could have inhibited PPARα-activated gene expression in ATGL-knockout mice. Most probably, ATGL provides ligands for PPARα-activation. This mechanism seems to be regulated by the diet in the liver but not in the heart - provided that changed expression levels in the heart of (fed) *Atgl*$^{-/-}$ mice are linked at all to PPARα. HPLC-MS/MS revealed that DHA levels were not increased in cardiac muscle of

Atgl$^{-/-}$ mice by induction of PPARα-activity upon administration of the synthetic PPARα agonist WY14,643. Therefore, the regulation of PPARα-induced gene expression of DHA-synthesizing enzymes is definitely not the only function of ATGL in this pathway. Most likely, ATGL is further needed to release the precursor for DHA-biosynthesis from triglycerides and/or phospholipids but this remains to be verified.

Zusammenfassung

Die Fettgewebstriglyzeridlipase (adipose (tissue) triglyceride lipase; ATGL) ist das primäre Enzym für die Katalyse des ersten und geschwindigkeitsbestimmenden Schrittes der stimulierten Lipolyse im weißen Fettgewebe. Dieser 3-stufige Prozess ist notwendig, um freie Fettsäuren aus den zytosolischen Triglyzeridspeichern, den Lipidtröpfchen, freizusetzen. Die Fettsäuren werden in verschiedene Teile des Körpers transportiert, vor allem zum Muskelgewebe und zur Leber. Sie sind die wichtigsten, da energiereichsten Substrate für die Produktion von ATP, werden aber auch als sekundäre Botenstoffe, als Regulatoren der Genexpression und als Komponenten von biologischen Membranen benötigt.

Mäuse, denen eine funktionelle ATGL fehlt, zeigen einen schwerwiegenden Phänotyp, der mit massiver Triglyzeridakkumulation im gesamten Körper und zahlreichen damit verbundenen Stoffwechselstörungen einhergeht. Die ersten Mäuse sterben infolge einer Herzschwäche im Alter von 12 Wochen. Im menschlichen Gen für ATGL wurden mehrere autosomal rezessive Mutationen beschrieben, die eine mit Myopathie assoziierte Neutrallipidspeicherkrankheit (NLSDM) verursachen, welche sich durch einen ähnlichen Phänotyp wie in ATGL-knockout-Mäusen beschrieben auszeichnet.

Die Analyse des Lipidprofils in *Atgl*$^{-/-}$-Mäusen ergab einen verminderten Anteil an DHA (C22:6n-3)-enthaltenden Phospolipiden und Triglyzeriden im Herzmuskel, wohingegen Lipide, die C18:0/C18:1/C18:2 enthalten, erhöht waren. Die Docosahexaensäure (docosahexaenoic acid/DHA) ist eine mehrfach ungesättigte ω3-Fettsäure, die hauptsächlich im Gehirn und der Netzhaut angereichert ist, für deren Entwicklung sie unabdingbar ist. DHA und ihre Stoffwechselprodukte haben vielerlei entzündungshemmende Wirkmechanismen. DHA muss entweder mit der Nahrung zugeführt werden oder wird aus ihrem Vorläufer, der α-Linolensäure (C18:3n-3), synthetisiert. Die α-Linolensäure ist eine essentielle Fettsäure, die hauptsächlich in pflanzlichen Ölen angereichert ist. Die Leber ist das Hauptorgan für die Synthese von DHA, auch das Hirn kann kleinere Mengen produzieren, während im Herzen nur ein verschwindend geringer Anteil synthetisiert wird.

Das Ziel dieser Arbeit war, die fehlende Verbindung zwischen mangelnder ATGL und verringerten Mengen an DHA-enthaltenden Lipiden herauszufinden. Mittels real-time PCR konnte die ATGL als Regulator der DHA (oder PUFA)-Synthese ermittelt werden. In der Mausleber wurde die Expression von ausgewählten Enzymen des DHA-Syntheseweges durch Fasten induziert, während dieser Effekt nicht auftrat, wenn die ATGL fehlte. Die Expression im Herz war unabhängig vom Fütterungszustand, denn die relativen mRNA-Mengen waren sowohl in gefütterten als auch gefasteten ATGL-knockout-Mäusen reduziert. Von den (meisten der) untersuchten Enzyme konnte mittels

real-time PCR und Northern blot gezeigt werden, dass sie sowohl in der Leber auch als im Herz PPARα-Zielgene sind. Das Fehlen der ATGL könnte also die PPARα-vermittelte Genexpression verhindert haben. Wahrscheinlich stellt die ATGL die Liganden für die Aktivierung von PPARα während des Fastens bereit. Dieser Mechanismus wird in der Leber über die Nahrung reguliert, aber nicht im Herz – falls die Expressionsänderung im Herz von (gefütterten) ATGL-knockout-Mäusen überhaupt mit PPARα in Verbindung steht. Die HPLC-MS/MS zeigte, dass der Anteil an DHA im Herzmuskel von *Atgl*$^{-/-}$-Mäusen nach Aktivierung von PPARα durch den synthetischen Agonisten WY14,643 nicht wieder gestiegen ist. Daher ist die Regulation von PPARα-induzierter Genexpression in jedem Fall nicht die einzige Funktion der ATGL in diesem Stoffwechselweg. Am wahrscheinlichsten ist, dass die ATGL dazu benötigt wird, den Vorläufer für die DHA-Synthese aus Triglyzeriden und Phospholipiden freizusetzen; das muss aber erst bestätigt werden..

1. Introduction

1.1. Lipid Metabolism in mammals

Fatty acids (FA) are the main building blocks of all lipid classes throughout the body and the most important substrates for energy production by β-oxidation inside mitochondria (1). These carboxylic acids are characterized by a hydrophilic head and a hydrophobic tail. The tail is a hydrocarbon chain of varying length - naturally occurring chains range from four to 28 carbon atoms (1, 2, 3). The number of double bonds incorporated in the tail is used to classify fatty acids as saturated (no double bond), monounsaturated (one double bond) or polyunsaturated (2 or more double bonds) (Fig.1.1.1) (1). Fatty acids can also be classified according to their chain length as short chain (4 carbon atoms), medium chain (6-12 carbon atoms), long chain (>12-20 carbon atoms) and very long chain (22 – over 30 carbon atoms) fatty acids (4).

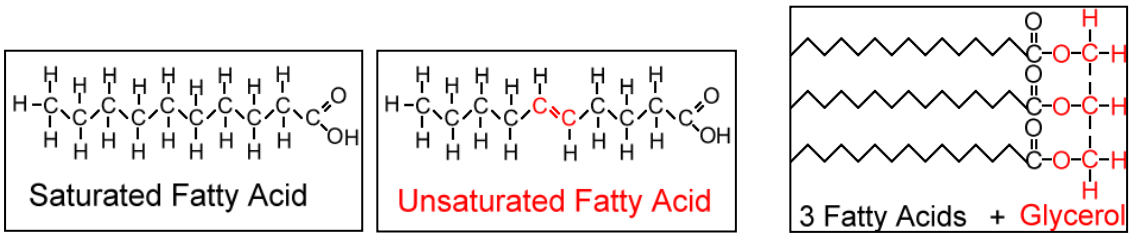

FIGURE 1.1.1. **Structure of saturated and unsaturated fatty acids (left) and triglycerides (right)**. Left: A saturated fatty acid with a chain of 10 carbon atoms. Middle: A monounsaturated C10 fatty acid. Right: A triglyceride (TG), also called triacylglycerol (TAG), formed by esterification of three FA on a glycerol backbone (Image source: (5)).

Fatty acids in food, taken up by ingestion of animal or vegetable fat and oil, mostly form triglycerides (TG), where three FA at a time are esterified onto a glycerol backbone (6). These triglycerides account for about 90% to 95% of daily human energy supply provided by dietary fat (7). Some triglycerides are already broken down into diglycerides and free fatty acids (FFA) in the stomach by lingual and gastric lipases. They are further processed into monoglycerides and fatty acids by pancreatic lipases in the duodenum (8, 9). In the small intestine monoglycerides, free fatty acids, glycerol, and cholesterol are emulsified by bile salts and form micelles which are absorbed by intestinal enterocytes (10). Inside these epithelial cells, fatty acids are reesterified into triglycerides by monoacylglycerol acyltransferase (MGAT) and diacylglycerol acyltransferase (DGAT) (11, 12) and packaged into lipoprotein particles called chylomicrons together with cholesterol, phospholipids and apolipoprotein B-48 (ApoB-48). These particles first enter the lymph system and are subsequently released into the blood system and transported to various organs (13, 14). As a result of lipoprotein lipase activity fatty acids are again released

from triglycerides (and thereby from lipoprotein particles) and then taken up via passive or facilitated diffusion by cells of extrahepatic organs for energy supply or storage (15). The remainder of these particles (chylomicron remnants) is taken up by liver cells and metabolized (16).

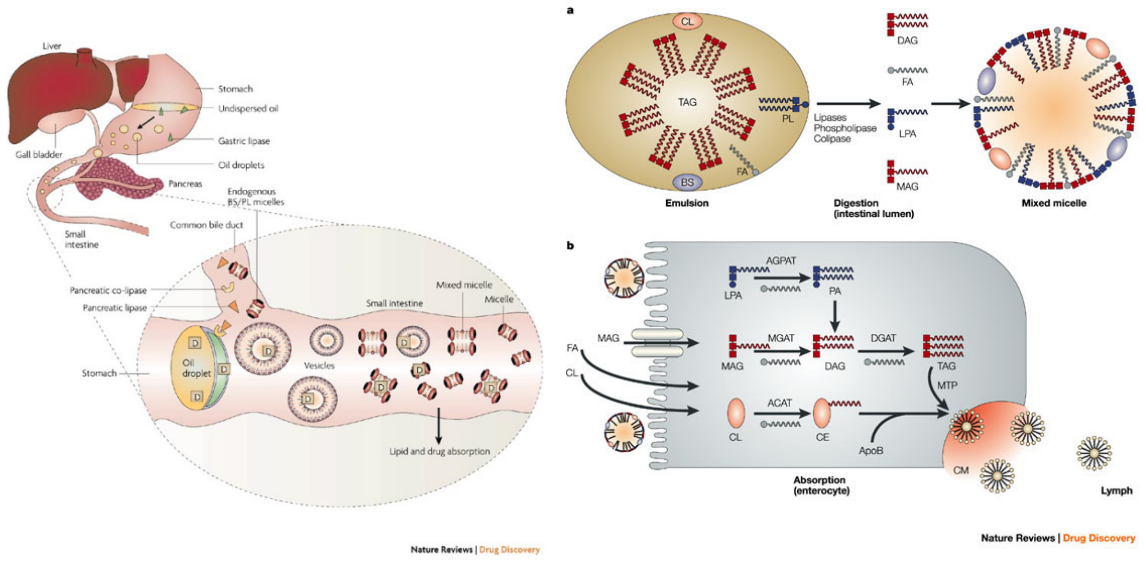

FIGURE 1.1.2. **Digestion and absorption of dietary TAG**. Left: The digestion of dietary TAG already starts in the stomach where lingual and gastric lipases cleave part of the TAG into DAG, FA and glycerol. DAG and remaining TAG are further processed to MAG, glycerol and FA in the small intestine by pancreatic lipase (image source: (17)). Right: The cleavage products form micelles through the emulsifying action of bile salts and are absorbed by enterocytes. Inside these epithelial cells, fatty acids are reesterified to TAG by the action of MGAT and DGAT and together with cholesterol esters and apoB are packaged into chylomicrons and released into the lymph system (image source: (18)). CL, cholesterol; BS, bile salt; FA, fatty acid(s); PL, phospholipid; MAG, monoacylglycerol; MGAT, monoacylglycerol acyltransferase; DGAT, diacylglycerol acyltransferase; CE, cholesterol ester; ApoB, apolipoprotein B; CM, chylomicron.

If nutritional energy supply exceeds the energy requirements, fatty acids are stored in form of TG in small and very dynamic cytosolic organelles called lipid droplets (19, 20). Lipid droplets exist in every organ and cell of the body (21). Nevertheless, mammalians store fat mainly in the white adipose tissue (WAT) (21). The storage of excess fatty acids not only serves as energy source but also prevents toxic concentration of free fatty acids in the cell which would severely disrupt cell function, for instance by destroying biological membranes (22).

During times of increased energy demand like fasting or exercising stored fatty acids need to be released from these cytosolic triglyceride stores by a process called lipolysis (23). Lipolysis is a three-step process which is catalyzed by three different enzymes. The first and rate-limiting step, which is catalyzed by the adipose triglyceride lipase (ATGL), is the hydrolysis of triglycerides into diglycerides (DG) and free fatty acids (FFA). Next, the hormone sensitive lipase (HSL) cleaves diglycerides into monoglycerides (MG) and free fatty acids. In the last step monoglycerides are hydrolyzed into glycerol and free fatty acids by the monoglyceride lipase (MGL) (21, 24). These free fatty acids enter the

blood stream where they bind to serum albumin and are transported to various organs and tissues, mainly muscle tissue and liver. They are used for energy/ATP production, for membrane biogenesis, for regulation of gene expression (e.g. as ligands for nuclear receptors) and for ketogenesis/gluconeogenesis in the liver (20, 21, 22). Furthermore FFA but also other lipolysis intermediates (e.g. DG) serve as second messengers in signal transduction pathways (21, 25). Energy is also consumed by brown adipose tissue (BAT) which needs fatty acids for thermogenesis/heat production inside mitochondria. Humans lose this specialized adipose tissue during childhood whereas rodents and hibernating animals keep it throughout life (26, 27).

1.2. ATGL

The adipose triglyceride lipase (ATGL) was discovered only recently, in 2004, by three different research groups (28, 29, 30). Until then, the hormone sensitive lipase (HSL) was thought to catalyze both the first and the second step of lipolysis. ATGL cleaves triglycerides with 10-fold higher substrate specificity than diglycerides (21). It is highly expressed in white and brown adipose tissue. At lower levels it is found in cardiac muscle, skeletal muscle and testis (28). Transcription of ATGL is regulated by hormones, cytokines and fasting/refeeding which confirms its critical role in lipolysis (28, 31).

ATGL is a member of the patatin-like phospholipase domain containing family of proteins (PNPLA1-5) (21). It is also called PNPLA2 (official designation), desnutrin (29), or calcium-independent phospholipase $A_2\zeta$ (iPL-$A_2\zeta$) (30, 31). The murine gene spans nine exons on chromosome 7 with a size of 4.9 kb. The protein is built up by 486 aa with a calculated molecular mass of 54 kDa (32). The human gene (504 aa) comprises ten exons on chromosome 11p15.5 with sequence similarity of 84% to its mouse homologue and, regarding the patatin domain, even of more than 95% (21, 28, 33). The N-terminal patatin domain is structurally characterized by a three-layered α/β/α sandwich architecture and contains the lipase consensus sequence motif GXSXG with the nucleophilic serine at position 47 (Ser47) (34, 35). The enzymatic activity of this phospholipase domain untypically is given by a catalytic dyad instead of a triad (36). In addition to the active serine, the catalytic dyad is made up by an asparagine (Asp166) outside the central β-sheet (37). A hydrophobic stretch in the C-terminal region, which is composed mainly of α-helices and loop regions, is needed for the localization of ATGL to the lipid droplet but compromises the enzymatic activity (38). It also includes two phosphorylation sites (Ser^{404};Ser^{428} in human ATGL) but it remains to be elucidated whether the phosphorylation status influences the protein's activity (21, 38).

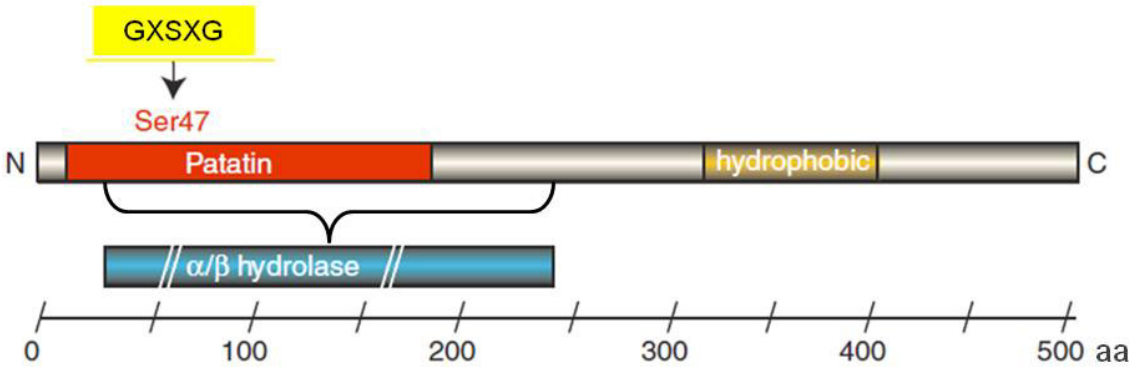

Adapted from Fischer et al., 2007

FIGURE 1.2.1. **Predicted structure of the human ATGL protein (39)**. Protein map of human ATGL displaying the N-terminal patatin domain that contains the lipase consensus sequence motif GXSXG with the active serine at position 47. The α/β-hydrolase fold (represented by the blue box underneath) is also N-terminally located inside the ATGL protein whereas the C-terminus harbors a hydrophobic region. aa, amino acid(s); GXSXG: G, glycine; S. serine; X, any aa (image adapted from: (39)).

1.3. Regulation of lipolysis

The protein encoded by *comparative gene identification-58*, CGI-58, was shown to bind to murine ATGL thereby increasing its activity by up to 20-fold (40). The same effect, although much weaker, was observed for human ATGL with a 5-fold induction of the enzyme's activity through binding of CGI-58 (21, 40).

CGI-58 belongs to the esterase/thioesterase/lipase family of proteins which is structurally characterized by α/β-hydrolase folds (41). In CGI-58 the active serine within the lipase motif GXSXG is replaced by an asparagine (42) therefore it has no lipolytic activity. At basal level, CGI-58 binds to lipid droplets within adipocytes by interacting with perilipin A and therefore can no longer bind to and activate ATGL (43). Perilipin A is a member of the PAT or perilipin family of proteins that are lipid droplet coat proteins (41). Activation/regulation of lipolysis includes a series of phosphorylation/dephosphorylation events (44). During fasting, for instance, glucagon and/or catecholamines (e.g. adrenaline) are secreted. They bind to their respective (glucagon or β-adrenergic) receptors thereby stimulating G-proteins which in turn activate the adenylyl cyclase (45). The induction of this enzyme results in increased cyclic AMP (cAMP) levels. cAMP molecules bind to the regulatory subunits of the cAMP-dependant protein kinase (PKA) and free its catalytic subunits (6). PKA phosphorylates perilipin A which releases CGI-58. CGI-58 can now bind to and activate ATGL, however the exact mechanism of activation is not yet known. PKA-phosphorylated HSL gets translocated to the lipid droplet where its enzymatic activity is induced by perilipin A (46, 47). ATGL gets phosphorylated at some sites as well (by other unknown kinases) but whether these phosphorylations have an inhibitory or stimulating effect on its activity remains unclear (21). Only recently, a potent inhibitor of the adi-

pose triglyceride lipase was identified, the product of the so-called *G0/G1 Switch Gene 2* (G0S2) (48). G0S2 was shown to bind to the patatin domain of ATGL thereby inhibiting its TAG hydrolyzing activity. The inhibitory mechanism still hasn't been described in detail (48).

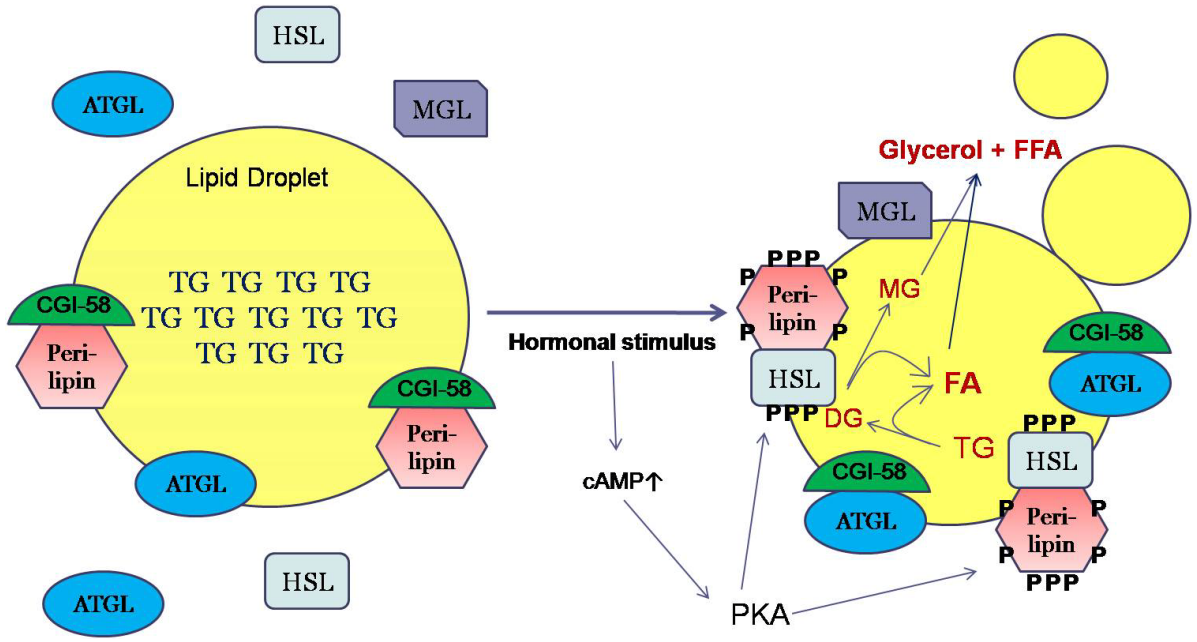

FIGURE 1.3.1. **A model for the regulation of lipolysis.** In the basal state, CGI-58 binds to perilipin A and locates on the lipid droplet (49, 50). ATGL is either in the cytosol or on lipid droplets and displays only minimal activity. Inactive HSL and MGL are found in the cytosol. Upon hormonal stimulation, perilipin A gets phosphorylated by PKA and releases CGI-58 which now can bind to ATGL and stimulate its activity. Phosphorylated HSL translocates from the cytosol to the lipid droplet where it binds to perilipin A and gets activated. ATGL that is stimulated by CGI-58 and located on the lipid droplet hydrolyzes triglycerides (TG) into diglycerides (DG) and fatty acids (FA). Diglycerides are further cleaved by HSL into monoglycerides and fatty acids. And finally, MGL catalyzes the hydrolyzation of the monoglyceride into glycerol and fatty acids (51). Fatty acids are released into the blood stream.

Mutations in the C-terminal region of ATGL lead to an increased enzymatic activity but inhibit its association with lipid droplets. These findings suggest that the C-terminal region of ATGL interferes with the binding of CGI-58 but is needed for its translocation to the lipid droplet (38). The N-terminal hydrophobic stretch in CGI-58, which is rich in tryptophan, has been shown to be necessary for lipid droplet binding and also for stimulating ATGL activity although it has no influence on interaction with ATGL (40). Truncated C-termini in CGI-58 go along with a complete loss of ATGL-activating function but have no effect on the localization of CGI-58 (40).

1.4. ATGL-knockout mice (*Atgl*$^{-/-}$)

For functional analysis of ATGL, homozygous null-mice were produced. They suffer from generalized metabolic dysfunction (52) and accumulate triglycerides essentially in all organs of the body (31). Most of the triglycerides are obviously found in WAT and BAT but also in cardiac and skeletal muscle and to a lesser degree in testis, liver, and kidney

(22). Compared to wild type littermates, *Atgl*$^{-/-}$ mice exhibit an increased whole body fat mass (and therefore increased plasma leptin levels) but a similar lean body mass at identical food intake rates (31). Knockout mice display mild obesity with an increase in lipid droplet size and hypertrophy of adipocytes (31). Basal lipolysis is similar in wild type and knockout mice but there is a drastic reduction in stimulated lipolysis in mice deficient for ATGL (31). FFA release following a hormonal stimulus is reduced by about 75% in KO mice (21). As the liver is no longer provided with fatty acids plasma levels of triglycerides, total and HDL cholesterol, and ketone bodies are lowered (21). Since fatty acids are no longer available as energy source, uncoupled mitochondrial respiration needed for heat production/thermogenesis is defective in brown adipose tissue. KO mice are cold-sensitive (22) and die upon exposure to coldness for several hours. Furthermore, reduced FFA release leads to an increased glucose uptake as alternative energy supply what explains increased glucose tolerance and insulin sensitivity in *Atgl*$^{-/-}$ mice during fasting (52, 53, 54). Moreover, carbohydrate oxidation is increased in KO mice during exercise what leads to a depletion of glycogen stores in muscle and liver (54). During fasting, the respiratory quotient (RQ) decreases in WT mice due to an increased β-oxidation but stays elevated in KO mice as they can't mobilize stored triglyceride for energy production (31). This goes along with a decrease in oxygen consumption and reduced endurance capacity during running exercises in knockout mice (54). These results are in line with the fact that ATGL mRNA is upregulated by exercise in healthy young men (55).

The obviously most harmful and in fact mortal phenotype is the fatty degeneration of the heart. Due to the massive TG accumulation, the heart weight is increased in *Atgl*$^{-/-}$ mice going along with a thickening of the left ventricle wall and a drastically reduced ejection volume (31). The first mice die around the age of 12 weeks from cardiac insufficiency and at this age, TG content of the heart is 20-fold increased in comparison to wild type mice (31).

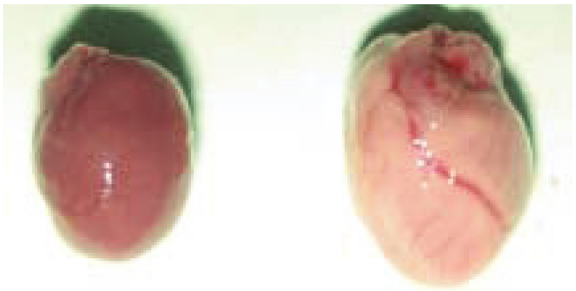

FIGURE 1.4.1. **Isolated hearts of wild type and *Atgl*$^{-/-}$ mice.** Left: heart of a wild type mouse. Right: heart of a knockout mouse. The yellowish-white discoloration and increased size result from the massive TG accumulation (image source: (31)).

Since reduced fatty acid release and triglyceride accumulation was observed not only in adipose tissue but essentially in every organ of the body (except for the brain), ATGL seems to be important for lipolysis everywhere in the organism and its activity obviously cannot be compensated by other lipases (31).

An interesting discovery was that while mutations in CGI-58 provoke the same phenotype as mutations in ATGL they also have an effect on the skin permeability barrier function (41) (56). Therefore, CGI-58 seems to have an ATGL-independent function in the skin. CGI-58-KO mice already die within 16 hours after birth (56).

1.5. Human pathology

Several autosomal recessive mutations that result in a phenotype similar to the one described for *Atgl*$^{-/-}$ mice and are classified as neutral lipid storage disease (NLSD) have been described in the human *ATGL* gene but also in the gene encoding CGI-58 (34). Humans deficient for a functional ATGL accumulate triglycerides in various tissues and cells like granulocytes (22). The lipid vacuoles inside these white blood cells lead to a morphology called Jordans' anomaly which is one of the diagnostic characteristics for NLSD (57). In contrast to KO mice, human patients are not obese. This would suppose that ATGL has another, less important function in humans than in mice or that alternative lipases exist in humans which can in part replace ATGL activity. However, the hypotheses on the exact role of ATGL in human lipid metabolism are still discussed very controversially (58) (59) (60). ATGL-deficient humans suffer from severe cardiac and milder skeletal myopathy. To date two patients have died from cardiac insufficiency but contrary to KO mice it is not clear if this was caused by lipid accumulation (39, 61): Furthermore, a common feature associated with mutations in the *ATGL* gene is some kind of liver disease (21, 22).

Humans with mutated forms of CGI-58 show more or less the same symptoms as described above except for an additional phenotype affecting the skin named nonbullous congenital ichthyosiform erythroderma (34). Ichthyosis describes the scaly, wrinkled skin which can no longer perform its permeability barrier function. Furthermore, defective CGI-58 results only in a very mild form of myopathy but displays additional neurological disorders (34). Therefore, people having mutations in the gene encoding ATGL suffer from neutral lipid storage disease with myopathy (NLSDM) whereas mutations in CGI-58 cause neutral lipid storage disease with ichthyosis (NLSDI) also called Chanarian-Dorfman syndrome (CDS) (42).

1.6. Docosahexaenoic acid (DHA)

Docosahexaenoic acid (C22:6n-3; trivial name: cervonic acid) is a ω-3 long chain polyunsaturated fatty acid (LC-PUFA) with a tail of 22 carbon atoms and six double bonds (62). It is the main PUFA in the mammalian retina and human breast milk and highly concentrated in the brain (62, 63, 64, 65).

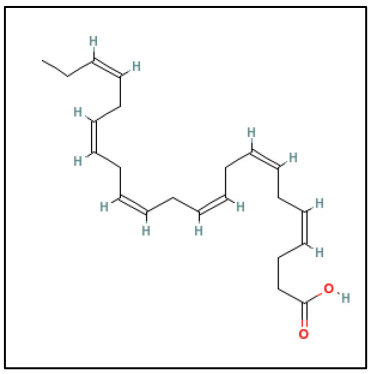

FIGURE 1.6.1. **Structure of docosahexaenoic acid (DHA).** Schematic representation of DHA with its 22 carbon atoms and six double bonds. The carboxylic acid head group is marked in red (image source: (66)).
.

DHA is either directly taken up by ingestion of cold water fish oil, alternatively it can be synthesized from its precursor α-linolenic acid (ALA; C18:3n-3) (67). Most of the 20- and 22-carbon PUFAs in human tissue are derived from conversion of C18:2n-6 (linoleic acid; LA) and C18:3n-3 (ALA), respectively (68). α-linolenic acid (ALA) is an essential ω-3 polyunsaturated fatty acid with a chain of 18 hydrocarbons and 3 double bonds which has to be taken up with the diet. It is highly concentrated in vegetable oils (69, 70). There exist three different pathways for DHA biosynthesis: one anaerobic (marine bacteria/unicellular eukaryotes) and two aerobic (Δ4-desaturase-dependant (unicellular eukaryotes) and Δ4-desaturase-independent (mammals)). (71). In mammals, a pathway involving a peroxisomal retroconversion step, the so-called Sprecher pathway, is at work (72). The retroconversion is necessary due to the absence of a specific desaturase, the Δ4-desaturase, which was believed for a long time to be present in mammals, too (73). This enzyme would be needed for the introduction of one double bond into C22:5n-3. But instead, C22:5n-3 first gets elongated and desaturated to C24:6n-3 which is transported to the peroxisomes and finally β-oxidized to form C22:6n-3 (64, 73). Patients suffering from Zellweger syndrome show reduced DHA brain levels and synthesis rates (67, 70) what further indicates that the last steps of DHA biosynthesis take place in peroxisomes.

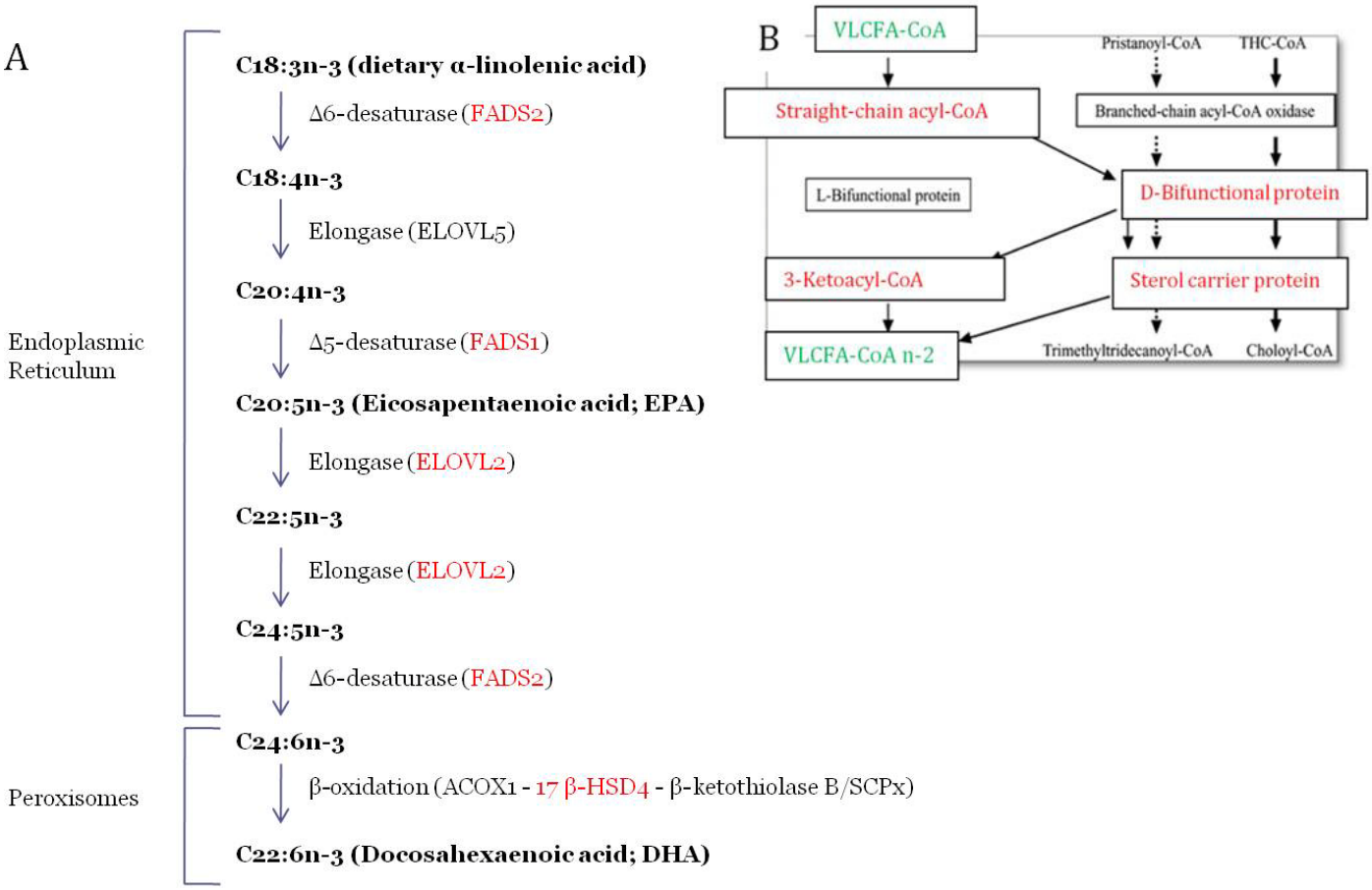

FIGURE 1.6.2. **Pathway for DHA biosynthesis in mammals.** A, The sprecher pathway for DHA synthesis comprises a series of elongations and desaturations. The last (β-oxidation) steps are taking place in the peroxisomes. Red marked enzymes were investigated in our study. B, A more detailed view of β-oxidation inside peroxisomes (image source (67)).

The main organ for DHA synthesis is the liver where ALA gets converted by a number of desaturation and elongation events. After injection of the radioactively labeled precursor, DHA appears first in the liver and later in the brain and the retina (62). This suggests that the liver secretes DHA into the blood stream in the form of lipoprotein particles (mainly acylated in PL) which are taken up by brain and retina and incorporated into cell membranes (62). Liver synthesis rate exceeds the brain consumption rate by about 30 times, so the liver is able to “feed” the whole organism with DHA (69). Brain and heart also have the capacities to synthesize DHA although compared to the liver the levels of DHA produced in the heart are marginal (69). The brain either takes up preformed DHA incorporated into phospholipids but it can also synthesize minor amounts itself. DHA biosynthesis in the brain takes place mainly in astrocytes (74). It could be part of the supporting role of astroglia to ensure the DHA supply of neurons (63).

1.7. Functions of DHA

Omega-3 and omega-6 FA are mainly incorporated in the inner membrane leaflet of cells (neurons, erythrocytes, cardiac myocytes, etc.) at the sn-2 position of phospholipids (75). Hydrolytic release of PUFA from this position is catalyzed by the Ca^{2+}-dependant isoform of phospholipase A_2 (Ca^{2+}-$PLA_{2)}$ which frees them for cell signaling and eicosanoid synthesis (75). Many actions of DHA rely on the fact that it can be transformed to bioactive lipid mediators.

Anti-inflammatory/inflammation resolving mechanisms

The main omega-6 PUFA is arachidonic acid (AA; C20:4n-6) which is metabolized to eicosanoids classified as thromboxanes, prostaglandins, and leukotrienes that fulfill mainly important pro-inflammatory actions (76). The most abundant omega-3 PUFA are DHA and EPA (C20:5n-3) which have especially anti-inflammatory functions. On the one hand omega-3 FA compete with omega-6 FA for the same transport, acylation, and synthesis pathways and for incorporation into cell membranes (77). EPA and DHA are incorporated into phospholipid membranes of inflammatory cells in a time- and dose-dependent manner, partly at the expense of AA, and thereby inhibit AA metabolism and the production of AA-derived eicosanoids (76). On the other hand, EPA and DHA serve as precursors for the production of anti-inflammatory players like resolvins (E- and D-series), docosanoids and protectins, especially DHA-derived neuroprotectin D1 (NPD-1) (78, 79). DHA/EPA further negatively influence the production of peptide mediators (e.g. cytokines) and other inflammatory agents (adhesion molecules, platelet activating factor, TNFα,..) because they affect transcription factors that regulate inflammatory gene expression (NFκB, PPARγ) (78). DHA alters lipid raft organization and function since it is stereochemically incompatible with sphingolipids and cholesterol and thereby affects these pro-inflammatory signal-transduction pathways that are compartmentalized by such lipid rafts (78). PPAR/RXR-heterodimers can be activated already by µmol-concentrations of DHA and EPA and in turn inhibit NFκB-activation (78). A link between PPAR activation and n-3 PUFAs has also been described in another study. They could show that PPARβ/δ binding to DNA is increased when primary cultures of rat cardiomyocytes where provided with EPA or DHA and this is attributed to an upregulated ACOT (acyl-CoA thioesterase) activity which guarantees high NEFA concentration and therefore a constant supply with PPAR ligands (80). Since EPA and DHA are PPAR ligands themselves this could be some kind of a positive feedback loop (78).

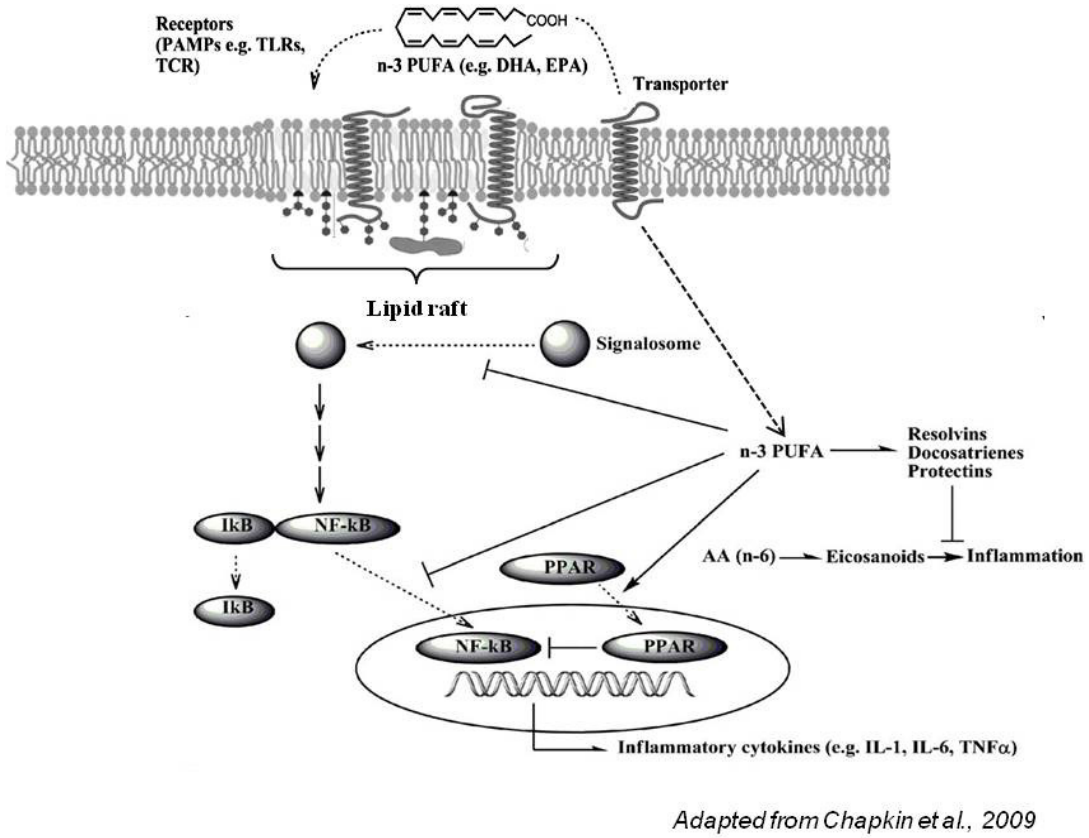

FIGURE 1.7.1. **Proposed model of anti-inflammatory actions mediated by EPA and DHA (78)**. EPA/DHA are either incorporated into lipid raft domains or transported into the cell and have several functions: modification of lipid raft organization by EPA/DHA important for signal transduction via TLRs (and/or other receptors incorporated into lipid rafts) and further transcription factor activation (e.g. NFκB); alteration of nuclear receptor activity (PPAR) thereby inhibiting expression of inflammatory mediators; interference with the production of pro-inflammatory metabolites from AA; production of anti-inflammatory metabolites from n-3 PUFAs. AA, arachidonic acid (C20:4n-6);DHA, docosahexaenoic acid (C22:6n-3); EPA, eicosapentaenoic acid (C20:5n-3); NF-kB, nuclear factor kB; IkB, inhibitor of NF-kB; IL, interleukin; PPAR, peroxisome proliferator-activated receptor; PUFA, polyunsaturated fatty acids; TLR, Toll-like receptor; these receptors recognize highly conserved pathogen-associated molecular patterns (PAMPs) and then generate an immune response; TNFa, tumor necrosis factor alpha (image adapted from: (78)).

Development and maintenance of the nervous system

DHA is the ω-3 fatty acid preferentially taken up by the brain where it is incorporated into brain phospholipids (especially phosphatidylserine (PS)) - the main constituents of neuronal membranes (63). DHA is important for synaptogenesis/neurogenesis (62, 79), neurotransmitter metabolism (81) and normal brain development (64). It promotes neurogenesis by regulating transcription factors and the cell cycle of neural stem cells (82). Moreover, DHA is the major structural component of the gray matter (83) and the major fatty acid transported across the placenta during fetal development (62, 81). This might be a reason for circulating DHA levels being higher and ALA conversion rates being increased in women during the reproductive cycle (75). Fluidity of synaptic membranes increases when DHA is incorporated (due to its stereochemistry (84)) what improves learning ability (64). In (passive or active) avoidance tests (to measure learning behavior) DHA-fed mice perform better compared to mice on a standard chow-diet (85, 86). DHA

incorporated into phosphatidylserine (PS) inside neuronal membranes has an anti-apoptotic effect because DHA-containing PS preferentially interacts with membrane proteins. Thereby PS accumulates inside nerve cell membranes further facilitating Raf-1 translocation to the membrane (63). Raf-1 is involved in anti-apoptotic signaling mechanisms. That's possibly why neuronal cells take up that much DHA to retain PS in the membranes (63). Another anti-apoptotic effect is the activation of Bcl-2 by NPD-1 (79). Bcl-2 also plays a role in regulating the programmed cell death. Since Bcl-2 and Raf-1 are involved in the same functional processes, there might be a link between these anti-apoptotic functions. Furthermore, brain phosphatidylethanolamine (PE) plasmalogen levels are higher in DHA-fed mice (85). Plasmalogen is important in lowering the ability of cholesterol to be oxidized in brain phospholipid bilayers – therefore it is needed for maintaining and improving the brain's function (85). During ischemic injury or convulsions, the brain was shown to release free 22:6n-3 which is converted to docosanoids that have neuroprotective functions and fight/resolve inflammation (62, 79).

Patients with generalized peroxisomal disorders (Zellweger syndrome; Refsum's disease) have low DHA levels in brain – supplementation with DHA improves many of the symptoms: plasmalogen concentration increases in erythrocytes, liver enzymes return (almost) to normal, brain myelin normalizes (87).

Vision

DHA accumulates in retinal tissues during fetal development where it is needed for photoreceptor membrane biogenesis and represents over 60% of the fatty acids in the outer membrane segment of retinal photoreceptor cells (62, 71, 88). There it guarantees visual acuity since proper function of rhodopsin has been shown to depend on DHA levels (71). Moreover DHA attenuates microglial activation and delays retinal degeneration (89).

Cardiovascular system

The anti-arrhythmic functions of DHA/EPA rely on the incorporation into myocardial cell membranes where they affect trafficking of channels in lipid rafts and have direct effect on the sinus node and depolarization/repolarisation rate (90). The endothelial function improves upon DHA-supplementation; furthermore large artery stiffness and blood pressure are reduced. Anti-atherosclerotic functions further rely on the reduction of pro-atherogenic cytokines and growth factors like interleukins, TNFa, PDGF, and MCP-1 which is again closely connected with its anti-inflammatory action (90).

Serum lipids

TG-reducing properties – maybe due to increased beta-oxidation and reduced lipogenesis by regulation of gene expression – are controversially discussed (85, 91). At least for EPA it was shown that it increases beta-oxidation when changing from fed to fasted status (92).

Other functions

DHA might have anticancer activity since it downregulates SOD-1 gene expression thereby enhancing oxidative stress what might be killing cancer cells more effectively (93). DHA is likely to have a number of other beneficial functions, especially in the brain. Neurological disorders like depression (71) or Alzheimer's disease (85) were discussed to be closely connected with changes in DHA levels of the brain. Preterm infants not supplemented with DHA displayed reduced cognitive development (94). The beneficial functions of DHA seem to be manifold but detailed information on its mode of actions still remains elusive.

1.8. Lipid profiling by tandem MS[1]

Lipid profiling of *Atgl*$^{-/-}$ mice by MS/MS without prior HPLC separation revealed some interesting new insights into the physiology of ATGL (Ingo E. Streith, unpublished data). Phospholipids (PC, PE, PS, PI, and CL) were examined for fatty acid composition in cardiac muscle, skeletal muscle, liver, WAT, BAT and testis by tandem MS. The results showed a significant decrease in DHA-containing phospholipids in the heart of *Atgl*$^{-/-}$ mice (compared to WT and HSL$^{-/-}$ mice) whereas most of C18:0/C18:1/C18:2-containing PL species were increased (Fig.1.8.1). This effect was most pronounced for PC and PE but was also observed concerning fatty acid composition of PS, PI, and CL.

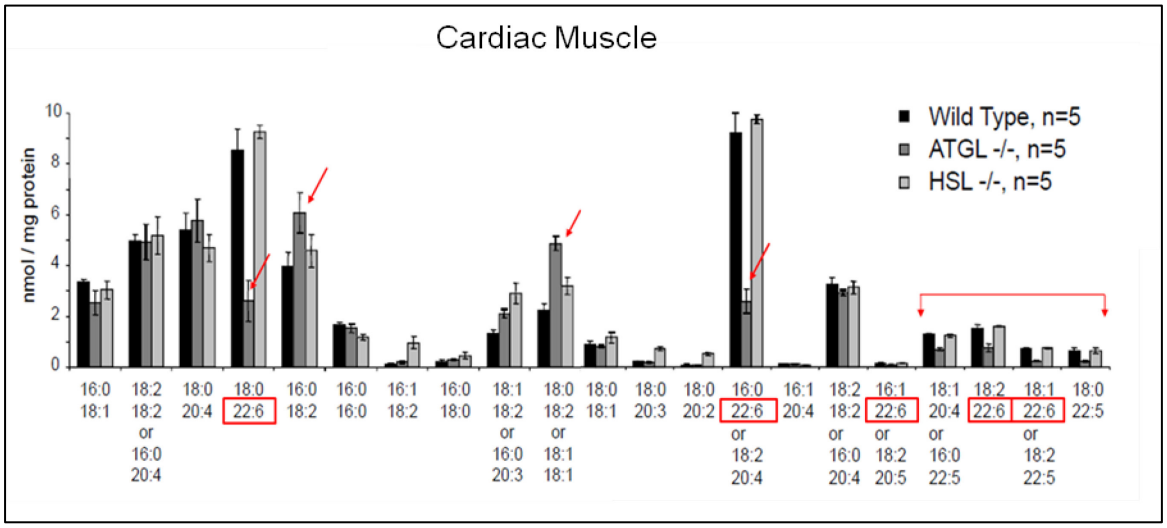

FIGURE 1.8.1. **Lipid profiling analysis by MS/MS**. Mass spectrometric analysis of PC composition in cardiac muscle of wild type mice and ATGL/HSL deficient mice (absolute values). DHA-containing PC species are marked in red. n, number of mice.

Looking at the TAG profile (Fig.1.8.2), again most DHA-containing triglycerides were reduced in CM of mice deficient for ATGL compared to wild type mice (C56:7; C58:6; C58:9) whereas triglycerides containing linoleic acid (C18:2) were increased (C54:4;

[1] All figures in chapter 1.8 provided with courtesy by Ingo E. Streith

C54:5). However, it has to be kept in mind that concerning particular triglycerides there can be an overlay of many different species (e.g. C58:6 could be composed of C22:6/C18:0/C18:0 but also of C20:4/C:20:0/C18:2). For an exact determination of the composition of triglycerides a further analyzation step would have been necessary.

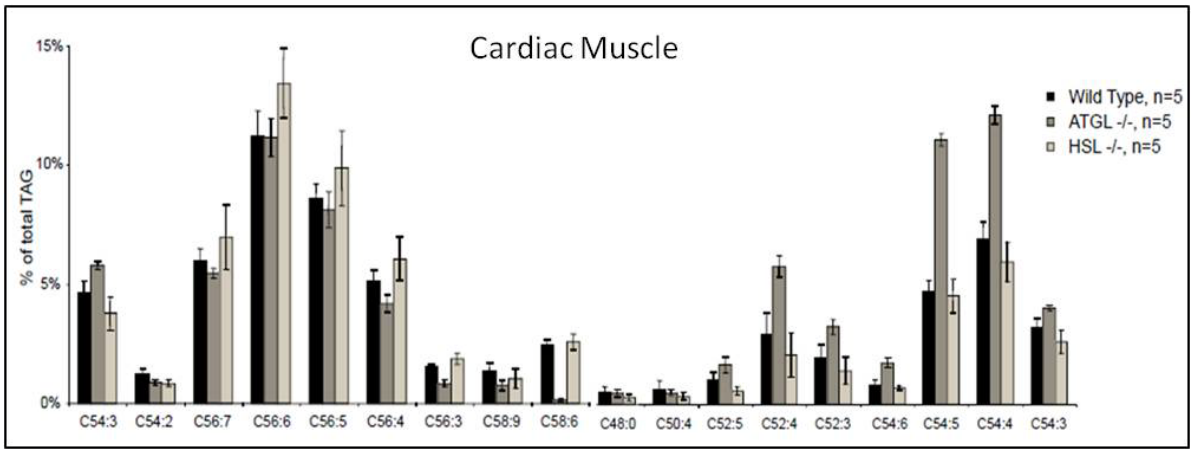

FIGURE 1.8.2. **Quantitative fatty acid composition of TAG species.** Fatty acid composition of TAG species was investigated in cardiac muscle of WT, *Atgl*$^{-/-}$, *Hsl*$^{-/-}$, and *Cgi-58*$^{-/-}$ mice by MS/MS.

The same pattern was obtained for free fatty acids in the cardiac muscle (Fig.1.8.3). C22:6n-3 was again decreased in ATGL-deficient mice whereas C18-fatty acids were increased compared to wild type mice although these results were not significant due to high standard deviations.

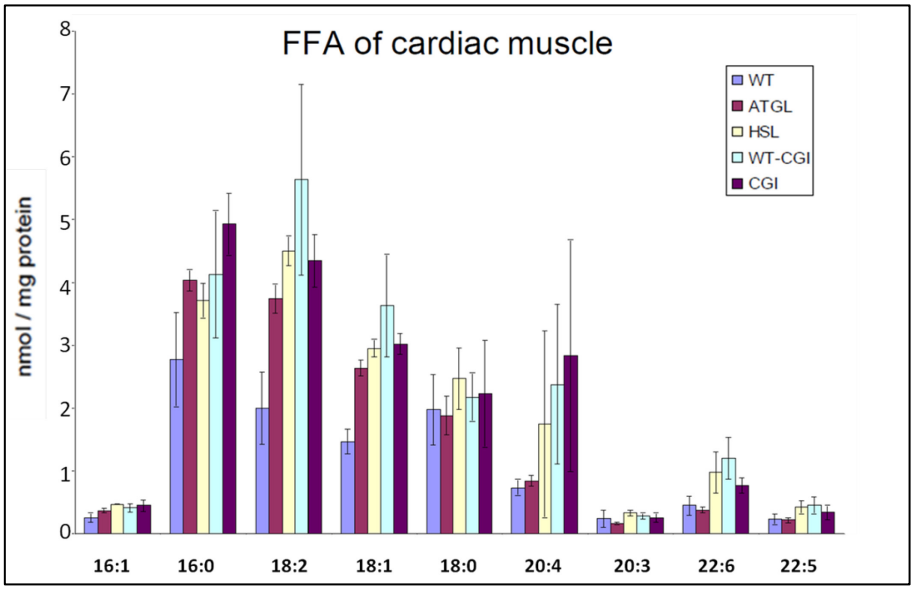

FIGURE 1.8.3. **FFA composition analyzed by MS/MS.** WT, wild type; ATGL, *Atgl*$^{-/-}$; HSL, *Hsl*$^{-/-}$; WT-CGI, wild type with functional CGI-58; CGI, *CGI-58*$^{-/-}$.

In summary, precursors of LC-PUFAs incorporated into phospholipids and triglycerides were increased in *Atgl*$^{-/-}$ mice compared to WT mice whereas LC-PUFAs, especially DHA, were reduced.

2. Aim of the study

The results of the lipid profiling analysis (chapter 1.8) suggested a causal relationship between ATGL deficiency and reduced levels of DHA-containing lipid species. Therefore, we wanted to elucidate the role of ATGL in DHA biosynthesis.

We followed two main approaches both connected to the TG-hydrolyzing activity of ATGL:

- Release of FFA by ATGL could influence signaling pathways/regulate gene expression, thereby exerting an effect on DHA synthesis
- ATGL could release those FA from triglycerides/phospholipids that are needed as precursors for LC-PUFA synthesis

Additionally, feedback regulation could have an impact on DHA levels since DHA is a PPAR ligand itself. The main approach to answer some of these questions was to compare the mRNA levels of selected enzymes involved in DHA-synthesis in various mouse tissues by doing quantitative real-time PCR measurements. DHA (C22:6n-3) is synthesized from α-linolenic acid (C18:3n-3) mainly in the liver but also in the brain and the heart (67, 69). The first desaturation and elongation steps take place in the endoplasmic reticulum. The C22:5n-3-intermediate produced inside the ER is transported to the peroxisomes where it gets β-oxidized to form DHA (64, 73). We chose following enzymes of the DHA-synthesis pathway to take a closer look at:

- **FADS1**: fatty acid desaturase 1; Δ5-desaturase
- **FADS2**: fatty acid desaturase 2; Δ6-desaturase; rate-limiting enzyme which fulfills the first desaturation step
- **ELOVL2**: elongation of very long chain fatty acids-like 2; elongase with high substrate specificity for C20:5 and C22:5
- **17β-HSD4**: 17β-hydroxysteroid dehydrogenase type 4; peroxisomal β-oxidation enzyme

FADS1 and FADS2 were selected as they are the rate-limiting enzymes of DHA biosynthesis (68). Furthermore, FADS2 but also ELOVL2 are rather important for this pathway as both of them are catalyzing two synthesis steps. 17β-HSD4 was selected as one of the peroxisomal enzymes involved in β-oxidation of DHA and has been shown to be essential for DHA synthesis (64).

The expression of these enzymes was examined primarily in the liver being the main organ of DHA synthesis (69) but also in the heart since the changes in DHA-containing phospholipid levels were observed in the heart.

3. Materials and Methods

MATERIALS

3.1. Plastic- and glassware

Nuclease/DNA-free 1.5 ml/2 ml PP reaction tubes, 15 ml/30 ml sterile PP tubes with screw cap, pipette tips, Petri dishes, sterile serological pipettes, and 96-well microplates were purchased from Greiner bio-one (Kremsmünster, Austria), Sarstedt (Nümbrecht, Germany) and Corning Inc. (NY; USA). Fast optical 96-well reaction plates for real-time PCR were used from Applied Biosystems (United States). Glass vessels, for instance beakers, Erlenmeyer flasks, and graduated cylinders, were bought from the company Lactan (Graz, Austria). Glassware was washed and autoclaved (121°C) before usage.

3.2. Chemicals

All chemicals listed, if not indicated otherwise/separately, were purchased from the companies Merck (Darmstadt, Germany), Carl Roth (Karlsruhe, Germany), J.T. Baker (Phillipsburg, NJ, USA) or Sigma Aldrich (St. Louis, MO, USA) and had a purity grade/degree of *pro analysi* (p.a.).

3.3. Radiochemicals

α-^{32}P-dATP (red) was purchased from Hartmann Analytic GmbH (Braunschweig, Germany)

3.4. Enzymes

DNaseI/10x DNaseI buffer (Invitrogen)
Phusion Hotstart DNA-polymerase/5x High Fidelity buffer (Finnzymes)
Restriction enzyme EcoRI/10x EcoRI buffer (Fermentas)
T4-DNA-Ligase/appropriate 10x buffer (New England Biolabs)
Calf Intestine Phosphatase (CIP, New England Biolabs)
DNA Polymerase I, Large (Klenow) Fragment (New England Biolabs)/Labeling 5x buffer (Promega)

3.5. Kits

BCA Protein Assay Reagent (bicinchoninic acid) (Thermo Scientific)

BigDye® Terminator v3.1 Cycle Sequencing Kit (Applied Biosystems)

High Capacity cDNA Reverse Transcription Kit (Applied Biosystems)

HR series NEFA-HR(2) kit (Wako Diagnostics)

Maxima™ SYBR Green/ROX qPCR Master Mix (Fermentas)

Power SYBR® Green PCR Master Mix (Invitrogen)

3.6. Equipment

ABI PRISM® 310 Genetic Analyzer (Applied Biosystems)

Accela High Speed LC/UHPLC system (Thermo Scientific)

Balances (ScalTec)

Benchtop centrifuge 5415R (Eppendorf)

Biotrak II Visible Plate Reader (Amersham Biosciences)

C1000 Thermal Cycler (Bio-Rad)

Centrifugal vacuum concentrator (ATR Heto)

Centrifuge GS-6/GS-6R (Beckman Coulter)

CFX96 Real-Time System (Bio-Rad)

DNA Engine DYAD™ Thermal Cycler (Bio-Rad)

Dri-Block DB-3 (Techne)

Electrophoresis Power Supply EPS 600 (Pharmacia Biotech)

GE Image Quant 3000 (GE Healthcare)

Horizontal DNA Electrophoresis Gel Boxes (Bio-Rad)

Model 285 Vacuum Blotter (Bio-Rad)

Nanodrop ND-1000 (Peqlab)

Prism 310 Genetic Analyzer (ABI)

Sample Concentrator (Techne)

StepOnePlus RT PCR Systems (Applied Biosystems (ABI))

STORM 860 Phosphorimager (Molecular Dynamics)

Test-tube rotator/Rotating wheel (Labinco)

Thermomixer compact (Eppendorf)

TriPlus™ Autosampler (Thermo Scientific)

Trace GC Ultra (Thermo Electron Corporation)

Trace DSQ Mass Spectrometer (Thermo Electron Corporation)

Ultra Turrax (IKA works)

Ultraviolet Crosslinker (UVP Inc.)

3.7. Buffers and Solutions

All buffers and solutions were prepared and/or diluted using “Fresenius” Aqua bidest. from Fresenius Kabi (Graz, Austria). For RNA applications ddH_2O was treated with DEPC. Solutions were autoclaved if they had to be sterile.

3.7.1. Solutions and Stocks

DEPC-ddH_2O
900 ml ddH_2O
900 µl DEPC (0.1% DEPC)
autoclaved

0.5M EDTA
186 g/l

Ethidium bromide
10 mg/ml ddH_2O

IPTG (Isopropyl β-D-thiogalactopyranoside)
23.8 mg/ml ddH_2O

X-Gal (5-Bromo-4-chloro-3-indolyl β-D-galactopyranoside)
40 mg/ml DMSO

20% SDS
200 g SDS/l dissolved at 65°C

1000x ampicillin stock
100 mg/ml

RNase
10 mg/ml
Boil for 10 min

1 M Tris-HCl
121.1 g Tris
adjusted to pH 7.5 with HCl

5x DNA loading dye
3 ml 30% glycerol
7 ml ddH_2O
25 mg bromophenol blue
25 mg xylene cyanol

3 M Potassium acetate
294 g 3 M potassium acetate
115 ml glacial acetic acid

Hybridization solution
50 ml 1 M sodium-phosphate buffer
70 ml 20% SDS
80 ml ddH_2O
400 µl 0.5 M EDTA pH 8.0
pH to 7.2

Prehybridization Solution
Hybridization solution + 1% BSA

1000x protease inhibitor (Pi)
20 mg leupeptin
2 mg antipain
1 mg pepstatin
dissolved in 1 ml DMSO

Sevac

1.18 M $CHCl_3$

0.04 M isoamyl alcohol

DNA: overlaid with ddH_2O; RNA: covered with 0.1 M Tris-HCl (pH 8.0) dissolved in DEPC-ddH_2O

Acidic Folch reagent

20 ml $CHCl_3$

10 ml MeOH

1% glacial/pure acetic acid

Lysis Solution

0.3 M NaOH

0.1% SDS

TRIzol (Invitrogen): TRIzol® Reagent is a solution containing phenol and guanidine isothiocyanate and was used for isolating total RNA from cells and tissues by phenol-chloroform extraction. Phenol-chloroform extraction relies on phase separation by centrifugation.

RNase away (Molecular Bioproducts): RNase away is an alkali hydroxide solution used as a surface decontaminant to remove nucleases.

3.7.2. Buffers

50x TAE buffer

242 g Tris-HCl

57.1 ml CH_3COOH

100 ml 0.5 M EDTA

ddH_2O to 1 l, pH to 8.0

10xMOPS

21 g MOPS

3,6 g NaOAc

10 ml EDTA (0.5M)

DEPC-H_2O to 500 ml

pH to 7.0 (10N NaOH)

1 M sodium-phosphate buffer, pH 7.0

57.7 ml 1 M Na_2HPO_4

42.3 ml 1 M NaH_2PO_4

1x TE buffer

10 mM Tris pH 7.4

1 mM EDTA pH 8.0

HSL buffer

0.25 M sucrose

1 mM EDTA

1 mM DTT

to pH 7.0 with acetic acid

20xSSC

3 M NaCl

0.3 M $C_6H_5O_7Na_3 \cdot 2H_2O$ (trisodium citrate dihydrate)

ddH_2O to 1 l, pH to 7.0

Lysis Buffer I

5 ml 1 M glucose

2.5 ml 1 M Tris-HCl (pH 7.5)

2 ml 0.5 M EDTA

90.5 ml ddH_2O

Lysis Buffer II

0.2 ml 10 M NaOH

0.5 ml 20% SDS

9.3 ml ddH_2O

3.8. Media

Media were sterilized by autoclaving at 121°C and stored at 4°C.

LB medium

10 g peptone

5 g Yeast Extract

10 g NaCl

ddH_2O to 1 l, pH to 7.0

LB-agar plates

10 g peptone

5 g Yeast Extract

10 g NaCl

ddH_2O to 1 l, pH to 7.0

15 g agar agar

3.9. Standards

GeneRuler™ 1kb DNA ladder (Fermentas)

MassRuler™ Low Range DNA ladder (Fermentas)

3.10. Primers

Primers were designed using Harvard PrimerBank (95) (96) (97), NCBI Primer-BLAST and Primer Designer, version 2.0 (Scientific & Educational Software, NC, USA) and purchased from Invitrogen or Eurofins MWG Operon.

Gene	Forward primer (5' → 3')	Reverse primer (5' → 3')	Length (bp)	Amplicon (bp)	NCBI Gene ID
m*Fads1*	agcacatgccatacaaccatc	tttccgctgaaccacaaaataga	21/23	110	76267
m*Fads2*	aagggaggtaaccagggagag	ccgctgggaccatttggtaa	21/20	150	56473
m*Elovl2*	tctggtggtgtgttttgaactg	acaggccgtagtaggagtaca	22/21	102	54326
m*17β-Hsd4*	aggggacttcaagggaattgg	gcctgcttcaactgaatcgtaa	21/22	112	15488
m*Actb*	agccatgtacgtagccatcca	tctccggagtccatcacaatg	21/21	81	11461
m*Fads1*-probe	ttgaattcacaacatcagcgacttcagc	ttgaattcgcggcatgtaagtgaagaag	28/28	810	76267
m*Fads2*-probe	ttgaattcggagaagatgctacggatgc	ttgaattcggctctccaggaacctgata	28/28	802	56473

TABLE 3.1. **Sequences of forward and reverse primers designed for real-time PCR and Northern blot probe preparation**. Underlined sequences represent EcoRI restriction site.

3.11. Plasmids

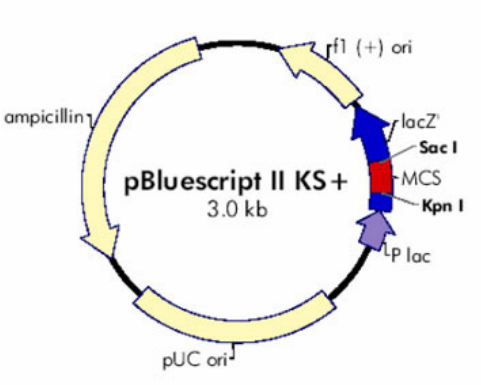

pBluescript II SK+:

ampicillin resistance (100µg/ml)

blue/white screening

general cloning vector

3.12. Animals

Mice were housed under standard conditions (24°C; 14h light/10h dark) and had free access to water and the standard laboratory chow diet (ssniff® M-Z Extrudate; 4.5% w/w fat). For some experiments mice were fasted for 12 hours (o/n) or chow diet was supplemented with 0.1% of the synthetic PPARα agonist WY14,643 (Cayman Chemical Company) for three weeks. *Atgl*$^{-/-}$ mice (Pnpla2^{tm1Rze}/Pnpla2^{tm1Rze}) were generated by targeted homologous recombination (Fig.3.12.1) (31).

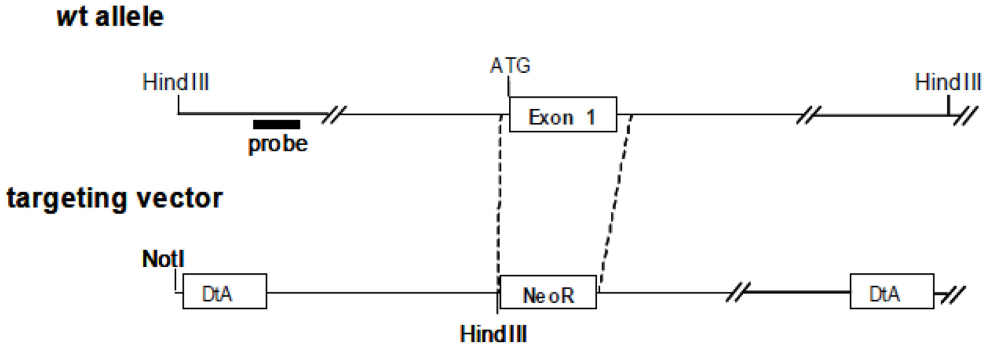

FIGURE 3.12.1. **Targeting strategy for generating *Atgl*$^{-/-}$ mice** (31). Murine gene encoding ATGL was knocked out by homologous recombination. Depicted at the bottom is the site-specific cassette introducing a neomycin resistance and disrupting the ATGL coding sequence (image source: (31)).

Heterozygous mice were bred for the deleted allele. Experimental KO mice were generated by breeding *Atgl*$^{+/-}$ or *Atgl*$^{-/-}$ males to *Atgl*$^{+/-}$ females. Male offspring was used at 8 to maximum 10 weeks of age and backcrossed at least 5 times on the C57BL/6J background (31). Transgenic mice overexpressing *Atgl*-cDNA specifically in cardiac muscle were generated as described (98). Liver-specific adenoviral expression of ATGL in *Atgl*$^{-/-}$ mice was performed as illustrated (99).

Animals were killed by cervical dislocation between 8 and 12 a.m., and liver, heart, and brain tissues were collected. All experiments were performed with male mice.

3.13. Real-time PCR

3.13.1. Primers

Primers were dissolved in an appropriate volume of ddH_2O (as indicated in the instructions) to a final concentration of 200 pmol/µl by placing them on a thermomixer at 500 rpm and 37°C for about half an hour. 2 and 4 µl of dissolved primers were loaded on a 1.5% agarose gel to check the actual concentration. Depending on the intensity of the bands, primers were diluted until forward and reverse primers were equally concentrated. This was of especial importance for quantitative real-time PCR.

3.13.1.1. Agarose gel electrophoresis

Agarose (Invitrogen) was dissolved in 1xTAE (1%: 3 g/300ml; 1.5%: 4.5 g/300ml), boiled in the microwave, cooled down to approx. 60°C and mixed with ethidium bromide. For polymerization, the gel was poured into the tray fixed in the gel caster. The electrophoresis chamber was filled with 1×TAE, the polymerized gel was added and the samples (mixed with 5x DNA loading dye) were loaded on the gel.

3.13.2. RNA preparation

For the handling with RNA it is very important to be as RNase-free as possible. Therefore everything was done wearing gloves, working benches were cleaned with RNase-away and water was treated with DEPC.

DEPC-ddH_2O: diethylpyrocarbonate added to double distilled water inactivates RNases by covalent modifications. The flask containing DEPC-ddH_2O was placed into the hood overnight with the lid not screwed down so that DEPC volatilized overnight and was autoclaved the next day.

3.13.2.1. Tissue isolation

Blood samples were collected under anesthetic by puncture of the retrobulbar venous plexus. Mice were killed by cervical dislocation. Liver, heart, and brain were dissected and immediately transferred into a reaction tube containing TRIzol®. If not used immediately, tissue was kept in cryovials in liquid nitrogen at about -210°C.

3.13.2.2. RNA isolation

The isolated tissue was weighed and 1 ml TRIzol® (Invitrogen) was added for up to 100 mg tissue, 2 ml were used for more than 100 mg tissue. TRIzol works by maintaining RNA integrity during tissue homogenization, while at the same time disrupting and breaking down cells and cell components. Guanidinium thiocyanate denatures proteins, including RNases, and separates rRNA from ribosomes. The tissue was homogenized with an Ultra Turrax (samples not being handled with were kept on ice in the meantime) and incubated at room temperature for 5 minutes. 0.1 ml 1-bromo-3-chloropropane (instead of chloroform – less toxic) were added per ml TRIzol® and tubes were mixed vigorously. Samples were incubated at RT for another 15 minutes and in the meantime were shaken from time to time. Next, they were centrifuged for 15 min at 4°C and maximum 12,000×g. The solution then had separated into three distinct phases: an upper aqueous phase containing the RNA, an interphase containing the proteins (visible as a white precipitate), and the lower organic phase (reddish) containing the DNA. The aqueous phase was transferred into a fresh reaction tube. 0.5 ml isopropanol were added per ml TRIzol®, mixed vigorously and incubated at RT for 10 minutes. The samples were centrifuged at 4°C and maximum 12,000×g for 10 minutes. The supernatant was removed and 1 ml 75% EtOH was added to the pellet. The pellet was washed at 4°C and maximum 7500×g for 5 minutes. The supernatant was again removed and the pellet was air-dried until the smell of ethanol had vanished completely. The pellet was resuspended in 100 – 600 µl DEPC-ddH_2O (depending on the size and the RNA concentration).

3.13.2.3. RNA concentration

For determination of RNA concentration, samples were measured with NanoDrop 1000 spectrophotometer. Therefore, 1 µl of each resuspended pellet was loaded on the NanoDrop. Each sample was measured at least twice. RNA can be quantified using absorption of light at 260 and 280 nm (A260/280). Ideally, this ratio should be close to 2 for high quality nucleic acid. For RNA, an absorption value of 1 equates a concentration of 40 µg/ml whereas for DNA an absorption of 1 is equivalent to a concentration of 50 µg/ml.

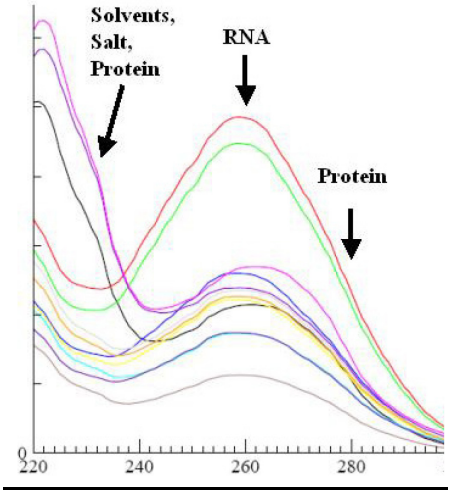

FIGURE 3.13.1. **Spectrogram showing the maximum absorbance of several substrates** (source: (100))**.**

With the determined concentration, volume of concentrated RNA needed for 50 µl of a 0.2 µg/µl-solution was calculated and prepared for every sample (c1∗V1 = 0.2 µg/µl*50µl → c1: measured concentration, V1: volume of the sample needed for preparation of the 0.2 µg/µl-solution). 2 µl of all diluted samples were merged in a separate reaction tube as negative control (a so-called "RT minus sample") for qRT-PCR.

3.13.2.4. RNA agarose gel electrophoresis

For examination of RNA quality, isolated RNA samples were denatured and visualized on an agarose gel. Due to the nature of RNA, the separation on gels is a bit different compared to DNA. RNA that is usually single stranded can fold up itself to form stable secondary structures (such as hairpins). This is a problem when you need to separate RNA on a gel. Therefore RNA was denatured by incubating with formaldehyde at 55°C.

1% RNA agarose gel

3 g agarose were dissolved in 250 ml DEPC-H_2O, heated in the microwave until the agarose had completely dissolved and cooled down to approx. 60°C. 30 ml 10xMOPS and 17.5 ml 37% formaldehyde were added. The gel equipment was washed with 20% SDS and DEPC-H_2O before usage to destroy any nucleases. The gel was prepared under the fume hood about 1 hour before loading the samples because of the formaldehyde. Ethidium bromide had not to be added to the gel since there was enough contained in the sample buffer.

RNA sample preparation

5 µg RNA (200 ng/µl) were mixed with 6 µl 5xRNA sample buffer and filled up with DEPC-ddH_2O to 30 µl. The samples were denatured for 15 min at 55°C. They were loaded on the gel and the gel was run for 20 min at constant 90 V. 1xMOPS was used as running buffer.

3.13.2.5. DNase digest

If the quality of RNA was good, RNA samples were digested with DNase I to destroy any unwanted DNA-contamination. For the DNase digest a kit from Invitrogen was used.

	µl
RNA (=1µg*)	5
DNase	1
10xDNase-buffer	1
DEPC-H2O	3

*5 µl of the prepared 0.2 µg/µl-dilutions → equivalent to 1 µg RNA

A mastermix was prepared containing DNase, buffer and water (on ice!). 5 µl of the mastermix were pipetted into reaction tubes, 5 µl RNA were added and samples were incubated for 15 min. at RT and 350 rpm in a thermomixer. DNaseI was inactivated by addition of 1 µl 25 mM EDTA and incubation at 65°C for 10 minutes. Samples were kept on ice afterwards.

3.13.2.6. Reverse transcription

The DNase-digested samples were immediately subjected to reverse transcription with a kit from Applied Biosystems since cDNA is much more stable than RNA.

	µl
10x RT-buffer	2
dNTPs (100mM)	0,8
10x Random Primer	2
Reverse transcriptase	1
RNase inhibitor	1
H2O	3,2

A mastermix was prepared for all samples except the RT minus sample. For the RT minus sample the reverse transcriptase was excluded, instead 1µl of water was added. The RT minus sample was used during real-time PCR as a control to know if DNase-digest worked and to see potential DNA contaminations. The mastermixes were pipetted into PCR strips and the DNase-digested samples (11µl) were added. Reverse transcription was performed in the 1000 Thermal Cycler from BioRad using following protocol:

	Step1	Step2	Step3	Step4
Temperature	25°C	37°C	85°C	4°C
Time	10min	120min	5min	Forever

3.13.3. Quantitative Real-Time PCR

Real-time PCR was performed using the CFX96 real-time PCR detection system combined with the 1000 Thermal Cycler (Bio-Rad) or using the StepOnePlus RT-PCR system (ABI).

SYBR Green is a fluorescent dye that binds double-stranded DNA like EtBr but with much higher sensitivity. In real-time PCR, a very simple principle is followed: the more target-mRNA was expressed in the various tissue samples, the more cDNA should be obtained by reverse transcription, the more SYBR Green should bind to the cDNA and the earlier the fluorescence measured during real-time PCR should reach a certain threshold. This happens at a specific cycle what determines the **threshold cycle value** or **Ct-value**.

3.13.3.1. Optimal primer concentration

For determination of the concentration of forward and reverse primer resulting in a sufficient template amplification rate, three different primer concentrations were tested:

0.5 µl (c=10 pmol/µl in 20 µl → 100 pmol) = 250 nM

1.0 µl (200 pmol) = 500 nM

1.5 µl (300 pmol) = 750 nM

For this primer testing a 1:25-dilution of the 50 ng/µl-stock of a WT cDNA-template was used and three different mastermixes were prepared:

MM **1** ($\times$ $\boldsymbol{x}$)	MM **2** ($\times$ $\boldsymbol{x}$)	MM **3** ($\times$ $\boldsymbol{x}$)
- 10 µl SYBR Green	- 10 µl SYBR Green	- 10 µl SYBR Green
- 4 µl cDNA	- 4 µl cDNA	- 4 µl cDNA
- 5 µl H_2O	- 4 µl H_2O	- 3 µl H_2O

$\boldsymbol{x}$...number of primer pairs to test multiplicated with 3 (for triplicates). For blank measurements, 4 µl ddH2O (BL) or RT minus probe (RT-) were added instead of cDNA.

Either 19µl (MM**1**), 18µl (MM**2**/blank) or 17µl (MM**3**) of the mastermixes were pipetted into a 96-wells microtiter-plate first and 0.5 µl, 1 µl or 1.5 µl of each forward and reverse primer were added to MM 1, MM 2/blank or MM 3, respectively. The products of the real-time PCR were loaded on a 1.5% agarose gel together with a 100 bp-DNA-ladder to verify the expected and therefore correct size. Furthermore, the amount of product obtained using the different primer concentrations was compared on the gel and the lowest primer concentration resulting in a sufficient amplification and a threshold Ct-value in a range of 20 to 25 was chosen for further analyses.

Melt curve analysis was performed to see whether the primers build dimers (if negative controls produce a melt curve peak) or amplify unspecific products (melt curve with 2 peaks).

3.13.3.2. Cycle sequencing

The real-time PCR products from the primer concentration test run were used for a cycle sequencing reaction to check if the amplified gene fragments had the correct sequence. This chain-termination method requires a single-stranded DNA template, a primer, a DNA polymerase, all four of the standard deoxynucleotides (dATP, dGTP, dCTP and dTTP) and four dideoxynucleotides (ddATP, ddGTP, ddCTP, or ddTTP). The dideoxynucleotides are the chain-terminating nucleotides which lack a 3'-OH group that would be needed for the formation of a double bond between the nucleotides. Thereby DNA strand extension is terminated and results in DNA fragments of varying length. All four dideoxynucleotides are labeled with fluorescent dyes with different wavelengths of fluorescence and emission. This enables sequencing in a single reaction and is called Dye-terminator sequencing.

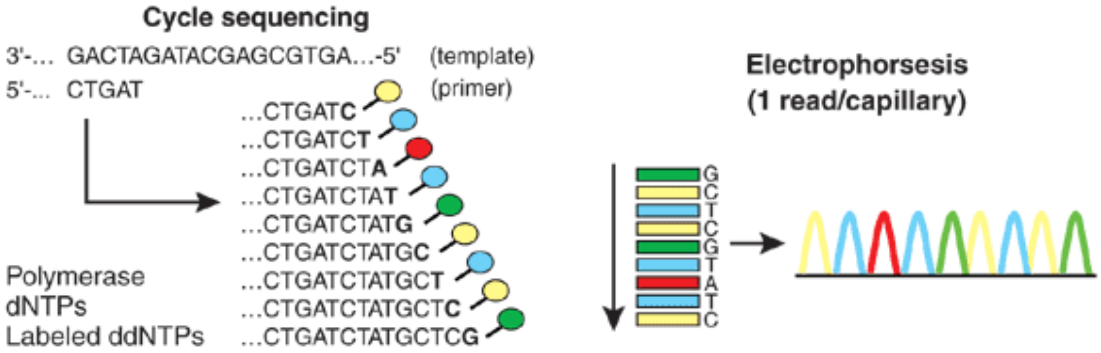

FIGURE 3.13.2. **Schematic view of the cycle sequencing reaction** (image source: (101)**).**

cDNA concentration of the PCR products was measured with NanoDrop 1000 and 50 ng/µl-dilutions were prepared for every sample.

For sequencing, BigDye® Terminator v3.1 Cycle Sequencing Kit was used.

BigDye v3.1		2 µl
5x Sequencing Buffer		2 µl
Primer	≤ 5pmol	1 µl
DNA template **PCR product:** **Plasmid:**	 10-50 ng 150-300 ng	x µl
ddH_2O	ad 10 µl	x µl

Four batches were mixed for every PCR product, two containing the forward and two the reverse primer.

PCR program:

	1	2	3	4	5
Temperature	96°C	96°C	53°C	60°C	4°C
Time [min]	1:00	0:15	0:30	1:30	∞
		30 repeats			

1…initial denaturation
2…denaturation
3…annealing
4…elongation/extension

Purification
2.5 µl 125 mM EDTA and 25 µl 100% EtOH were added to the PCR products. The samples were transferred into 1.5 ml reaction tubes and centrifuged for 20 min. at 13,000 rpm (Eppendorf 5415R) and 4°C. The supernatant was removed and samples were washed two times with 250 µl 70% EtOH for 15 min. at 13,000-15,000 rpm and 4°C. The pellets were dried in the SpeedVac concentrator, dissolved in 15 µl HiDye formamide and transferred into PCR tubes. The PCR products were sequenced with the ABI PRISM® 310 Genetic Analyzer and the resulting sequences were blasted against the mouse genome.

3.13.3.3. PCR efficiency

The PCR efficiency had to be tested for every gene. Therefore, a dilution series (1:5, 1:25, 1:125, 1:625) was prepared from a pool of all cDNA samples, the relative expression of all genes was measured in these diluted, pooled samples and a straight calibration line was created. This served multiple purposes. For every gene the highest sample dilution resulting in Ct-values between 20 and 25 was determined. The standard equation (y=kx+d;k, slope) was calculated for different thresholds. Finally, the threshold, that resulted in a coefficient of determination (R^2) of at least 0.997 and a slope as close to -3.32 as possible, was chosen. A slope of -3.32 indicates a PCR reaction that is 100% efficient. Slopes that are more negative than -3.32 indicate reactions with less than 100% efficiency. Slopes that are more “positive” than -3.32 may be caused by bad sample quality or pipetting problems. Reactions with 100% efficiency result in a 10-fold increase

of the PCR amplicon every 3.32 cycles during the exponential phase of amplification (log2 10 = 3.3219) (102). The coefficient of determination close to 1 indicates that the fluorescence decreases exponentially with the higher degree of dilution.

The dilutions were prepared from the pooled aliquots of the 50 ng/µl-stocks:

	Dilution	**Concentration [ng/µl]**	**[ng cDNA/4µl]**
V_1	1:5	10 ng/µl	40 ng
V_2	1:25	2 ng/µl	8 ng
V_3	1:125	0.4 ng/µl	1.6 ng
V_4	1:625	0.08 ng/µl	0.32 ng

A separate mastermix was prepared for every single target gene.

MM

- 10µl SYBR Green
- 0.5-1.5µl primer forward
- 0.5-1.5µl primer reverse
- 3-5 µl H_2O

Wells were preloaded with 16 µl of the mastermix and 4 µl of cDNA were added. For statistical reliability at least duplicates should be measured for every dilution. The straight calibration line (so-called “real-time PCR standard curve”) was created by plotting the logarithm of input nucleic acid (amount of cDNA) on the x-axis and the associated Ct-values on the y-axis.

3.13.3.4. Housekeeping Gene

Housekeeping genes are genes involved in basic functions needed for the sustenance of the cell. Therefore they are constitutively expressed (they are always turned ON).
The PCR efficiency of the housekeeping gene has to be consistent with the efficiency of the target gene and the threshold Ct-values should be similar. If the efficiency is not the same, the amplification rate is different, too. Therefore the values are no more quantitative and mRNA-expression of the target gene can no longer be related to the expression of the housekeeping gene.

3.13.3.5. Measurement of the samples

As the optimal primer concentrations and template dilutions have been ascertained and the best-fitting housekeeping gene has been chosen, samples were measured. Real-

time PCR is used to compare the expression of specific genes (target genes) under special conditions (e.g. deficiency of a lipase (KO)) with the expression of these genes under "normal" reference conditions (e.g. functional lipase (WT)). For comparison it is necessary to normalize the relative mRNA levels of the target genes in every sample to the levels of a housekeeping gene in the same sample since housekeeping genes principally are expressed at same levels in all tissues/under all conditions.

For reliability, 6 batches were prepared for every sample (target sample or reference sample) to have one triplicate for target gene expression and one triplicate for housekeeping gene expression. The mastermixes were prepared the same way as described for the PCR efficiency test run.

Quantitative Real-Time PCR protocol (Bio-Rad CFX96)

	1	2	3	4		5 (Melt Curve)
Temperature	50°C	95°C	95°C	60°C	**Plate Read**	45°C – 85°C (increment 0.5°C)
Time [min]	2:00	10:00	0:30	1:00		5:00
		40 repeats				

1...UDG pretreatment for carryover decontamination; OPTIONAL

2...initial denaturation

3...denaturation

4...annealing/extension

3.13.3.6. Evaluation

For relative quantification the Ct value obtained for the respective target gene of each sample had to be related to the corresponding Ct value of the housekeeping gene to obtain a standardized ΔCt-value.

ΔCt = Ct (Target Gene x (Sample y)) – Ct (Housekeeping Gene (Sample y))

For the comparison of mRNA expression of the samples of interest (e.g. knockout) with mRNA expression of the reference samples (e.g. wild type), all ΔCt-values were normalized to the mean reference ΔCt-value.

ΔΔCt = ΔCt – Mean ΔCt (reference)

The relative mRNA expression levels which actually were compared in the resulting diagrams were obtained by following equation:

Relative mRNA expression levels: $2^{-\Delta\Delta Ct}$

3.14. Northern Blot

A northern blot enables the visualization of (target gene) (m)RNA in various tissues by labeling with a radioactive probe specifically binding to this RNA.

3.14.1. Preparation of Northern blot probe I

3.14.1.1. PCR

For amplification of a specific probe a PCR was done with the primers designed for real-time PCR. Liver cDNA from wild type mice was used as a template. First, a temperature gradient was applied to establish the optimal annealing temperature resulting in the most specific and abundant product. In a 2nd PCR, multiple batches were run at this temperature for each gene to obtain enough cDNA for the Northern blot probe.

PCR-batch (**30 µl**):

cDNA template	1 µl
Primer fwd	0.5 µl
Primer rev	0.5 µl
dNTP	0.5 µl
Phusion polymerase	0.3 µl
5x High Fidelity buffer	6 µl
ddH_2O	21.2 µl

PCR-Program:

	1	2	3	4	5	6
Temperature	98°C	98°C	variable	72°C	72°C	4°C
Time [min]	2:00	0:30	0:30	0:30	10:00	∞
		36x				

The PCR products (mixed with a dye) were loaded on a (depending on the size of the amplicon) 1% or 1.5% agarose gel together with an appropriate DNA ladder. The gel was run at 90V for about 45 minutes and specific products were cut out of the gel with a sterile scalpel and purified.

3.14.1.2. Elution of DNA from an agarose gel ("Freeze & Squeeze")

Gel pieces were frozen at -70°C for 10 min. or alternatively at -20°C o/n. For melting the gel, tubes were placed at 65°C for 5 minutes. With a yellow pipette tip the gel was squeezed and transferred into Ultrafree-MC centrifugal filter units with microporous

membrane (Millipore, Bedford, USA). The gel pieces were centrifuged for 20 min. at 8,000 rpm (Eppendorf 5415R), RT. DNA was contained in the eluate at the bottom afterwards. The volume of the eluate was estimated. For precipitation of DNA 1/10 of the volume of potassium acetate (3 M; pH 4.8) and the double of the volume of 100% ethanol were added. Tubes were placed at -20°C o/n (or alternatively at -70°C for 30 minutes). DNA got pelletized by centrifugation at 13,000 rpm and 4°C for 30 minutes. The pellet was washed with 600 µl of 70% ethanol and dried for max. 5 min. in the SpeedVac concentrator. Depending on its size the pellet was dissolved in 10 to 20 µl of ddH_2O. For determination of the concentration 1 µl of the resuspended DNA was loaded again on a 1% or 1.5% agarose gel together with a ladder designed for both DNA sizing and quantification.

3.14.2. Preparation of Northern blot probe II

New primers were designed (with Primer Designer, version 2.0) to amplify a piece of DNA of about 800 bp for higher specificity. Furthermore, EcoRI restriction sites were attached to the 5' end of the forward primer and the 3' end of the reverse primer to be able to clone the PCR product into a Bluescript vector to get a purified probe in a high copy number for Northern blotting.

First, PCR was run as described before. PCR products were purified from the gel again by the "Freeze and Squeeze" method and resuspended in 20 µl ddH_2O. As a control 1 µl of the DNA was loaded on an agarose gel as before. Next, insert (probe) and vector (pBluescript II SK+) were both digested with EcoRI.

3.14.2.1. Restriction digestion

Insert (30 µl)	**Vector (25 µl)**
19 µl cDNA	2 µl Blueskript
1 µl EcoRI	1 µl EcoRI
3 µl 10x EcoRI buffer	2.5 µl 10x EcoRI buffer
7 µl ddH_2O	19.5 µl ddH_2O

Insert and vector were digested for 2 hours at 37°C. The vector was additionally incubated with 1 µl of CIP at 37°C for half an hour. Calf intestinal phosphatase (CIP) inhibits the vector's religation by removal of the 5' phosphate groups.

Digested insert was filled up with ddH_2O to 100 µl and purified by a chloroform-phenol-extraction. First 75 µl $CHCl_3$ and then 100 µl phenol were added to the sample with mixing in between (vortex mixer). For phase separation the mix was centrifuged at 13,000

rpm (Eppendorf 5415R) for 5 min. at RT. 80 µl of the upper phase were mixed with 8 µl potassium acetate (3 M, pH 4.8) and 160 µl 100% ethanol and DNA was precipitated at -20°C o/n. The digested vector was loaded on a 1% agarose gel, cut out and eluted from the gel as described before and was also precipitated o/n. Both, vector and insert were pelletized the next day by centrifugation (see "Freeze and Squeeze") and dried pellets were dissolved in 15 µl ddH_2O. The resuspended pellets were desalted for half an hour by pipetting them onto mixed cellulose esters membrane discs (MF-Millipore™ Membrane Filters) which floated on the water surface of ddH_2O-filled Petri discs.

3.14.2.2. Ligation and transformation

1 µl of desalted vector and insert were loaded on an agarose gel (1%) to determine their concentration. 3 times as much insert as vector was used for the ligation. The appropriate volumes of insert and vector were mixed with 1 µl T4 ligase and 1.5 µl ligase buffer, filled up with water to a total volume of 15 µl and incubated for 2 hours at RT.
In the meantime, LB-agar plates were prepared. Therefore, LB-medium mixed with agar-agar was autoclaved. After cooling down, 1x ampicillin (1000x), 1x IPTG (2000x), and 1x X-Gal (2000x) were added and agar was poured into sterile Petri dishes.
For the transformation 5 µl ligation batch were added to 25 µl chemically competent E. coli (DH5T1R cells, Invitrogen) and put on ice for half an hour. Next the cells were heat-shocked at 42°C for 30 seconds and again cooled-down on ice. Then 200 µl of pre-warmed LB medium were added, the cells were transformed for 1 hour at 37°C and finally plated on the prepared Petri dishes. The plates were incubated o/n at 37°C (agar side on top).

3.14.2.3. Smale-scale preparation of plasmid DNA ("Mini prep")

Colonies having an insert were white since the multi-cloning side (MCS) of the Bluescript vector is inside the LacZ encoding sequence and insertion into the MCS disrupts this sequence. Each white colony was inoculated into 5 ml LB-Amp-medium and shaken at 37°C o/n. The overnight cultures were cooled on ice and centrifuged for 10 minutes at 3,500 rpm (Beckman GS-6R) and 4°C. The supernatant was removed, the pellets were carefully resuspended in 200 µl lysis buffer I and transferred into a 1.5 ml reaction tube. The resuspended cells were mixed with 200 µl freshly prepared lysis buffer II and incubated for 5 minutes at RT. After the addition of 150 µl 3 M potassium acetate, tubes were incubated at 4°C for 10 min. so that a white precipitate formed. For removal of the precipitate cells were centrifuged for 5 min. at 13,000 rpm (Eppendorf 5415R) and 4°C. The supernatant was moved into a new 1.5 ml reaction tube and extracted by addition of 400

µl phenol and 250 µl Sevac. For phase separation the tube was spun for 2 min. at 4°C and 13,000 rpm (5415R). The upper aqueous phase containing the DNA was transferred into another tube, mixed with 800 µl 100% EtOH and DNA was precipitated by incubation at -20°C for 30 min. The plasmids got pelletized by centrifugation at 13,000 rpm and 4°C for half an hour and pellets were washed with 400 µl 80% ethanol for 5 min. and 4°C at full speed (5415R). The supernatant was removed and pellets were dried in the Speed-vac. The pellets were dissolved in 48 µl ddH_2O mixed with 2 µl RNase (2.5 mg/ml) and incubated at 37°C for 15 minutes.

3.14.2.4. Control digest

For determination of positive clones, 3 µl of recovered plasmids were digested with Eco-RI as described previously and loaded on a 1 % agarose gel. For clones containing an insert, the remainder of the dissolved pellets was also digested with EcoRI, separated on an agarose gel, purified by the Freeze and Squeeze method and 15 ng were used for labeling with radioactivity.

3.14.3. Blot

3.14.3.1. Denaturing RNA agarose gel

RNA agarose gel and samples were prepared as described before. A bit of the agarose gel was kept at 55°C for later on. 10 µg of RNA mixed with the denaturing RNA dye were loaded on the gel. The gel was run for 1 and a half hour at 90V to get good separation of the RNA. Gel was checked under UV for RNA integrity and to see whether the same amount of RNA was loaded on the gel.

3.14.3.2. Blotting

After electrophoresis the agarose gel was placed into a plastic bowl and rinsed with ddH_2O for 20 to 30 minutes to get rid of the formaldehyde. After drying it (especially the slots), the slots were filled with the rest of the agarose gel. RNA was blotted on a membrane by vacuum blotting. Therefore, blotting paper was trimmed, layed in the vacuum blotter and dampened with 10xSSC. The blotting paper was covered with the nylon membrane (Hybond-N+; Amersham Biosciences) which was 1 cm longer and broader than the gel. Both, paper and membrane, were examined for and freed from airbubbles. Onto the membrane, a plastic foil was deposited which left open a cutout a bit smaller than the size of the gel. The gel was placed on the top and overlapped with the foil by about 1 cm. The vacuum pump was turned on (the under-pressure should not exceed 5 mm Hg), 1.5 l 10xSSC were added to the vacuum blotter and the gel was blotted o/n.

Next day, membrane was dried, trimmed and marked by cutting off the upper right corner. Blotted RNA was crosslinked with the membrane by UV-light in an ultraviolet crosslinker with 1200 kcal on the upper side and 600 kcal on the bottom side. The membrane was stored in a 50 ml tube with screw cap in the fridge at 4°C.

3.14.3.3. Labeling

For prehybridization, 1% BSA was added to an appropriate volume of the hybridization solution. For 50 ml tubes, 6 ml of prehybridization solution were needed. The plastic screw caps had to be punctured with a needle in the middle to prevent an elevated vapor pressure during heating. The plastic tubes were placed into hybridization glass tubes and incubated with the solution for 4 to 6 hours at 65°C in the hybridization oven (while permanently rotating). In the meantime the probes got labeled with ^{32}P.

For a small blot 15 ng of probe/DNA were used, filled up with water to 15 µl, denatured at 99°C for 5 min and immediately put on ice afterwards. Following reagents were added to the denatured cDNA for radioactive labeling:

Denatured probe + ddH_2O	**15 µl**
Nucleotide mix (CTG)	1 µl
10x BSA	1 µl
5x labeling buffer	5 µl
Klenow polymerase	0.5 µl
^{32}P-dATP	2.5 µl

The mix was incubated for 2 to 3 hours at room temperature. Then the probe was purified by size exclusion. Therefore a Pasteur pipette was plugged with glass wool and filled with Sephadex beads suspended in 1x TE-buffer. First the column got equilibrated with 500 µl 1x TE, then the probe was loaded on the column and washed off the column with 200 µl-fractions of 1x TE. Fractions were measured with a hand-held Geiger-Mueller counter to know which ones contained the probe. Labeled probes were eluted in the first peak. Loading of the column was continued until a second peak (containing the nucleotides) was measured. The 3 to 4 fractions that contained most of the radioactivity (from the first peak) were pooled, denatured for 5 min. at 99°C and cooled down on ice. The probe was added to the prehybridization solution and the blot was incubated o/n at 65°C in the rotating oven.

3.14.3.4. Washing and screening

Next day the hybridization solution was drained. The membrane was slewed in 2x SSC/0.1% SDS and washed for 20 to 30 min. in 1x SSC/0.1% SDS first and then in 0.5x

SSC/0.1% SDS by rotating again at 65°C in the hybridization oven. The membrane was layed on a paper towel and when being dry was wrapped in a cling film. A phosphor storage screen was exposed to the radioactivity on the membrane for at least 24 hours and imaged with the PhosphorImager (Storm860).

3.15. Analytical-chemical methods

Plasma free fatty acid composition

3.15.1. NEFA c kit (Wako)

For relative quantification of the free fatty acid – composition of the sera from *Atgl*$^{-/-}$ mice and wild type mice by GC-MS, a NEFA c kit was performed to determine the total amount of free fatty acids. This concentration then provided a reference for the quantitative analysis. The Wako enzymatic method uses the acylation of coenzyme A (CoA) by fatty acids in the presence of acyl-CoA synthetase (ACS). The produced acyl-CoA is then oxidized by acyl-CoA oxidase (ACOD) thereby generating hydrogen peroxide in the presence of peroxidase (POD). This enables the oxidative condensation of 3-methy-N-ethyl-N (β-hydroxyethyl)-aniline (MEFA) with 4-aminoantipyrine and forms a purple colored adduct which can be measured colorimetrically at 562 nm.

First, blood samples were centrifuged for 10 to 15 min. at 1,500-2,000xg and RT to separate the plasma from blood cells. Plasma partitioned in the upper phase, WBC in the interphase and RBC in the lower phase. Plasma was pipetted off and transferred to fresh reaction tubes. With the provided NEFA c kit standard solution a dilution series was prepared (concentrated - 1:2 – 1:4 – 1:8 – 1:16). 5 µl of every standard dilution and every sample were pipetted in duplicates into a 96 wells microplate. As blank measurement 5 µl ddH_2O were used instead. 150 µl of reagent #1 were added to the wells and plate was incubated for 10 min. at 37°C. Next, 75 µl of reagent #2 were added and again incubated for 10min. at 37°C. The absorbance was measured in a spectral photometer at 562 nm. To determine the concentration of NEFA in the plasma samples a standard calibration line was created with the known concentrations of the standard dilutions and the according measured absorbancies.

c (standard solution) = 28.2 mg/dl

conversion factor: $mg/dl \times 0.035 = mmol/l$

For further analysis equal quantities of NEFA were used (e.g. 10 µg NEFA = x µl sample) and were adjusted to 200 µl with ddH_2O.

3.15.2. Lipid extraction (acidic Folch)

For the extraction procedure it is very important to use clean PYREX® glass tubes since chloroform is able to degrade some types of plastics. Before using the tubes they were cleaned in the dishwasher and rinsed with $CHCl_3$ and ether or methanol to get rid of any disturbing substances that could interfere with the mass spectrometric analysis.

3.15.2.1. Lipid extraction of plasma

Every plasma sample was mixed with 1 ml of the acidic Folch reagent. For quantification, 45 µl of an internal standard solution (C17:0) were added per ml Folch solution. The samples were vortexed vigorously (to get bigger volumes for easier separation one could have added another ml of the Folch solution and vortexed again). 350 µl of ddH_2O were added and tubes were centrifuged for 15 min. at RT and 2,200 rpm (Beckman GS-6R). The upper aqueous phase and the proteins (white interphase) were removed. Once again the samples were vortexed and centrifuged for about 5 min. at 2,200rpm to remove remaining water drops. Finally, the organic phase was evaporated with N_2 at about 40°C. The lipid "pellets" were dissolved in 500 µl $CHCl_3$: MeOH (2:1) and transferred into amber glass vials. Lipids were ready then for measurement with HPLC-MS. For GC-MS, free fatty acids had to be silylated.

3.15.2.2. Silylation

Silylation is the introduction of a silyl group (R_3Si–) to a molecule so that functional groups which present a problem in gas chromatographic separation can be derivatized by silylating reagents. In our specific case, it was the replacement of acidic hydrogens in free fatty acids with the alkylsilyl group trimethylsilyl (-$SiMe_3$). N,O-Bis(trimethylsilyl)trifluoroacetamide (BSTFA) thereby served as trimethylsilyl donor. Thereby, the derivatives become generally less polar, more volatile and more thermally stable.

The samples were again evaporated with N_2 for at least 1 hour at about 40°C (samples had to be completely dry for further silylation). 50 µl BSTFA and 100 µl pyridine were added. Samples were vortexed until everything had completely dissolved and finally were transferred into a pointed glass insert/plastic outside vial for GC-MS-measurements.

3.15.2.3. Lipid extraction of tissue

Generally, lipid extraction from tissues follows the same principle as for plasma. Again, clean glass tubes were prepared. First, 1.5 ml MeOH were pipetted into the glass tubes. Liver, heart, and brain samples were weighed and added to the methanol. Tissue was homogenized with an ultra turrax. Homogenate was mixed with 3 ml $CHCl_3$ and 45 µl glacial acetic acid (1%). This mixture was rotated on a rotating wheel (Labinco) at RT for 2 to 3 hours. 1 ml HSL buffer containing 1% PI was added to every tube. Samples were centrifuged for 15 min. at 3,500 rpm (Beckman GS-6) and RT. The lower organic phase was soaked up with a Pasteur pipette and transferred into a new glass tube. The upper aqueous phase was disposed. The protein pellets of the interphase were dried under the fume hood. The organic phase was again evaporated with N_2 for about 1 hour at 40°C. Lipids were - depending on the approximate amount – dissolved in 100 to 500 µl of a $CHCl_3$:MeOH (2:1) mixture and transferred into amber glass vials for HPLC-MS measurements.

3.15.3. Protein determination

Protein determination of tissue samples was needed as a reference for quantification and comparison of lipid species among various samples. First, dried tissue/protein pellet was lysed in an appropriate volume of lysis solution composed of 0.3 M NaOH and 0.1% SDS. Therefore, samples were shaken in a water bath at 56°C over night.

Proteins were quantified by using the BCA protein assay kit (Thermo Scientific). In this assay, Cu^{2+} ions are reduced in an alkaline medium by proteins to Cu^{+} and form blue-colored chelate complexes with the proteins. BCA in a second step forms a purple colored adduct with the produced Cu^{+} ions which absorbs light at 562 nm. The BCA reagent (blue) first had to be diluted 1:50 with provided reagent 2 (white). With a protein standard (BSA; 2 mg/ml; Thermo Scientific) a dilution series (1 mg/ml – 0.75 mg/ml – 0.5 mg/ml – 0.25 mg/ml – 0.125 mg/ml – 0.0625 mg/ml - blank) was created. The protein standard was diluted with the lysis solution which also served as blank. One sample per tissue was used for preparation of three different dilutions (1:10, 1:25, 1:50) to find out which one had a protein concentration in the linear range of the straight calibration line. 10 µl of the standard and sample dilutions were pipetted into a 96 well microplate and 200 µl of the prepared BCA reagent were added. The plate was incubated at 37°C for half an hour. Absorbances were measured in a spectral photometer at 562 nm. A standard calibration line was created with the standard dilutions and protein concentration of tissue samples were determined with the linear equation (y=kx+d).

3.15.4. HPLC-MS

Phospholipids were analysed by tandem mass spectrometry. Samples dissolved in $CHCl_3$:MeOH (2:1) were further diluted and 4 µl were injected into the Accela ultra HPLC system (Thermo Scientific). The various lipids were separated by their different retention times in the HPLC system due to interactions with the C18-tails of the column. C18 columns with a hydrophobic alkyl phase are very retentive and give good separation over a broad spectrum. The C18 reversed phase Thermo Hypersil GOLD column, 100x1mm (0.9 µm), was operated at 50°C. As solvent A we used water (Millipore) and solvent B was acetonitrile/isopropanol (5:2, v/v). Both solvents contained 1% NH_4Ac (1 M aqueous solution) and 0.1% formic acid. For the gradient we started with 35% solvent B, increased to 70% in the first 4 minutes, reached 100% during the next 16.5 min. and stayed at 100% for 9.5 min. After each run, the column was equilibrated at starting conditions. The flow rate through the column was settled at 0.250 ml/min. Molecules were ionized by electrospray ionization (ESI) in the positive mode with a voltage of 4000 V. Thereby, stable MH+ ions were generated. By the electrospray ionization method all solvents were removed so that the ions could be injected into the high vacuum of the mass spectrometer.

Phospholipid species were detected by a triple quadrupole system (Quantum TSQ) from Thermo Scientific. A quadrupole is composed of four rods to which direct and alternating voltage can be applied at the same time. The two opposing rods always have the same phase and polarity. Through permanent changes of the electric field, ions start to oscillate in dependence of their m/z-ratio. The quadrupole is programmed in a way so that only ions of a certain m/z-ratio have a stable flight path through the detector. In the first quadrupole (Q1), the mass/charge-ratio of all incoming positively charged molecules is detected sequentially (full scan). In the collision cell (Q2) ions are fragmented by collision with gas molecules. The last quadrupole (Q3) is scanning again the mass/charge ratio.

For the detection of phosphatidylcholine, a precursor ion scan was done. In this case, Q1 scanned all m/z ratios and sequentially transferred the ions into Q2 where they were fragmented. In Q3 only these fragments with a specific m/z-ratio could pass to the detector. These specific fragments with a m/z-ratio of 184.1 represent the polar head group of phosphatidylcholine. If the detector measured ions, the m/z-ratio of the precursor was recorded. Argon was used as collision gas with an energy of 30 V and a collision gas pressure of 0.7 mTorr.

In the case of phosphatidylethanolamine, a neutral loss scan (loss of the uncharged head group of PE) was applied. Q1 did again a full scan as before, ions were fragmented in Q2 and this time Q3 scanned for the specific loss of the neutral head group of PE. The

neutral loss scan was done for a m/z-ratio of 141.0. This means that the mass detector was recording ions only in the case of this specific mass difference. Argon collision energy was 25 V this time with gas pressure remaining unchanged.
C24:0 (12:0/12:0, Avanti Polar Lipids Inc.) PC and PE were added as internal standards. Data were processed with the software Excalibur and peak areas were related to the internal standards.

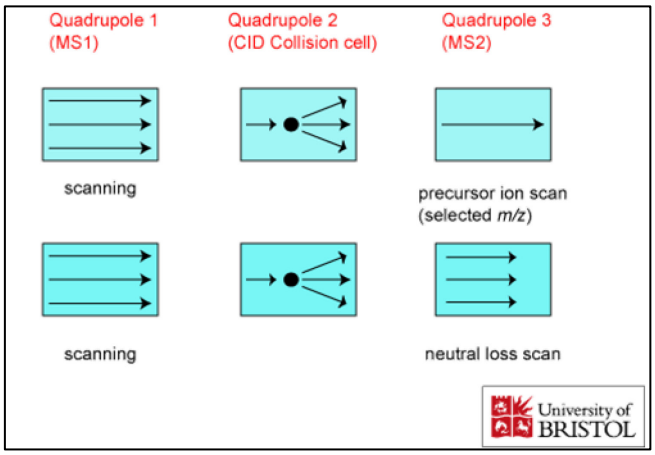

FIGURE 3.15.1. **Illustration of precursor ion scan and neutral loss scan by tandem MS** (source: (103))**.**

3.15.5. GC-MS

Free fatty acids were measured by GC-MS overnight.
The GC-MS is composed of two major building blocks: the gas chromatograph and the mass spectrometer. A difference in the chemical properties of the various fatty acids separates them as they travel the length of the column. The fatty acids need different amounts of time (retention time) to elute from the gas chromatograph and therefore reach the mass spectrometer consecutively. This allows the mass spectrometer to capture and detect the ionized molecules separately. Each fatty acid is broken into ionized fragments and detected using its mass to charge ratio in a full scan mode.

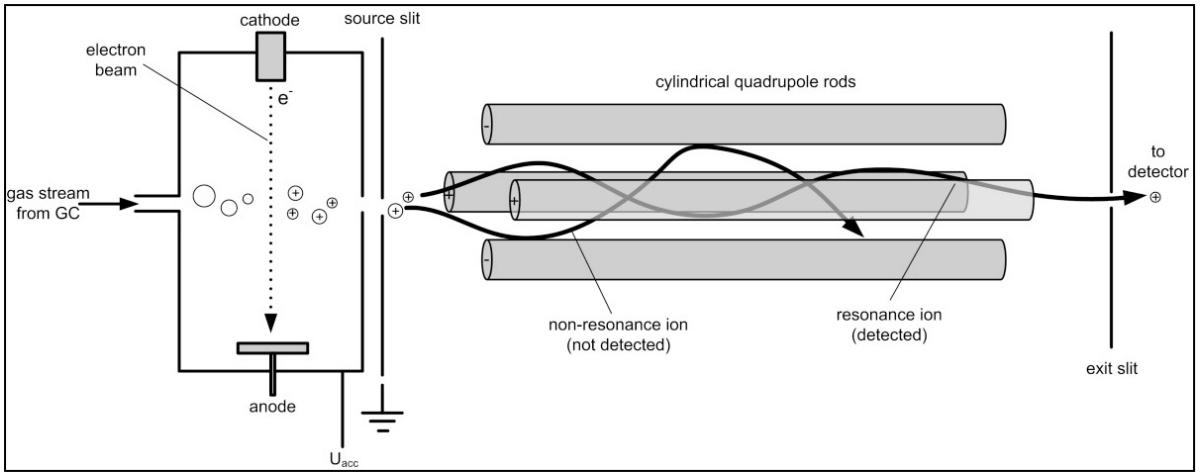

FIGURE 3.15.2. **Schematic representation of the quadrupole MS system** (image source: (104)**).**

A Thermo Trace GC ultra coupled to a Thermo DSQ quadrupole MS (ThermoElectron, Waltham, MA; USA) was used. The GC was fitted with a HP–5MS fused-silica capillary column (30 m x 0.25 mm (0.25 µm)). Helium was used as a carrier gas at a constant flow-rate of 1.5/1.0 ml/min. Initial column temperature was 110°C for 4 min, followed by an increase of 20°C/min to 300°C and an isothermal hold of 10 min. The mass spectrometer transfer line was kept at 310°C. Positive electron ionization (EI) was performed at an electron energy of 70 eV and an emission current of 0.150 A. Identity of analytes was verified in full-scan-mode. Data were again processed with Excalibur.

3.16. Statistical analysis

The results were expressed as a mean ± standard error of the mean for each group. Comparisons between groups were made by unpaired two-tailed Student's t-test. p values of <0.05 were considered statistically significant.

- $p < 0,05$ - *
- $0,05 > p > 0,001$ - **
- $0,001 > p$ - ***

4. Results

4.1. RNA experiments

4.1.1. Real-time PCR pretests

4.1.1.1. Primer test run

The actual real-time PCR measurements aimed at comparing mRNA levels of the four selected DHA-synthesizing enzymes (FADS1, FADS2, ELOVL2, 17β-HSD4) in wild type and *Atgl*$^{-/-}$ mice to determine whether ATGL deficiency had an impact on the expression of the enzymes. However, several preliminary tests had to be done in advance to ensure correct measurements and relevant results. First, the primer concentration resulting in a sufficient amplification of the respective cDNA had to be identified separately for every enzyme. Therefore, a preliminary real-time PCR was performed with varying primer concentrations and using a WT liver cDNA sample as template. The PCR products were loaded on a 1.5% agarose gel to identify the minimal quantity of primers required for sufficient amplification.

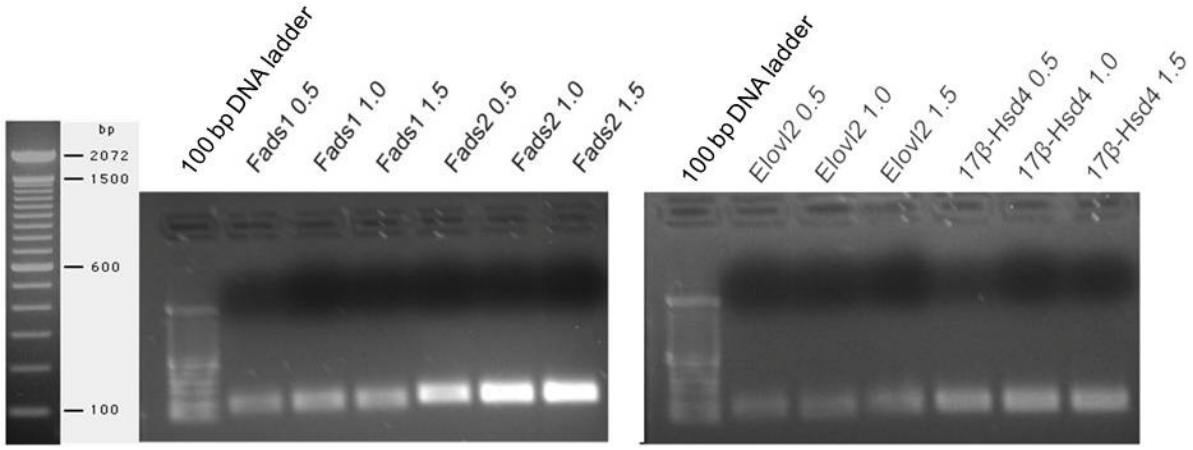

FIGURE 4.1.1. **Primer concentration test for real-time PCR.** Primer test real-time PCR was performed using a wild type liver cDNA sample and different volumes of the four primer pairs. One real-time PCR batch (20 µl) of each triplicate from the primer test run was loaded on a 1.5% agarose gel that was run at 100 V for 20 min. Obtained products were in line with estimated amplicon sizes. 100 bp DNA ladder depicted on the left was purchased from Invitrogen. *Fads1*, 110 bp; *Fads2*, 150 bp; *Elovl2*, 102 bp; *17β-Hsd4*, 112 bp. 0.5/1.0/1.5 stands for 0.5 µl/1.0 µl/1.5 µl of forward and reverse primer tested.

Based on the amount of product obtained for the different primer concentrations by real-time PCR (Fig.4.1.1), it was determined that 1 µl of forward and reverse primer was sufficient for good amplification of *Fads1* (Δ5-desaturase; 110 bp) and *17β-Hsd4* (peroxisomal β-oxidation enzyme; 112 bp); 1.5 µl were needed for *Elovl2* (elongase; 102 bp). It was found that the primers for copying part of the *Fads2* gene (Δ6-desaturase; 150 bp) bind better to the cDNA than the other primers and/or had more template to copy as they resulted in the highest quantity of product. That's why 0.5 µl of forward and reverse pri-

mer were applied for further measurements involving *Fads2* amplification. As *Fads2* presented the longest amplicon and *Elovl2* the shortest, the possibility that the varying signal intensities also could – at least partly – result from the different amplicon sizes was also taken into account. Additionally, the melt curves obtained for the four primer pairs were checked for primer dimers or unspecific product peaks.

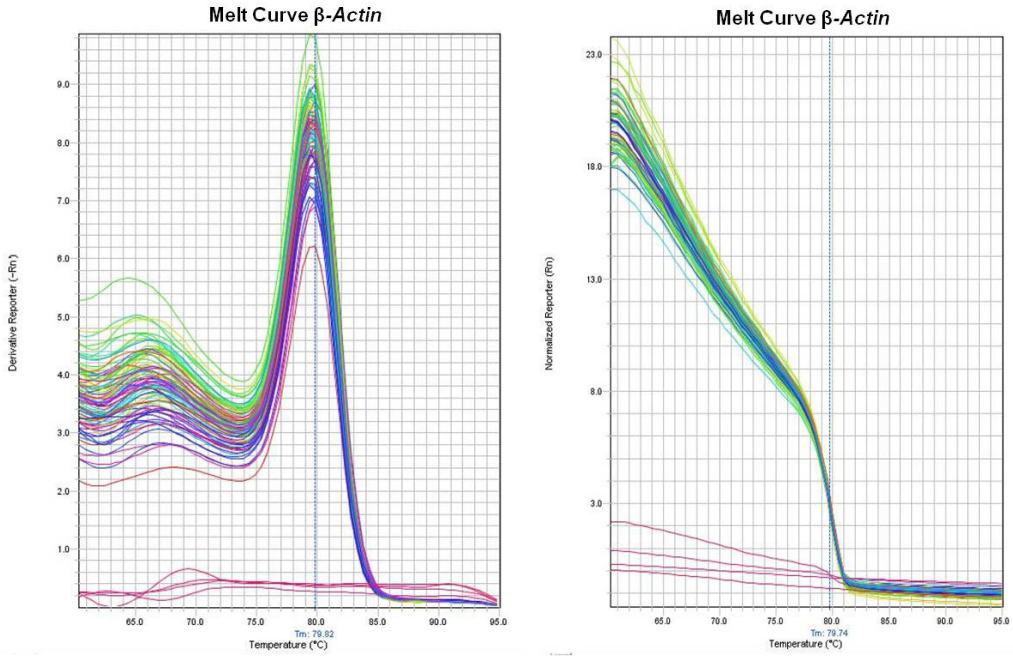

FIGURE 4.1.2. **Melt curves of *β-Actin*.** Verification of the absence of primer dimers and/or contamination by DNA. The pink lines at the bottom represent blank measurements with either water or RT-minus probe which should not result in melt curve peaks.

In case of primer dimers and/or unspecific amplification, a second melt curve peak would have been observed at a different melting temperature. Since blank measurements did not produce melt curve peaks, the absence of primer dimers and DNA contaminations was established (Fig. 4.1.2). All four primer pairs were specifically binding only to the genes of interest, not to other sequences or to one another. The small "peak" in the left graph (Fig. 4.1.2) could be explained by the configuration of the automatic graphical analysis of the real-time PCR machine. According to the manufacturer the analysis results are valid as long as in the second graph type (right) no further melting temperatures are obtained. These verifications by melt curve analysis were repeated for every single real-time PCR measurement.

4.1.1.2. Cycle Sequencing

The remaining two PCR batches from the primer test run were used for a sequencing reaction to confirm once more that the primers designed for real-time PCR were specifically amplifying the genes of interest. Usually purified or plasmid DNA is used for cycle

sequencing. Nevertheless, the real-time PCR products were sequenced although they still contained residual cDNA template, SYBR Green mastermix and primers which were not used up.

Four sequencing reactions were prepared for every gene, two with the respective forward primers and two with the reverse primers.

Fads1

Sequences producing significant alignments:

Transcripts	
Accession	Description
NM_146094.1	Mus musculus fatty acid desaturase 1 (Fads1), mRNA

QUERY 1 (Score: 84.2; E-value: 1e-14)

```
Query 1   CAAATACCTCTNCCTCNTCGGACCCCCNNCNNTCGCNGCCTCNNANACTTCCAGTGGTNC  60
          ||| ||| ||| |||| ||||||||||  |  | || |||||  | ||||||||||||
Sbjct 877 CAAGTACTTCTTCCTCATCGGACCCCCAGCCTT-GCTGCCTCT-ATACTTCCAGTGGTAT 934

Query  61   CTTTTCTNTTTTGTGGTTCAGCGGTAAAAA  90
             |||||| |||||||||||||||| |||||
Sbjct  935  ATTTTCTATTTTGTGGTTCAGCGGAAAAAA  964
```

Fads2

Sequences producing significant alignments:

Transcripts	
Accession	Description
NM_019699.1	Mus musculus fatty acid desaturase 2 (Fads2), mRNA

QUERY1 (Score: 194; E-value: 2e-47)

```
Query 1   CCGNGCGCCAGGCTCCGTTNCNNTCCTTCCGTTGGGAGGAGATTCAGANGCACAACCTGC 60
          ||| |||||||||||||| | |   |||||||||||||||||||||||| ||||||||||
Sbjct 109 CCGAGCGCCAGGCTCCGATGCCCACCTTCCGTTGGGAGGAGATTCAGAAGCACAACCTGC 168

Query 61  GCACCGACCGGTGGCTCGTCATCGACCGCAAGGTCTACAACGTTACCAAATGGTCCCAGC 120
          ||||||||||||||||||||||||||||||||||||||||||||||||||||||||||||
Sbjct 169 GCACCGACCGGTGGCTCGTCATCGACCGCAAGGTCTACAACGTTACCAAATGGTCCCAGC 228

Query  121  GG  122
             ||
Sbjct  229  GG  230
```

QUERY2 (Score: 201; E-value: 1e-49)

```
Query 1   CCGAGCGCCNGGCTCCGTTNCCNNCCTTCCGTTGGGAGGAGATTCAGAAGCACAACCTGC  60
          ||||||||| ||||||| | ||  ||||||||||||||||||||||||||||||||||||
Sbjct 109 CCGAGCGCCAGGCTCCGATGCCCACCTTCCGTTGGGAGGAGATTCAGAAGCACAACCTGC 168

Query 61  GCACCGACCGGTGGCTCGTCATCGACCGCAAGGTCTACAACGTTACCAAATGGTCCCAGC 120
          ||||||||||||||||||||||||||||||||||||||||||||||||||||||||||||
Sbjct 169 GCACCGACCGGTGGCTCGTCATCGACCGCAAGGTCTACAACGTTACCAAATGGTCCCAGC 228

Query  121  GG  122
             ||
Sbjct  229  GG  230
```

QUERY3 (Score: 145; E-value: 6e-33)

```
Query 18  GTTGTGCTTCTGAATCTCCTCCCAACGGAAGGTGGGCATCGGAGCCTGGCGCTCGGTGCT  77
          ||||||||||||||||||||||||||||||||||||||||||||||||||||||||||||
Sbjct 164 GTTGTGCTTCTGAATCTCCTCCCAACGGAAGGTGGGCATCGGAGCCTGGCGCTCGGTGCT 105

Query  78   CCCCTCTCCCTGGGTTACCTCCCTT  102
             |||||||||| ||||||||||||
Sbjct  104  CCCCTCTCCCT-GGTTACCTCCCTT  81
```

Elovl2

Sequences producing significant alignments:

Transcripts

Accession	**Description**
NM_019423.1	Mus musculus elongation of very long chain fatty acids (FEN1/Elo2, SUR4/Elo3, yeast)-like 2 (Elovl2), mRNA

QUERY1 (Score: 68; E-value: 9e-10)

```
Query 14   GCTTCTTNGGGCTTCCCCTGGAACGGCTTTATCCACATTCTCATGGTACTCCTACTACGG  73
           ||||||| || |   ||||| ||| |||||||||||||||||| ||||||||||||| |
Sbjct 542 GCTTCTTTGGACCCACCCTG-AACAGCTTTATCCACATTCTCAT-GTACTCCTACTAC-G 598

Query  74   GCCTG  78
             |||||
Sbjct  599  GCCTG  603
```

QUERY2 (Score: 59; E-value: 5e-07)

```
Query 10   AAGGTGTTCNGGGTGNNNTCAAGGAGGTTTNGACCACANGTTTTNCAGGTCCAAACACAC  69
           ||| ||||| |||||    ||| || | || ||||||| | | | ||| || ||||||||
Sbjct 569 AAGCTGTTCAGGGTGGGTCCAAAGAAGCTTTGACCACAAGGTATCCAGTTCAAAACACAC 510

Query  70   CACCAGATG  78
             |||||||||
Sbjct  509  CACCAGATG  501
```

17β-Hsd4

Sequences producing significant alignments:

Transcripts

Accession	Description
NM_008292.2	Mus musculus hydroxysteroid (17-beta) dehydrogenase 4 (Hsd17b4), mRNA

QUERY1 (Score: 68; E-value: 1e-09)

```
Query  41   AAGAAAGGGAAAGGGCGGAAAAAGCAGTGGCCAATTTACGATTCAGTTGAAGCAGGC  97
            |||||  ||||||| ||||||| |||||||||||| ||||||||||||||||||||
Sbjct  210  AAGAA--GGAAAGG-CGGAAAA-GCAGTGGCCAATT-ACGATTCAGTTGAAGCAGGC  261
```

QUERY2 (Score: 51.8; E-value:7e-05)

```
Query 9    TCTGCCACAACCTTGGTCTGGCAGGCTGGAGGAAGCCTTTACCAATTACCCTTGGAAAGT 68
           |||||||||||||| |||| ||||     |||| |||||||||||| ||||||   ||||
Sbjct 206 TCTGCCACAACCTT-GTCT-GCAG--CAGAGG-AGCCTTTACCAATT-CCCTTG--AAGT 155

Query  69   CCCC  72
             ||||
Sbjct  154  CCCC  151
```

QUERY3 (Score: 93.3; E-value: 3e-17)

```
Query 4    CTGCTTTTCNGCCTTTCCTTNTCNNC-CTGCCANAACCTTGTCTGCAGCTGCAGGAAGCC  62
           ||||||||| |||||||||| |    | |||||| |||||||||||||| | ||| ||||
Sbjct 232 CTGCTTTTCCGCCTTTCCTTCTTATCTCTGCCACAACCTTGTCTGCAGCAG-AGG-AGCC 175

Query  63   TTTACCNATTTCCCTTGAAGTCCCCT  88
             |||||| | ||||||||||||||||
Sbjct  174  TTTACCAA-TTCCCTTGAAGTCCCCT  150
```

FIGURE 4.1.3. **Results from the cycle sequencing reactions.** The sequences obtained from cycle sequencing were blasted against the mouse genome by using the nucleotide blast program (NCBI). Query, sequence obtained from cycle sequencing; Sbjct, aligned sequence from mouse genome. Score: similarity of two sequences over a range (dependant on the search parameters). E-value: probability of the score being generated by chance (dependant on the size of the database and the length of the hit).

The least exploitable sequencing reaction occurred for FADS1 where only one useable result was obtained with the forward primer. However, by blasting the sequence against the mouse genome (mus musculus; taxid: 10090) the one significant alignment that was found was for (mRNA) *Fads1*. In case of FADS2, three of the four reactions provided results whereas two of the four contained the forward primer. These two sequences were

almost identical. Again, significant alignments were produced only for the expected transcript. For ELOVL2, two sequences resulted in significant and correct alignments, one starting from the forward and one starting from the reverse primer. Nevertheless, the coverage was worse for ELOVL2 than for all other enzymes. For 17β-HSD4, two reactions containing the reverse primers and one reaction containing the forward primer produced sequences aligning with the expected mRNA. To sum up, all 4 primer pairs amplified the correct target sequences and were therefore specifically binding to the expected transcripts.

4.1.1.3. PCR-efficiency

For all four target genes and the housekeeping gene the cycle threshold with the ideal correlation between different amounts of cDNA used and fluorescence signal emitted had to be determined. Furthermore it had to be established which dilutions of cDNA samples would result in a Ct value of about 20 to maximum 25 at this cycle threshold. This test run was done with a pool including all samples. Of course it would have been preferable to test the samples separately but that wasn't reasonably practicable considering the time and/or costs involved. With the pooled samples, dilutions were prepared at ratios of 1:5 (10 ng(cDNA)/µl), 1:25 (2 ng/µl), 1:125 (0.4 ng/µl) and 1:625 (0.08 ng/µl) and Ct-values were determined for all genes by real-time PCR.

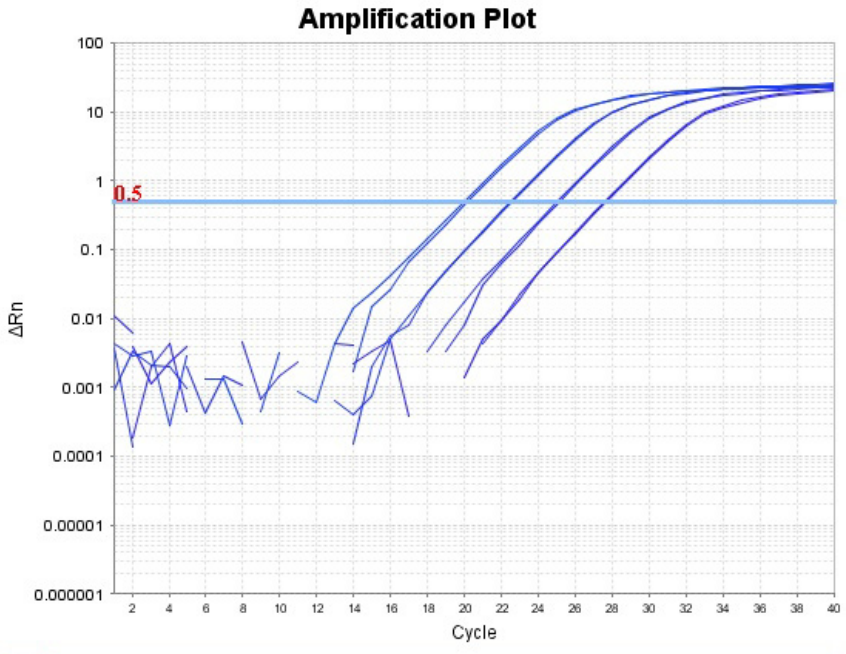

FIGURE 4.1.4. ***β-Actin* amplification plots of standard dilutions.** The higher the dilution ratio of the duplicates of the four standard dilutions the higher the threshold Ct-values. For perfect logarithmic amplification, Ct-values should be two cycles apart. The greater difference between the Ct-values in the graph above indicates that the PCR-reaction was not a 100% efficient. Cycle threshold set at 0.5 resulted in the best-fitting correlation (R^2) and slope (k) of the linear trend line. ΔRn, magnitude of normalized fluorescence.

The target genes' Ct-values were plotted on the y-axis against the logarithm of the respective amount of cDNA on the x-axis (Fig. 4.1.5). The correlation coefficient (R^2) that resulted from the linear trend line had to be at least 0.997.

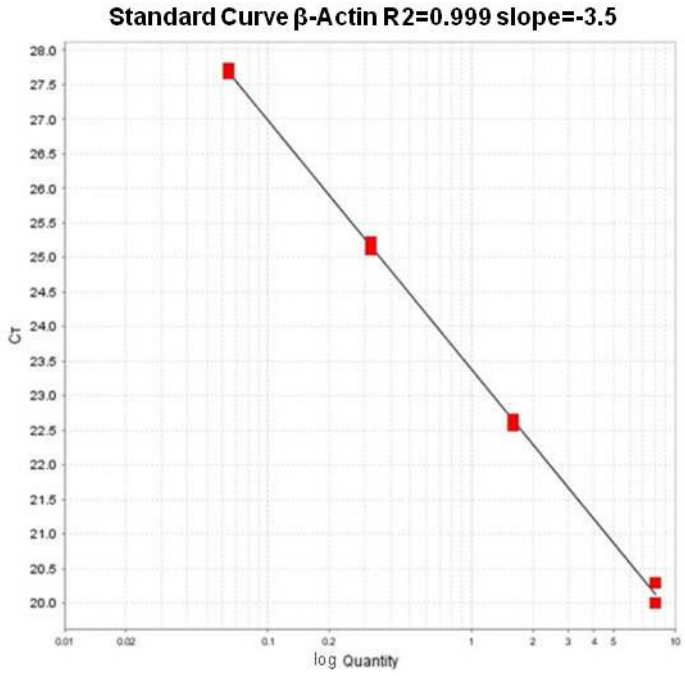

FIGURE 4.1.5. **Real-time PCR standard curve for *β-actin*.** This is the standard curve (linear trend line) resulting from the Ct-values at a cycle threshold of 0.5 on the y-axis plotted against the logarithmic quantity of cDNA used on the x-axis. The coefficient of determination (R^2) of almost 1 indicates a good correlation between the four dilutions. The slope of -3.5 shows that the PCR reaction efficiency was below 100%.

The PCR efficiency was tested for the housekeeping gene and the four target genes: the dilutions V1 and V2 resulted in threshold Ct-values between 20 and 25. For all further runs the V2 dilution was used in order to use as little cDNA as possible.

Concerning the PCR efficiency, some standard curve slopes were more positive than -3.32. This was most likely due to pipetting problems as it can be assumed that sample quality was acceptable since RNA quality was checked on an agarose gel. Most of the standard curves were more negative than -3.32. Accordingly, the PCR efficiency was not exactly 100% which is not unusual.

The blank measurements were negative.

In the following (4.1.2 – 4.1.5), the terms 'mRNA levels' and 'expression' stand for relative quantification (as opposed to absolute quantification). Relative quantification means that real-time PCR measurements do not result in absolute mRNA copy numbers. Instead, the values obtained are relative to the expression levels of a housekeeping gene (β-Actin) (Materials and Methods, p.30).

4.1.2. Fed mice

In the first actual real-time PCR measurements the expression of the selected DHA-synthesizing enzymes (FADS1, FADS2, ELOVL2, 17β-HSD4) in mice deficient for ATGL was compared with the expression in wild type mice.

Liver and heart of *Atgl*$^{-/-}$ and WT littermates were dissected. RNA was isolated using the TRIzol reagent (Invitrogen), the RNA concentration was measured with Nanodrop and its quality was checked on a 1% denaturing RNA agarose gel.

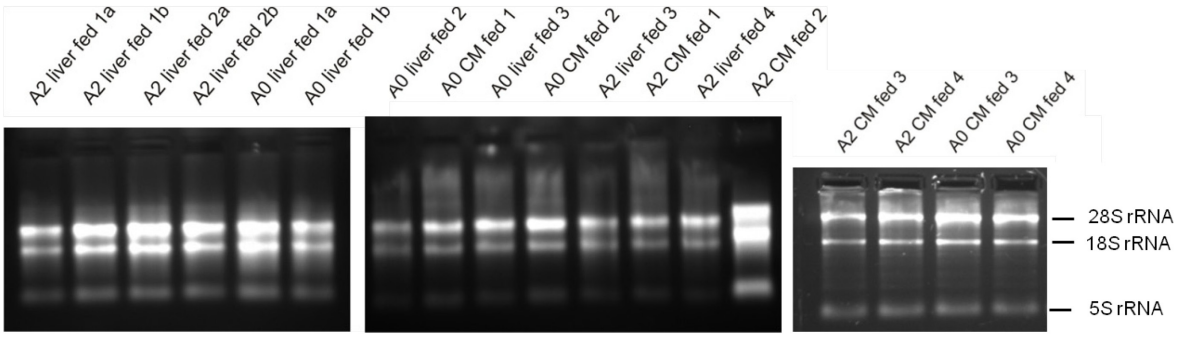

FIGURE 4.1.6. **RNA agarose gel**. RNA was isolated from liver and heart of fed mice. 5 µg RNA were loaded on a 1% RNA agarose gel and separated at 90 V for 20 min. A2, wild type; A0, *Atgl*$^{-/-}$; CM, cardiac muscle/myocytes; rRNA, ribosomal RNA.

RNA quality looked good as all three ribosomal RNA bands (28S rRNA, 18S rRNA, 5S rRNA) were detectable (Fig.4.1.6) and no smear was visible. RNA quality is highest if the 28S rRNA band is approximately twice as intense as the 18S rRNA band. This was the case for most of the RNA samples shown in figure 22 above.

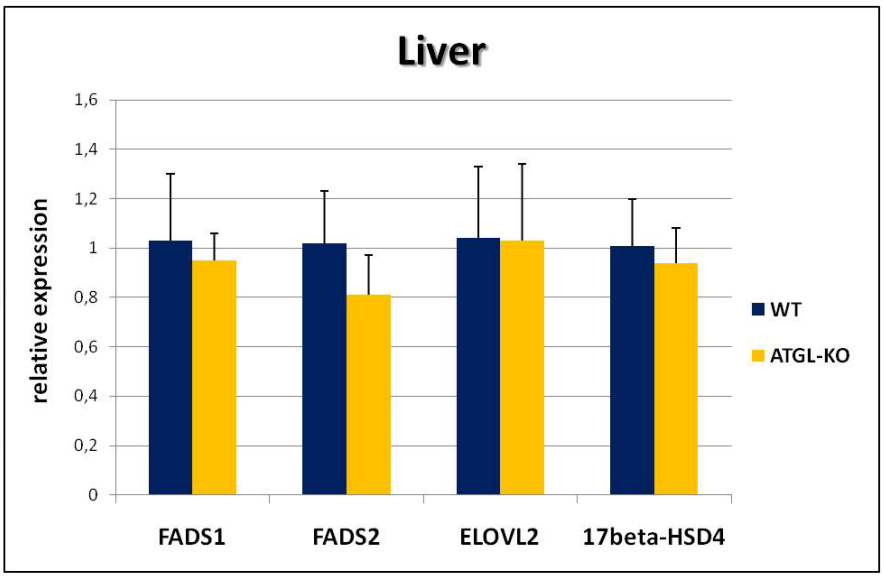

FIGURE 4.1.7. **Relative hepatic expression levels**. Reverse transcribed mRNA isolated from the liver of ATGL$^{-/-}$ and wild type mice was submitted to real-time PCR measurements of the four target enzymes. WT, wild type; KO, knockout. Data are means ± S.D. (n=7). Statistical significance was determined by the two-tailed Student's *t* test (*, $p<0.05$; **, $p<0.01$; ***, $p<0.001$).

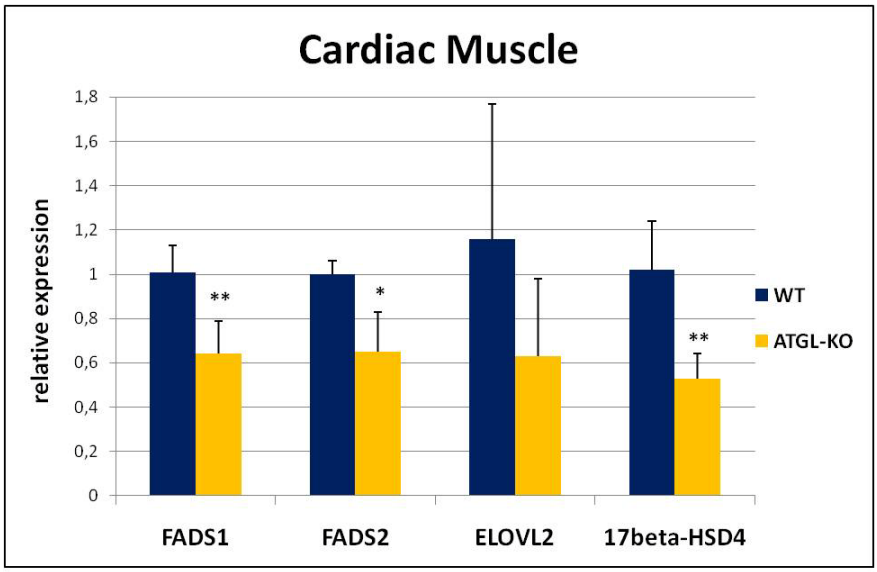

FIGURE 4.1.8. **Relative target gene mRNA levels in the heart**. Real-time PCR results from samples of wild type and ATGL-knockout hearts. WT, wild type; KO, knockout. Data are means ± S.D. (n=7). Statistical significance was determined by the two-tailed Student's *t* test (*, p<0.05; **, p<0.01; ***, p<0.001).

RNA isolated from liver and heart of fed *Atgl*$^{-/-}$ and WT mice was reverse transcribed and used to determine relative expression levels of selected enzymes involved in the DHA biosynthesis pathway. In the liver, expression levels were the same for KO and WT mice (Fig.4.1.7). mRNA levels were however downregulated in the heart of KO mice. This reduction was significant for all genes except for *Elovl2* (although this might be due to the high standard deviation) (Fig.4.1.8). FADS1 and FADS2 mRNA levels were reduced by 37% and 35%, respectively, ELOVL2 and 17β-HSD4 expression was decreased by 46% and/or 48%. The results suggested an involvement of ATGL in DHA biosynthesis in fed mice only in the cardiac muscle. Since there were no obvious differences in the fed liver at transcriptional level and since many hepatic lipogenic pathways are regulated by the nutritional status, enzyme expression was investigated in fasted mice.

4.1.3. Fasted mice

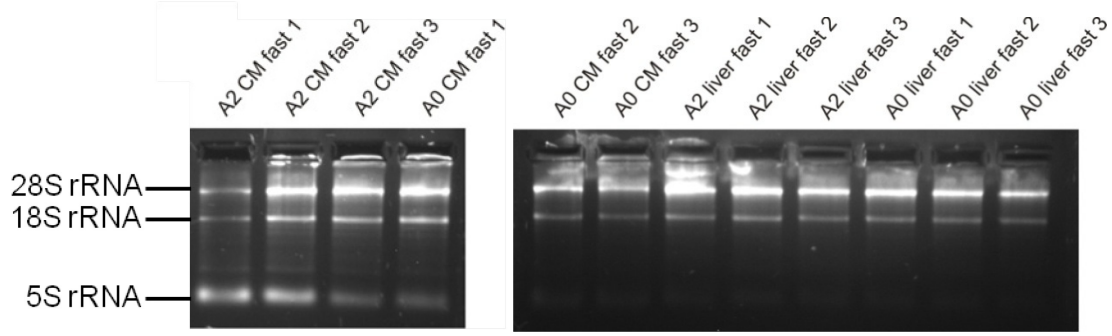

FIGURE 4.1.9. **RNA isolated from fasted mice.** Liver and heart were dissected from o/n (12h) fasted wild type and *Atgl*$^{-/-}$ mice. RNA was isolated and 5 µg were loaded on a 1% denaturing RNA agarose gel. The gel was run at 90 V for 20 min. rRNA, ribosomal RNA; A2, wild type; A0, *Atgl*$^{-/-}$; CM, cardiac muscle; fast, fasted.

On the picture at the right (Fig.4.1.9), the 5S rRNA band was very weak but 28S rRNA and 18S rRNA bands are far more relevant for RNA quality. As the 28S rRNA band was more intense than the 18S rRNA band the RNA quality was high.

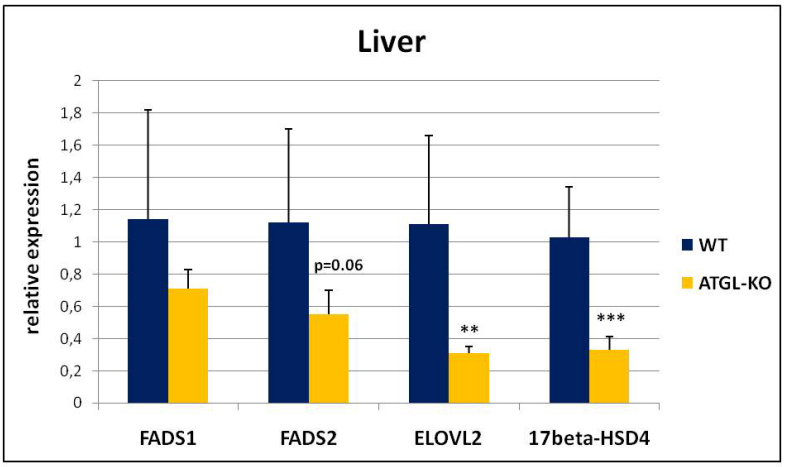

FIGURE 4.1.10. **Real-time PCR results from liver of fasted mice**. Relative expression levels of FADS1/2, ELOVL2 and 17β-HSD4 in the liver of over night fasted mice. WT, wild type; KO, knockout. Data are means ± S.D. (n=4/6 (WT/KO)). Statistical significance was determined by the two-tailed Student's *t* test (*, p<0.05; **, p<0.01; ***, p<0.001).

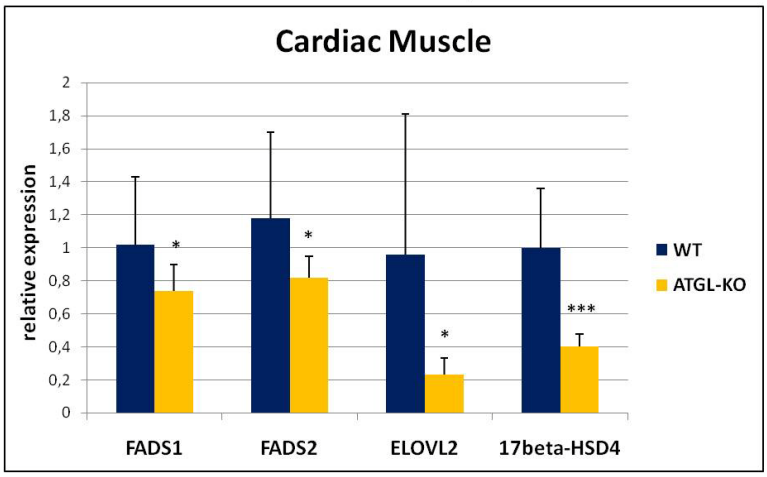

FIGURE 4.1.11. **Relative expression in cardiac muscle of o/n fasted mice.** WT, wild type; KO, knockout. Data are means ± S.D. (n=7). Statistical significance was determined by the two-tailed Student's *t* test (*, p<0.05; **, p<0.01; ***, p<0.001).

As expected the results for fasted mice were different. On transcriptional level a more or less pronounced downregulation of the enzymes was detected in the liver of knockout mice compared to wild type (Fig. 4.1.10). For FADS1 and FADS2 this downregulation was not significant, probably due to the high standard deviations. Nevertheless, the expression of FADS1 was reduced by 36%, of FADS2 by 53%. ELOVL2 mRNA levels were significantly decreased by almost 73% and 17β-HSD4 expression was only ⅓ (31%) of wild type levels. In the heart we obtained similar results as before except for ELOVL2. Reduction of ELOVL2 expression by 76% in knockout mice compared to wild type mice not only was significant but also more pronounced this time (Fig. 4.1.11). These observations supported the notion that ATGL has a putative function in DHA synthesis but is differently regulated in liver and heart.

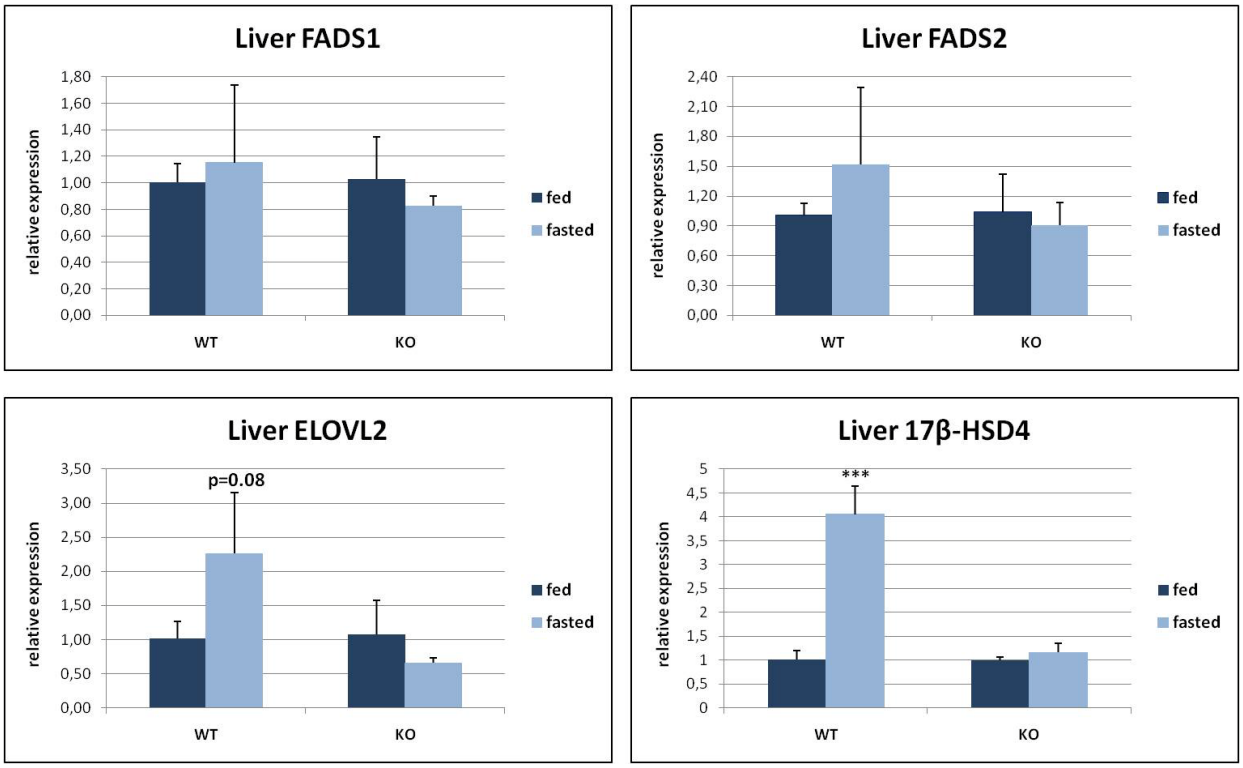

FIGURE 4.1.12. **Comparison of relative mRNA levels in fed and fasted mice.** Relative mRNA levels in the liver of fasted mice were compared to those in the liver of fed mice. WT, wild type; KO, knockout. Data are means ± S.D. (n=4/3 (fed WT/KO), n=3 (fasted)). Statistical significance was determined by the two-tailed Student's *t* test (*, p<0.05; **, p<0.01; ***, p<0.001).

Next, mRNA levels in fed mice were compared with those in fasted mice to verify that/examine if fasting has an influence on and/or induces the expression of target enzymes. Comparative analysis of mRNA levels in fed and fasted WT mice revealed that expression was higher in fasted mice. This effect was very pronounced for ELOVL2 (+122%) and especially for 17β-HSD4 (+301%). FADS1 and FADS2 mRNA levels increased only slightly (Fig.4.1.12). Relative expression tended to be downregulated for all genes except for *17β-Hsd4* in fasted KO mice compared to WT mice. But this reduction was only minimal and not significant. These results imply a regulation of DHA synthesizing enzymes by the nutritional status.

Since nuclear receptors, like peroxisome proliferator activated receptor alpha, are regulated by feeding/fasting and since a possible interaction between ATGL and nuclear receptors is assumed, a next step was to examine whether the expression changes in response to induced PPARα activity. Therefore, mice were fed a normal chow diet supplemented with the synthetic PPARα agonist WY14,643 during three weeks.

4.1.4. PPAR diet

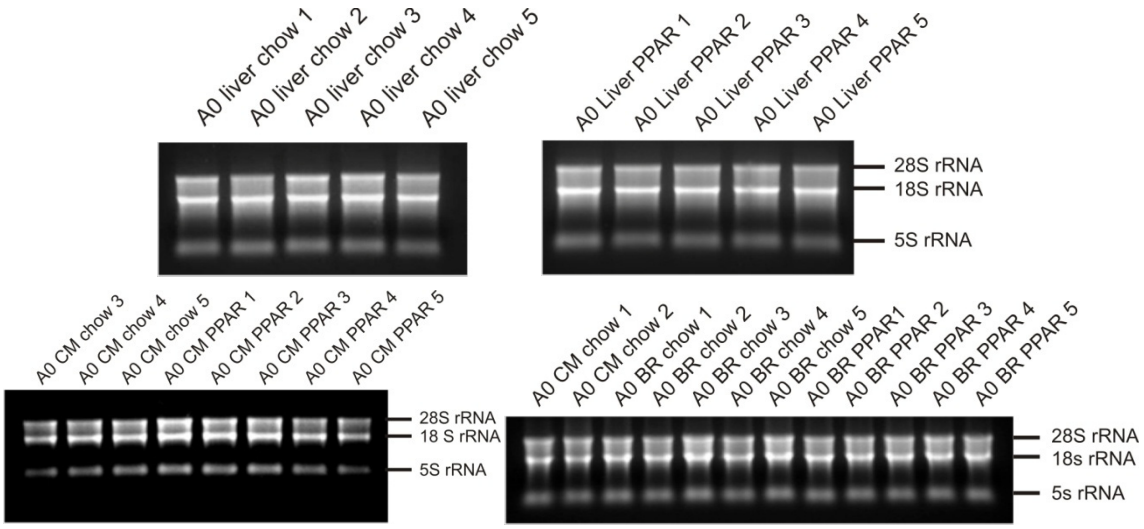

FIGURE 4.1.13. **RNA isolated from mice on a PPAR diet.** Mice were fed either a standard chow diet or a chow diet supplemented with the PPARα agonist WY14,643 during three weeks (PPAR diet). Liver, heart and brain were dissected, RNA was isolated and 5 µg RNA were loaded on a 1% RNA agarose gel and separated for 20 min. at 90 V. A0, *Atgl*$^{-/-}$; chow, chow diet; PPAR, chow diet + PPARα agonist; rRNA, ribosomal RNA; CM, cardiac muscle; BR, brain.

RNA was not degraded; no smear was visible. But RNA quality was not highest as the 18S rRNA band looked more intense than the 28S rRNA band (Fig 4.1.13). In spite of that we used this RNA for reverse transcription and subsequent real-time PCR measurements since according to various findings slightly degraded RNA can still be used for real-time PCR measurements without affecting the results (102).

4.1.4.1. Real-time PCR

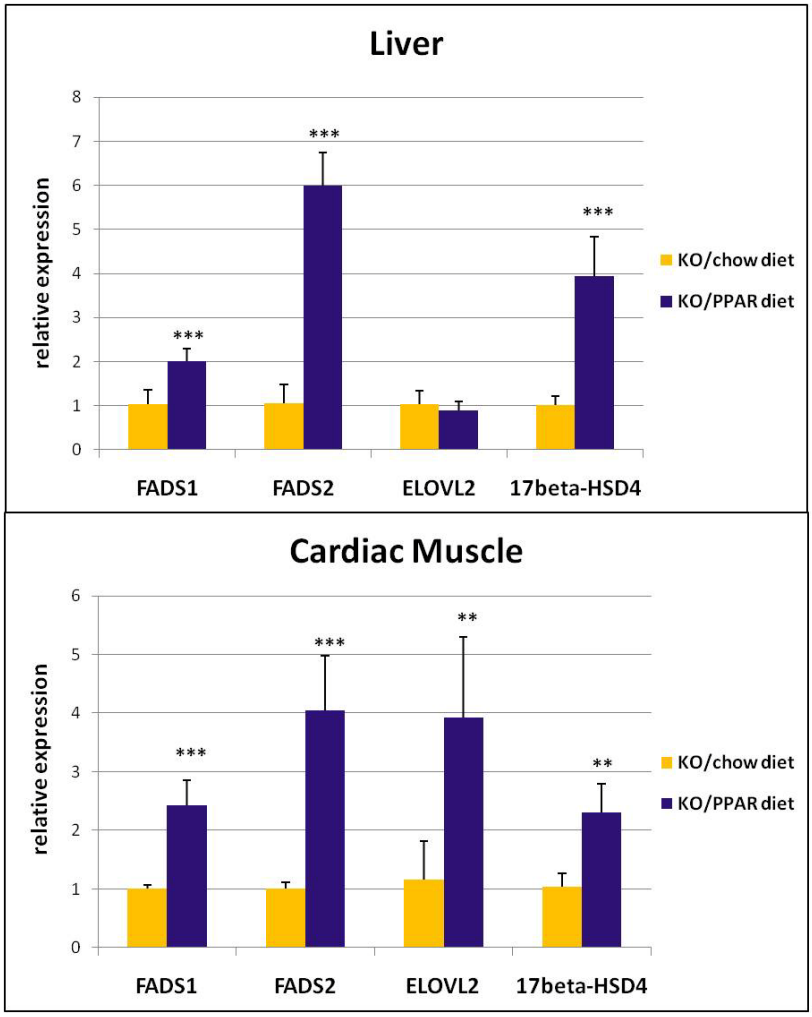

FIGURE 4.1.14. **Comparison of the relative expression in liver and heart of KO mice on a chow diet with the expression in KO mice on a PPAR diet**. RNA isolated from liver and heart of *Atgl*$^{-/-}$ mice that were fed a standard chow diet or a chow diet supplemented with a PPARα-agonist during three weeks was used for real-time PCR measurements. KO, knockout; Data are means ± S.D. (n=5). Statistical significance was determined by the two-tailed Student's *t* test (*, p<0.05; **, p<0.01; ***, p<0.001).

In the liver, all enzymes except ELOVL2 were highly significantly upregulated on transcriptional level in *Atgl*$^{-/-}$ mice after administration of the PPARα agonist (Fig.4.1.14 top). FADS1 expression was increased by 92%, FADS2 expression was almost six times higher (+465%) and 17β-HSD4 mRNA levels were almost 4 times (+289%) as high compared to KO mice on the standard chow diet. The same effect, although less pronounced, was observed in the heart except for cardiac mRNA levels of ELOVL2 which also were upregulated in KO mice fed the PPAR agonist (Fig. 4.1.14 bottom). FADS2 and ELOVL2 expression was increased by 304% and 238%, respectively, FADS1 and 17β-HSD4 mRNA levels were elevated more than twofold (FADS1: +134%; 17β-HSD4: +124%) upon feeding of the agonist. Accordingly, most (all) of the examined enzymes are PPARα target genes in the liver as well as in the heart.

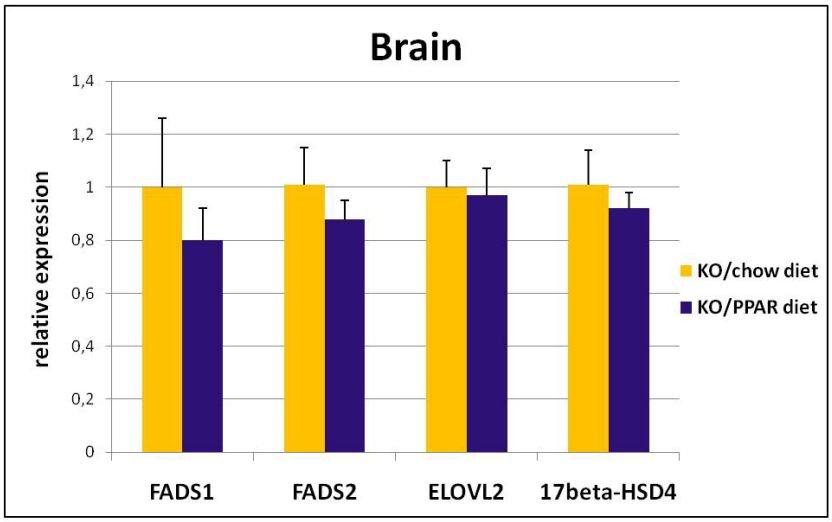

FIGURE 4.1.15. **Relative expression in brain**. mRNA levels were compared in brains of ATGL-knockout mice fed a chow or a PPAR diet. KO, knock out; PPAR diet, chow diet supplemented with 0.1% PPARα-agonist. Data are means ± S.D. (n=5). Statistical significance was determined by the two-tailed Student's *t* test (*, p<0.05; **, p<0.01; ***, p<0.001).

Expression of FADS1, FADS2, ELOVL2, and 17β-HSD4 was also examined in the brain this time because the brain is the organ with the second highest DHA-synthesis rate (69).

Relative expression of the enzymes did not change at all in the brain of *Atgl*$^{-/-}$ mice upon administration of WY14,643 (Fig. 4.1.15). This could be attributed either to different regulation of the enzymes in the brain or to failed transport of the agonist to the brain.

4.1.4.2. Northern Blot

For verifying purposes (to confirm the results obtained by real-time PCR), mRNA levels of DHA-synthesizing enzymes were examined in the liver and the heart of ATGL deficient mice on a PPAR diet and of ATGL deficient mice on a chow diet by doing a Northern blot.

4.1.4.2.1. Preparation of probe I

The first blots were done with probes synthesized from wild type liver cDNA templates using the primers designed for real-time PCR.

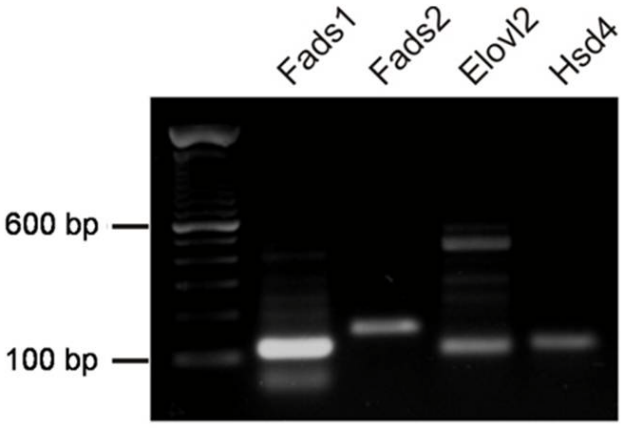

FIGURE 4.1.16. **PCR products from Northern blot probe preparation using WT liver cDNA.** Products from a test PCR run were loaded on a 1.5% agarose gel (100 V, 40 min.). *Fads1*, 110 bp; *Fads2*, 150 bp; *Elovl2*, 102 bp; *Hsd4*, 112 bp.

First, a PCR was run at 60°C which was consistent with the real-time PCR annealing temperature. At this temperature specific products were obtained only for *Fads2* and *17β-Hsd4* (Fig. 4.1.16) although real-time PCR reaction resulted in specific products for all four genes as shown before (pp.42-46). Therefore a temperature gradient was performed and PCR was repeated with multiple batches at 65°C for the best compromise between specificity and high quantity.

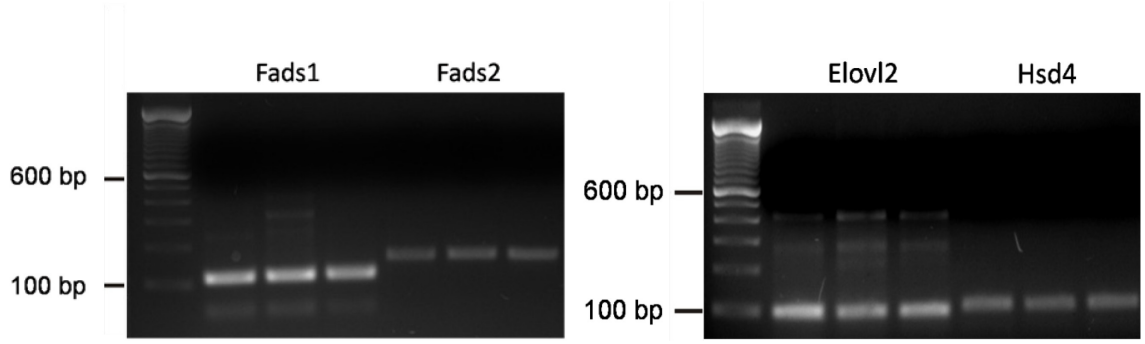

FIGURE 4.1.17. **Northern blot probes I.** PCR was run at an annealing temperature of 65°C with three batches for every enzyme/probe. PCR products were loaded on a 1.5% agarose gel, separated for 45 min. at 90V, cut out and eluted from the gel. *Fads1*, 110 bp; *Fads2*, 150 bp; *Elovl2*, 102 bp; *17β-Hsd4*, 112 bp.

PCR products were separated on an agarose gel (Fig. 4.1.17), cut out from the gel and purified by "freeze and squeeze". The precipitated and dried DNA was resuspended in ddH_2O and 1 µl of resuspended pellets was again loaded on a gel to determine the concentration of the probes and to see if the probes are specific now (only the correct band is visible).

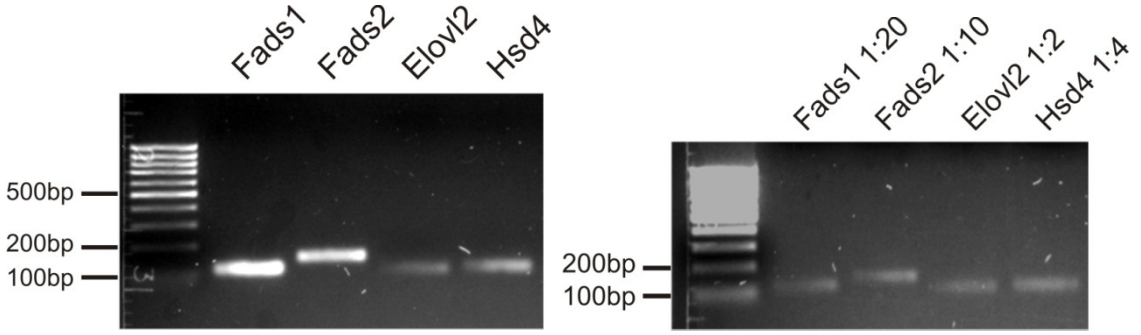

FIGURE 4.1.18. **Purified probes**. 1 µl of the resuspended pellets was again checked on a 1.5% agarose gel (90V, 30 min.) to determine their concentration. Dilutions were made and loaded on a second gel for better estimation. *Fads1*, 110 bp; *Fads2*, 150 bp; *Elovl2*, 102 bp; *17β-Hsd4*, 112 bp.

Purified cDNA separated on an agarose gel (Fig.4.1.18) displayed only one band of the correct size for all four genes. By comparing the intensities of the four probe bands with the ladder intensities the concentration of the resuspended pellets was estimated. 15 ng of the probe were then radioactively labeled.

4.1.4.2.2. RNA agarose gel I

Liver and heart RNA samples from *Atgl*$^{-/-}$ mice fed either a standard chow diet or a chow diet supplemented with the PPARα agonist WY14,643 were thawed on ice and 10 µg of RNA were separated on a 1% denaturing RNA agarose gel (Fig. 4.1.19).

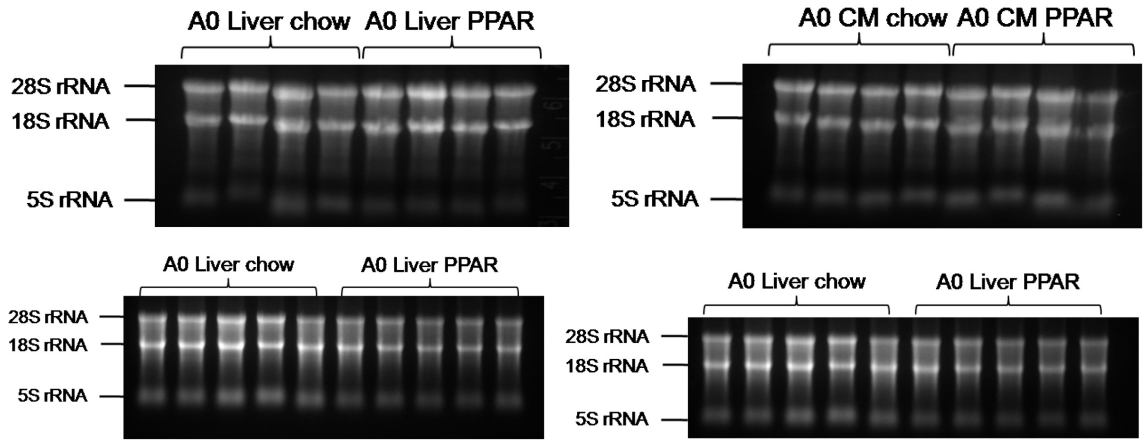

FIGURE 4.1.19. **RNA isolated from liver and heart of ATGL-knockout mice**. RNA samples that were already used for real-time PCR measurements were thawed and 10 µg RNA were loaded on a 1% RNA agarose gel (90 V, 1.5 h) for Northern blotting. 2 Gels were needed for the 17β-HSD4-blot (liver, heart (upper blots)), 2 gels for FADS1 and FADS2. 28S rRNA, 4.7kb; 18S rRNA, 1.9 kb.

RNA should be equally concentrated in all bands which was not the case (Fig. 4.1.19). The pictures were taken to see how much RNA was loaded in order to be able to take into account the differences in RNA quantity in the analysis.

4.1.4.2.3. Northern Blot I

The gel was blotted on a nitrocellulose membrane under vacuum o/n. The blot was hybridized with the radioactively labeled probe and a phosphor storage screen was incubated with the blot for 24 h, 72 h, and for 5 days to obtain a better signal with less noise.

FADS1

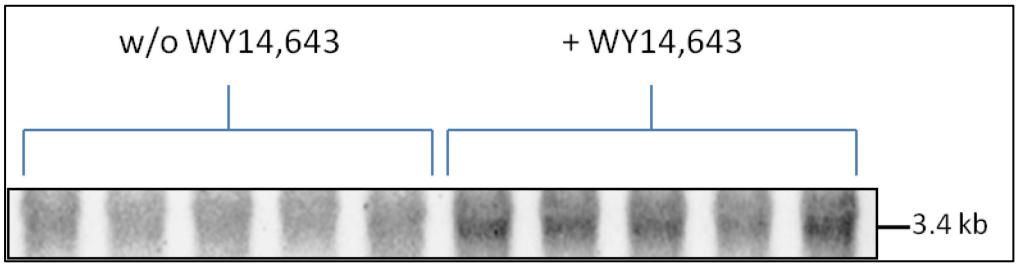

FIGURE 4.1.20. **Hepatic FADS1 mRNA levels.** RNA was isolated from the liver of *Atgl*$^{-/-}$ mice being fed/not being fed a PPARα agonist. 10 µg of total RNA were transferred to a nylon membrane and hybridized with a radioactive probe binding to *Fads1*. Screen was analyzed after 5 days. w/o, without.

Despite the long illumination time, there is still a lot of background noise. However, a band was obtained for FADS1 at 3.4 kb (GenBank™ accession number AB072976) which was detected only for the samples from KO mice which were fed the PPARα agonist (Fig.4.1.20). Taking into account that RNA intensity on the agarose gel was weaker for the PPAR-samples, the conclusion was that FADS1 mRNA levels were upregulated upon WY14,643 administration as it was seen by real-time PCR.

FADS2

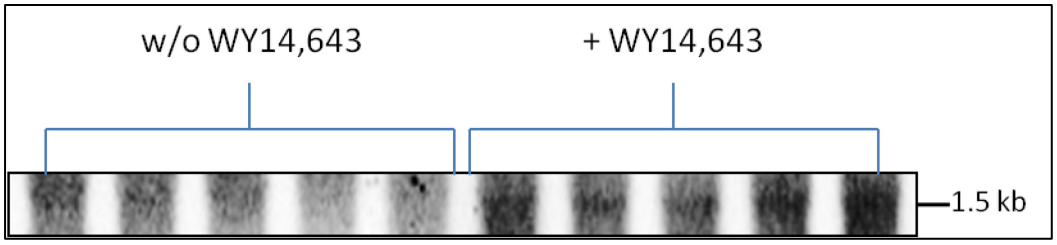

FIGURE 4.1.21. **FADS2 Northern blot**. 10 µg of RNA isolated from livers of *Atgl*$^{-/-}$ mice were blotted on a membrane o/n. Radioactive probe was binding to the *Fads2* mRNA (1.5 kb). w/o, without.

The radioactive *Fads2* probe was not perfectly working (Fig. 4.1.21). While the band at 1.5 kb (GenBank™ accession number AF126798) was slightly visible, it still looked more intense for PPARα agonist-fed mice. However, this signal was too blurred and there was too much background noise for a significant result.

17β-HSD4

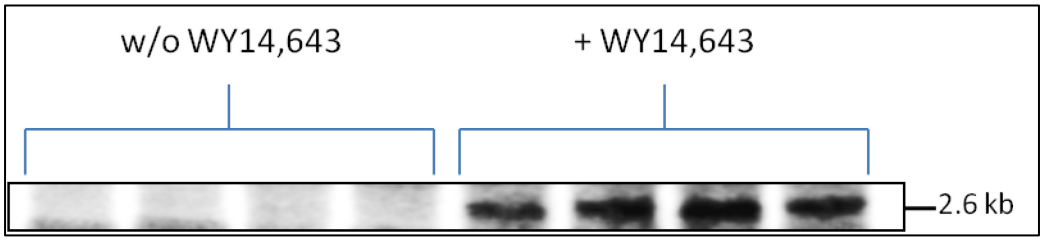

FIGURE 4.1.22. **Northern blot analysis of 17β-HSD4**. 10 µg RNA from livers of *Atgl*$^{-/-}$ mice on a chow diet or on a PPARα diet were blotted on a membrane. The blot was hybridized with a radioactive *17β-Hsd4*-probe. mRNA was detected at 2.6 kb (GenBank™ accession number BC022175). w/o, without.

Examining the blot labeled with the probe for 17β-HSD4, a tremendous difference in expression between KO mice that were fed the PPARα agonist and KO mice fed the standard chow diet was observed which was in concordance with the results obtained by real-time PCR (Fig.4.1.22). Regarding RNA samples isolated from KO mice on a chow diet, expression of 17β-HSD4 was completely blunted. Contrary to that, a large quantity of radioactive probe bound to RNA isolated from WY14,643-fed mice.

In conclusion, differences were registered in the expression of all three genes upon administration of the PPARα agonist but for FADS1 and especially for FADS2 the results

were not convincing. That's why the preparation of the probe was repeated with specifically designed primers.

Concerning the samples from cardiac muscle, no significant signal was obtained for 17β-HSD4 neither in the "normal" KO mice nor in the PPARα diet-fed mice. Therefore, FADS1 and FADS2 expression was no longer examined by Northern blotting. ELOVL2 expression in the liver was not verified by Northern blotting since no differences in expression were detected by real-time PCR measurements.

4.1.4.2.4. Preparation of probe II

Since primers designed for real-time PCR amplified a product of only about 100 bp, specificity was not as high as it would be for usual Northern blot probes with a length of at least 300 to 500 bp. For this reason new primers that amplified a PCR product of about 800 bp and had an additional EcoRI restriction site were designed. With the restriction site the PCR products were cloned into a Bluescript vector (pBluescript II SK+) and purified at a high copy number.

First, a PCR was done at an annealing temperature ranging from 65°C to 70°C using a wild type liver cDNA template and the newly designed primers.

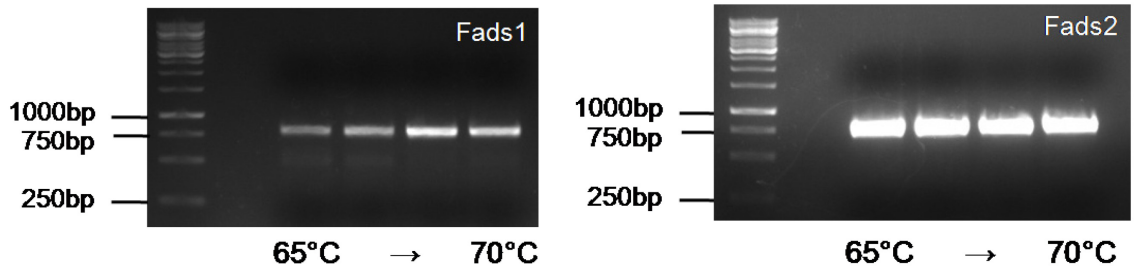

FIGURE 4.1.23. **Northern blot probe II**. A PCR with a temperature gradient from 65°C to 70°C was done to determine the optimal annealing temperature. Products were loaded on a 1% agarose gel (90V, 45 min.). *Fads1*, 810 bp; *Fads2*, 802 bp.

The PCR was repeated at 69°C with 8 more batches for FADS1 and 6 more for FADS2. All PCR products were separated on a gel (Fig.4.1.23) and then cut out and eluted from the gel. For verifying purposes, 1 µl of the precipitated and resuspended cDNA was loaded again on a 1% agarose gel (Fig.4.1.24).

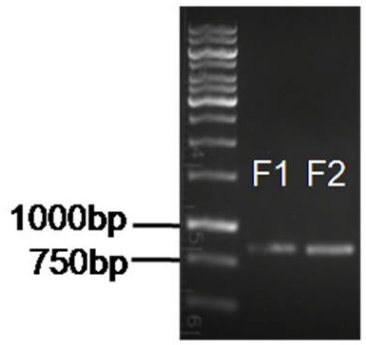

FIGURE 4.1.24. **Purified probes**. 1 µl of the resuspended pellets were visualized on a 1% agarose gel that was run at 90 V for about 1 hour. F1, *Fads1* (810 bp); F2, *Fads2* (802 bp).

The resuspended pellets and 2 µl of the Bluescript vector were digested with EcoRI (the vector was additionally treated with calf intestinal phosphatase (CIP) to remove 5' phosphate groups and inhibit its religation). The inserts were purified by a chloroform-phenol-extraction. The vector was loaded on an agarose gel (Fig.4.1.25), cut out and eluted from the gel.

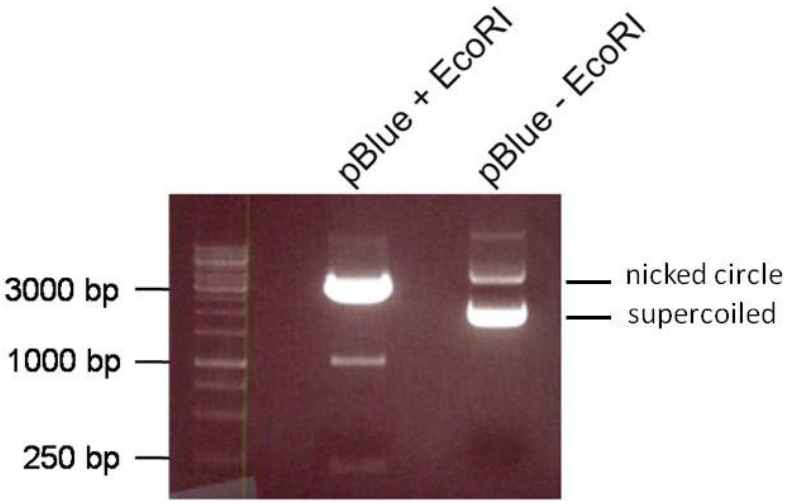

FIGURE 4.1.25. **EcoRI digested pBluescript II SK+**. The vector was digested with EcoRI for 2h at 37°C and loaded on a gel. The 3000 bp fragment representing the digested and linearized vector (pBlue + EcoRI) was cut out from the gel. For verifying purposes, the undigested vector (pBlue – EcoRI) was also loaded on the gel (1.5%, 90 V, 45 min.). pBluescript II SK+, 3.0 kb; pBlue, pBluescript II SK+; + EcoRI, digested with EcoRI; - EcoRI, undigested vector.

On the gel it was detected that the vector already contained some unknown insert (Fig.4.1.25; 1000 bp fragment, lane 'pBlue + EcoRI'). Since the vector (3000 bp) was cut out from the gel, this insert was eliminated. The undigested vector migrated differently in the gel – not according to its size – due to its circulated plasmid form. Most of the vector ran faster because of being supercoiled. The upper band migrating slower represented the nicked circle form of pBluescript II SK+.

Vector and inserts were desalted and 1 µl, respectively, was again visualized on an agarose gel (Fig.4.1.26) to determine their approximate concentration since 3 times more insert than vector was used for ligation.

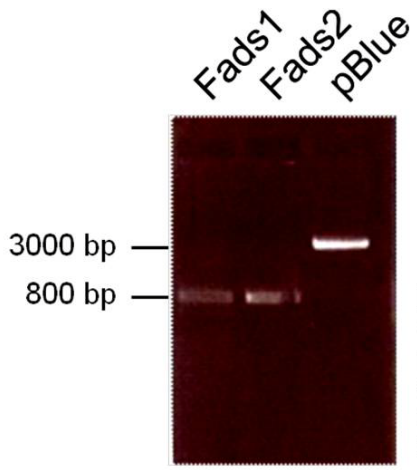

FIGURE 4.1.26. **Purified insert and vector**. 1 µl of purified probes and pBluescript vector was separated on a 1% agarose gel for 40 min. at 90 V to estimate their approximate concentrations. *Fads1*, 810 bp; *Fads2*, 802 bp.

Vector and inserts were ligated and transformed into chemically competent E.coli and plated onto LB-Amp plates supplemented with X-Gal and IPTG. Plates were incubated at 37°C o/n and were checked for white colonies the next day. One white colony was detected for the *Fads1* probe, two colonies for *Fads2*. The small number of positive clones was probably due to an inefficient digestion with EcoRI caused by disturbing ions since insert and vector were not desalted before digestion. These colonies were inoculated into 5 ml LB+Amp o/n and a "Mini prep" was done the next day. For verifying purposes, 3 µl of the purified plasmid DNA were cut with EcoRI and analyzed by DNA electrophoresis to see whether these colonies were no false-positive clones (Fig.4.1.27).

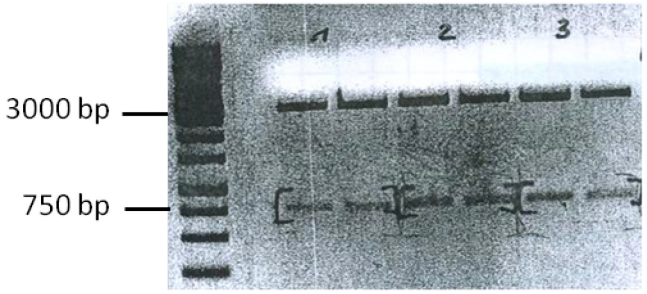

FIGURE 4.1.27. **Control digest with EcoRI.** Aliquots of the DNA purified from positive clones by "Mini-Prep" were digested with EcoRI and separated on a 1% agarose gel for 45 min. at 90V to verify integration of the insert. 1, *Fads1*; 2,3, *Fads2*. *Fads1*, 810 bp; *Fads2*, 802 bp.

Since all three colonies were positive, the remainder of the purified DNA was loaded on a 1% agarose gel, cut out and eluted from the gel, precipitated with 100% ethanol and potassium chloride and dissolved in ddH_2O. 1 µl of the resuspended pellets was examined on another gel (1%) to estimate their concentration and 15 ng DNA were radioactively labeled.

4.1.4.2.5. RNA agarose gel II

Again, 10 µg RNA of liver samples from *Atgl*$^{-/-}$ mice with or without PPAR agonist were loaded on a denaturing 1% agarose gel (Fig.4.1.28). Two gels were prepared, one for FADS1 and the other for FADS2.

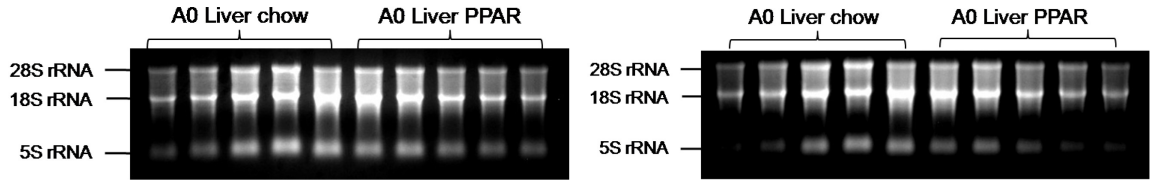

FIGURE 4.1.28. **RNA agarose gel loaded with liver samples.** RNA samples isolated from liver of *Atgl*$^{-/-}$ mice fed or not fed the PPAR-agonist WY14,643 were thawed and 10 µg were separated on a denaturing 1% agarose gel for 1.5 h at constant 90 V. rRNA, ribosomal RNA; A0, *Atgl*$^{-/-}$; chow, standard chow diet; PPAR, standard chow diet supplemented with WY14,643.

Once more RNA was not equally concentrated (Fig.4.1.28). Since the intensity of bands looked different than on the previous gel, it might rather be due to a pipetting error than to an imprecise measurement of concentration.

4.1.4.2.6. Northern Blot II

The gel was vacuum blotted on the nitrocellulose membrane o/n, the membrane was incubated with the radioactive probes o/n and the phosphor storage screen was exposed to ^{32}P-radioactivity for 72 hours (Fig.4.1.29/Fig.4.1.30).

FADS1

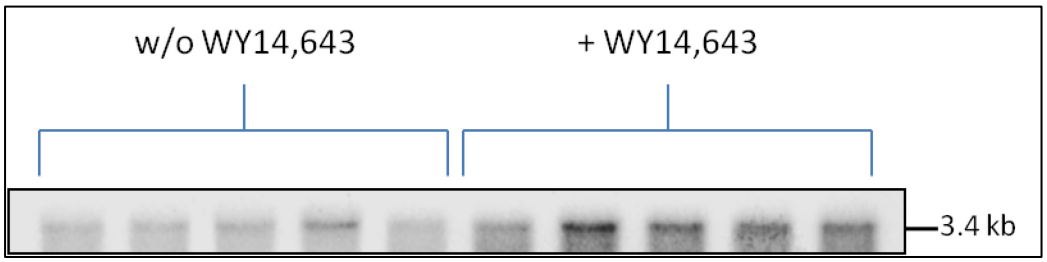

FIGURE 4.1.29. **Hepatic FADS1 mRNA levels evaluated by Northern blot.** Blotting analysis was performed with 10 µg of total RNA. Nylon membrane was hybridized with ^{32}P-labeled *Fads1* probe. w/o, without; +, with; WY14,643, PPARα agonist.

This time a more distinct band was obtained for the new FADS1 probe binding to the target (Fig.4.1.29). There was still some smear/background visible, maybe resulting from partial degradation of the RNA since RNA was thawed already for the 4th time (although it didn't seem to be degraded on the gel). Anyway, an upregulation of mRNA levels was clearly visible for FADS1 in PPARα agonist-fed KO mice compared to those on standard chow diet and this result confirmed real-time PCR experiments.

FADS2

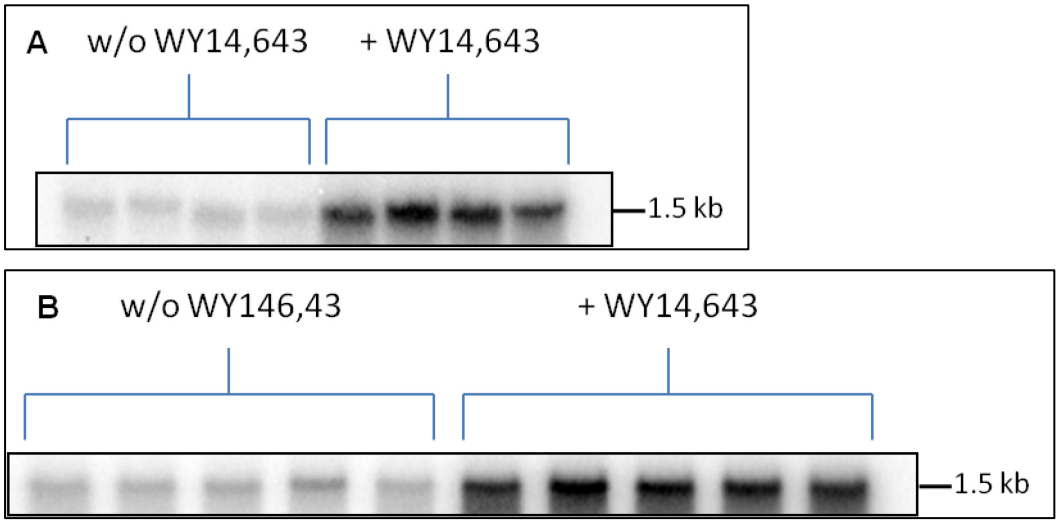

FIGURE 4.1.30. **FADS2 Northern blots with liver RNA samples**. Blot A had previously been hybridized with radioactive *17β-Hsd4*-probe and was now incubated with the new Fads2 probe. The *17β-Hsd4*-radioactivity on this membrane had decayed over a period of 4 weeks (half-life of ^{32}P: 14 days). Blot B was a newly prepared membrane also hybridized with the *Fads2* probe. Screen was exposed to radioactivity during 72 hours.

There was a clear difference in expression for FADS2 this time (Fig.4.1.30). While mRNA was only slightly detectable in livers of knockout mice on a standard chow diet, the expression was highly induced upon administration of the PPARα agonist WY14,643 on both blots.

As seen by real-time PCR measurements, upregulation of expression by WY14,643 was much stronger for FADS2 and 17β-HSD4 than for FADS1.

4.1.5. Transgenic ATGL

Since mRNA levels of the selected enzymes were reduced in (fasted) *Atgl*$^{-/-}$ mice, the next attempt was to examine whether expression of FADS1, FADS2, ELOVL2, and 17β-HSD4 changes when ATGL is overexpressed in wild type as well as knockout mice. If ATGL is inducing the transcription of the selected enzymes, mRNA levels should go up in response to the overexpressed ATGL protein. Therefore, livers of fasted WT mice overexpressing ATGL (99) and hearts of fed WT/KO mice expressing exogenous ATGL under a cardiac-muscle specific promoter (α-myosin heavy chain promoter (MHC)) (98) were used for following measurements.

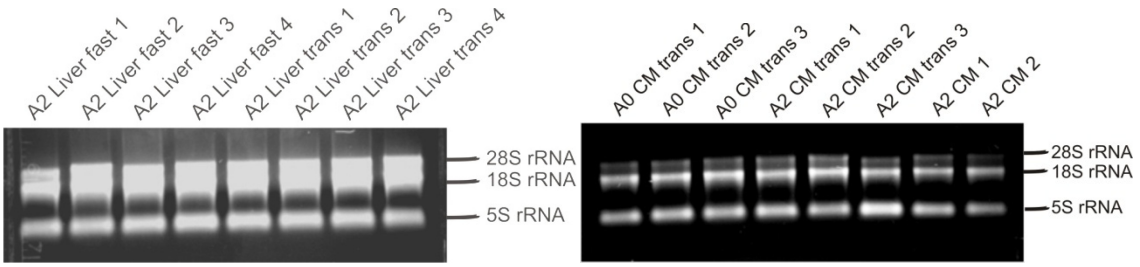

FIGURE 4.1.31. **RNA isolated from mice overexpressing transgenic ATGL.** RNA was isolated from liver and heart of mice that were expressing only endogenous ATGL or that were overexpressing transgenic ATGL specifically in heart and liver. RNA was checked on a 1% RNA agarose gel (90V, 20 min.). A2, *Atgl* wild type; fast, fasted; trans, overexpression of transgenic ATGL; A0, *Atgl*$^{-/-}$; CM, cardiac muscle; rRNA, ribosomal RNA.

Transgenic mice were created overexpressing exogenous ATGL specifically either in the heart or in the liver. RNA was isolated without being degraded but again (at least in case of CM) the 18S rRNA band was more intense than the 28S rRNA band which indicates that RNA quality wasn't perfect (Fig.4.1.31).

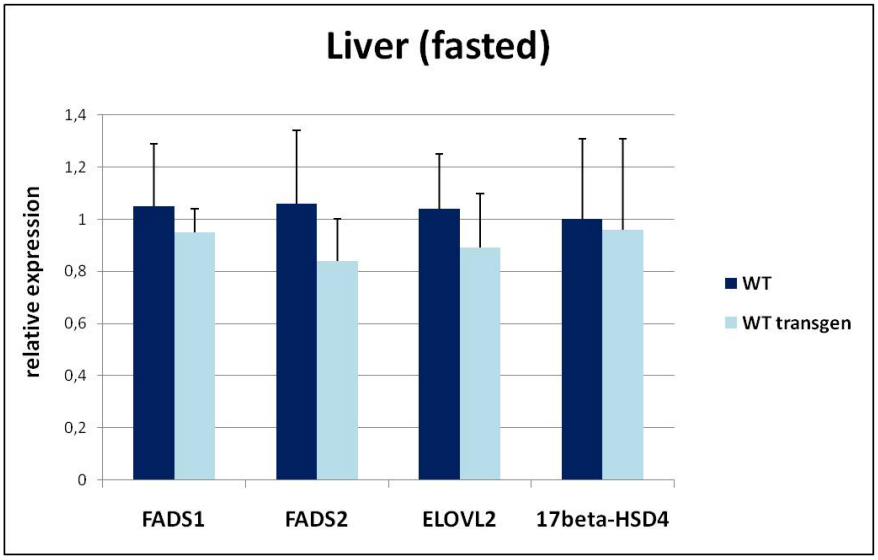

FIGURE 4.1.32.**Relative mRNA levels in the liver of wild type mice with or without transgenic ATGL.** RNA was isolated from fasted wild type mice that were either or not overexpressing transgenic ATGL specifically in the liver. WT, wild type; transgen, transgenically overexpressed ATGL. Data are means ± S.D. (n=4). Statistical significance was determined by the two-tailed Student's *t* test (*, p<0.05; **, p<0.01; ***, p<0.001).

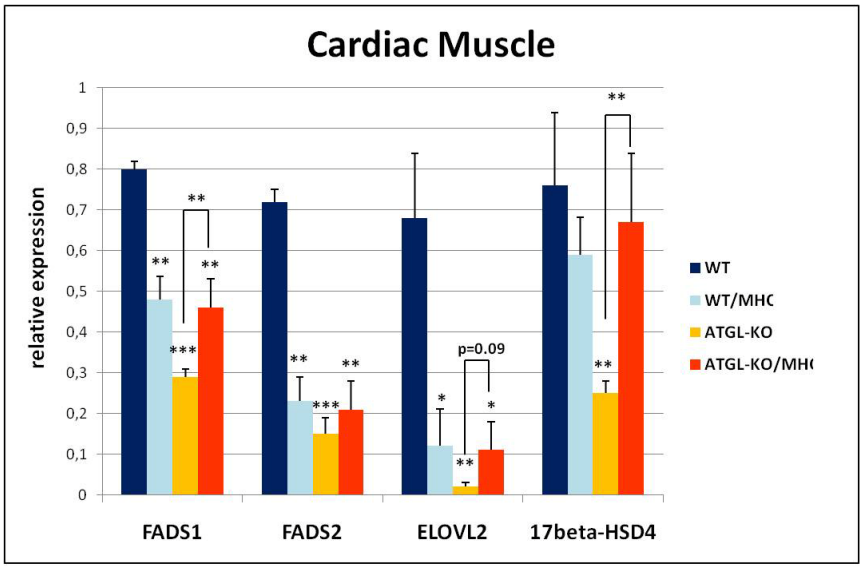

FIGURE 4.1.33. **Relative expression in the hearts of wild type and knockout mice.** RNA was isolated from fed wild type and KO mice that either or not overexpressed transgenic ATGL specifically in the cardiac muscle. WT, wild type; MHC, myosin heavy chain (heart-specific promoter for transgenic ATGL expression); KO, knockout. Data are means ± S.D. (n=3). Statistical significance was determined by the two-tailed Student's *t* test (*, p<0.05; **, p<0.01; ***, p<0.001).

Liver samples were isolated from fasted wild type mice with or without transgenic ATGL being expressed exclusively in the liver. The relative expression of the four target enzymes was not significantly different between the two phenotypes (Fig.4.1.31). Looking at the relative expression levels in the heart of fed mice, again a significant decrease in the expression of DHA synthesizing enzymes was observed in *Atgl*$^{-/-}$ compared to WT mice (FADS1: -64%; FADS2: -79%; ELOVL2: -97%; 17β-HSD4: -67%) (Fig.4.1.32). This reduction was more pronounced than during the first measurements. It was surprising that wild type mice with transgenic ATGL expression in the heart had lower relative mRNA levels for all four enzymes than "normal" wild type mice. The more so as this reduction was significant - except for 17β-HSD4. *Atgl*$^{-/-}$ mice overexpressing ATGL exclusively in the heart raised their relative expression levels to those of wild type hearts with transgenic ATGL but they didn't reach "normal" wild type levels. Only for 17β-HSD4, mRNA levels were almost as high as in wild type hearts (88%).

As these results were unexpected, expression of MCAD (medium-chain acyl-CoA dehydrogenase) which was already shown to be regulated by ATGL on transcriptional level (Haemmerle et al., unpublished data) was checked and could therefore indicate whether overexpressed ATGL actually displayed the anticipated activity.

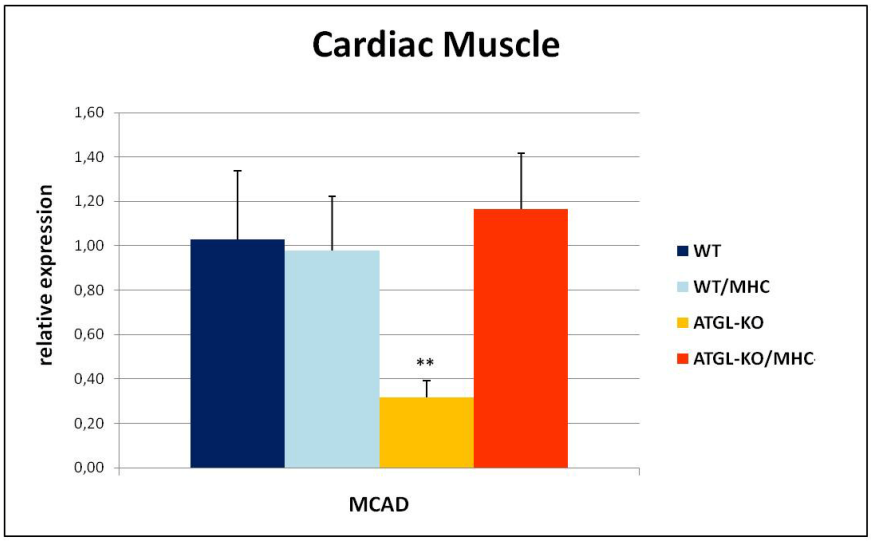

FIGURE 4.1.34. **Expression of MCAD in mouse heart.** RNA was isolated from hearts of different genotypes and subjected to real-time PCR. WT, wild type; MHC, myosin heavy chain (heart-specific promoter for transgenic ATGL expression); KO, knockout. Data are means ± S.D. (n=3). Statistical significance was determined by the two-tailed Student's *t* test (*, $p<0.05$; **, $p<0.01$; ***, $p<0.001$).

In the cardiac muscle a clear influence of ATGL activity on MCAD expression was detected (Fig.4.1.34). Although again mRNA levels were not upregulated in wild type mice overexpressing ATGL, no reduction of MCAD expression was registered compared to WT mice. Additionally, in KO mice overexpressing ATGL the expression was normalized and wild type values were reached. So it was concluded that the observed downregulation of DHA-synthesizing enzymes in wild type mice overexpressing ATGL had to be a pathway-specific regulation.

4.2. Lipid profiling analyses

4.2.1. Plasma free fatty acid composition

In order to determine differences in the composition of free fatty acids between the plasma of wild type and ATGL-knockout mice, free fatty acids were extracted from plasma of wild type, *Atgl*$^{-/-}$ and *Hsl*$^{-/-}$ mice by an acidic Folch extraction procedure. The concentration of free fatty acids was determined with the NEFA c kit from WAKO.

Dilutions of the extracted fatty acids were further subjected to a derivatization with BSTFA (trimethylsilyl-donor) and then analyzed by GC-MS.

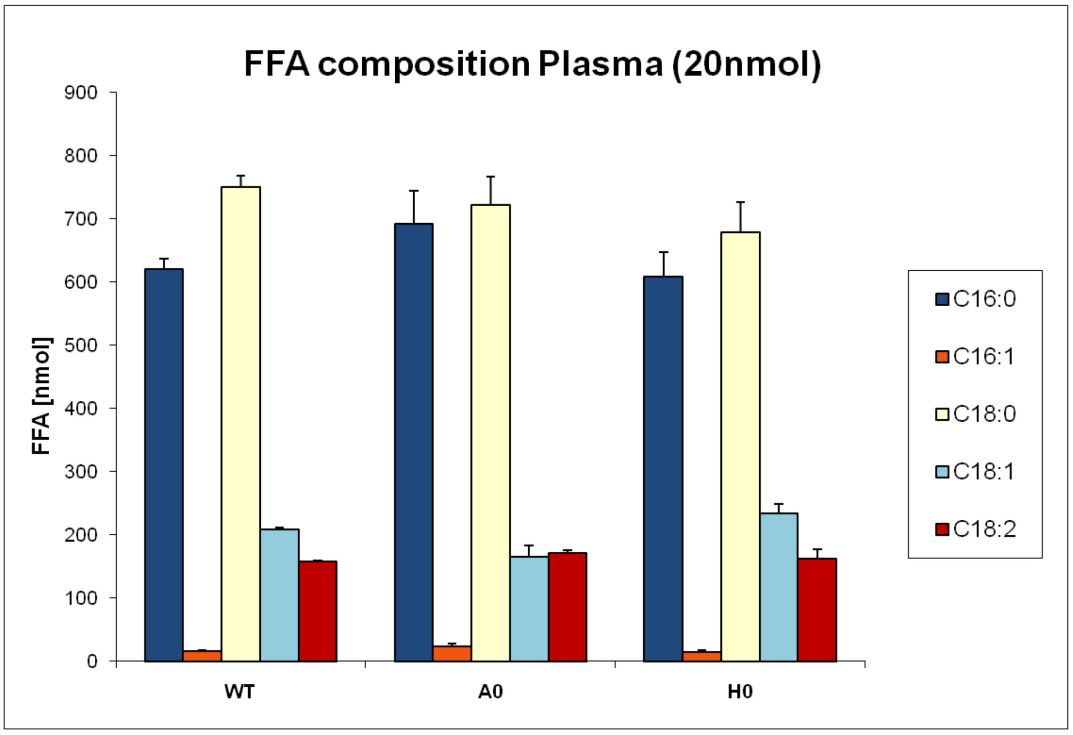

FIGURE 4.2.1. **Plasma free fatty acid composition determined by GC-MS.** Blood samples were taken from wild type, *Atgl*$^{-/-}$ and HSL$^{-/-}$ mice, plasma was separated and lipids were extracted for FFA composition by GC-MS: FFA, free fatty acids; WT, wild type; A0, *Atgl*$^{-/-}$; H0, *Hsl*$^{-/-}$; C16:0, palmitic acid; C16:1, palmitoleic acid; C18:0, stearic acid; C18:1, oleic acid; C18:2, linoleic acid.

No real difference was observed concerning the plasma FFA-composition of wild type, *Atgl*$^{-/-}$ (A0) and *Hsl*$^{-/-}$ (H0) mice (Fig.4.2.1). Levels of saturated fatty acids C16:0 and C18:0 were extraordinarily high. In contrast to the very first FFA measurement by direct injection MS/MS (St.Louis; USA), C22:6n-3 or other PUFAs were not detected at all – perhaps the concentration was too low for the applied GC/MS measurement. For the quantification of these long-chain fatty acids in the plasma, the method still needs to be adapted. It was also unclear where the high levels of unsaturated fatty acids came from. In any case, the composition of all reagents, buffers and solutions did not explain the "contamination" with these saturated fatty acids.

4.2.2. Phospholipid analysis

First let us summarize the lipid profiling results that constituted the starting point of our study (p.13/14). The distribution of different lipid species and free fatty acids in cardiac muscle was compared between *Atgl*$^{-/-}$ mice and WT mice. Looking at the TAG profile, DHA (C22:6n-3)-containing triglycerides were reduced in mice deficient for ATGL compared to wild type mice whereas mainly triglycerides containing linoleic acid (C18:2) were increased (Fig.1.8.2). Very similar results were obtained for phospholipids (Fig.1.8.1). A decrease in DHA-containing phosphatidylcholins (PC) and phosphatidylethanolamines (PE) being less pronounced for PS, PI, and CL was observed in ATGL$^{-/-}$ compared to WT mice. On the other hand, C18:0/C18:1/C18:2-containing phospholipids were elevated in KO mice. In addition the FFA composition revealed reduced levels of DHA and increased levels of C18 fatty acids (Fig.1.8.3).

In order to further understand the correlation between the presence or absence of ATGL and changes in the lipid profile, lipids were extracted from liver, heart, and brain of KO and WT mice under various conditions. The lipid composition was studied by performing a HPLC-MS/MS analysis for phosphatidylcholines and phosphatidylethanolamine.

4.2.2.1. Cardiac Muscle

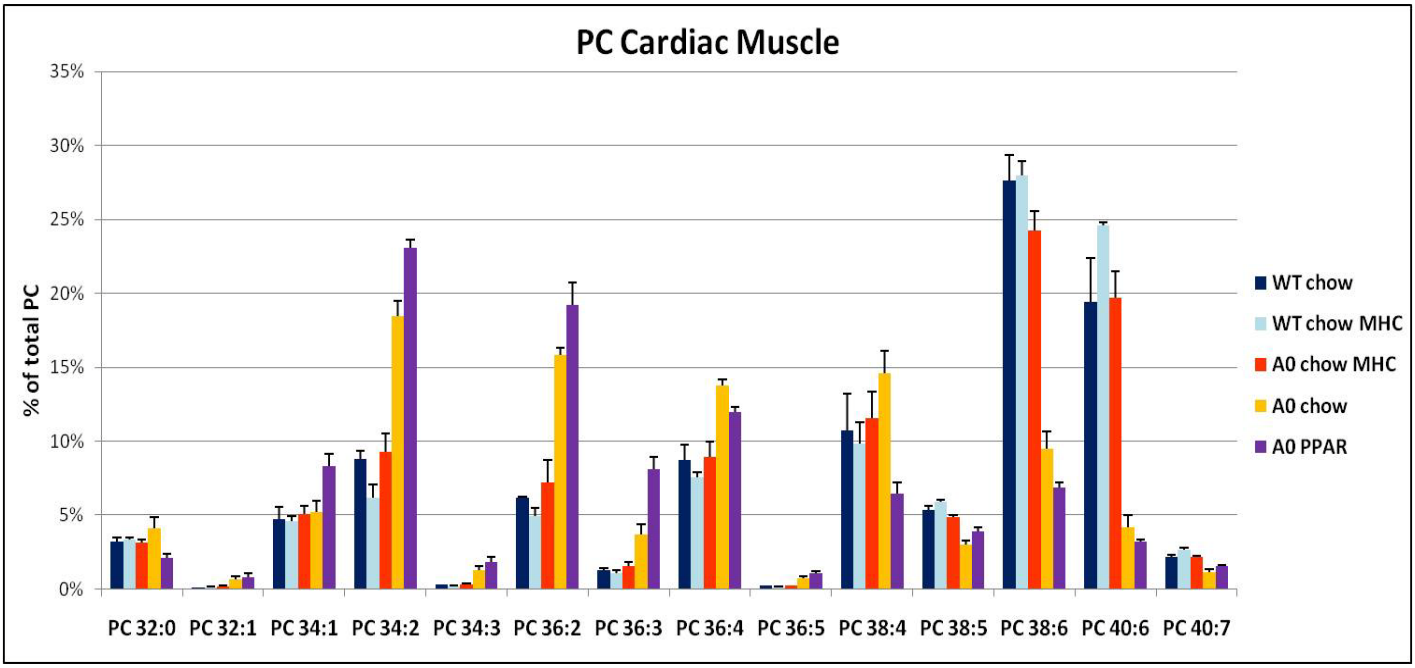

FIGURE 4.2.2. **Mass spectrometer analysis of phosphatidylcholine in mouse hearts.** Lipids were extracted from hearts of wild type and transgenic mice by an acidic Folch and PC composition was measured by HPLC-MS/MS. The detailed fatty acid composition of the single PC species is described in table 4.2.1. PC, phosphatidylcholine; WT, wild type; chow, fed a chow diet; MHC, myosin heavy chain (heart specific promoter for transgenic ATGL); A0, *Atgl*$^{-/-}$; PPAR, fed a chow diet supplemented with a PPARα agonist.

First, we looked into the fatty acid compositions of the various phospholipid species.

PC species	Fatty acid composition I	Fatty acid composition II	Possible C18:3 involvement
PC 32:0	C16:0/C16:0		
PC 32:1	C16:0/C16:1		
PC 34:1	C16:0/C18:1		
PC 34:2	C16:0/C18:2		
PC 34:3	C16:1/C18:2	C16:0/C18:3 (?)	
PC 36:2	C18:0/C18:2	C18:1/C18:1	
PC 36:3	C18:1/C18:2	C16:0/C20:3	C18:0/C18:3 (?)
PC 36:4	C18:2/C18:2	C16:0/C20:4 (?)	C18:1/C18:3 (?)
PC 36:5	C16:1/C20:4	C16:0/C20:5 (?)	C18:2/C18:3 (?)
PC 38:4	C18:0/C20:4		
PC 38:5	C18:1/C20:4	C16:0/C22:5	
PC 38:6	C16:0/**C22:6**	C18:2/C20:4	
PC 40:6	C18:0/**C22:6**		
PC 40:7	C18:1/**C22:6**	C18:2/C22:5	

TABLE 4.2.1. **Fatty acid composition of PC species**. For phospholipids of a specific number of C- and H-atoms there is sometimes more than one possible combination of fatty acids. Column I represents the most common composition, column II a lesser common one. Column III lists possible C18:3-incorporation which is usually not considered as possibility due to the normally very low concentration of C18:3 in wild type mice.

Fatty acid composition of PC in cardiac muscle was more or less the same for fed wild type mice with or without transgenic expression of ATGL (Fig.4.2.2). Nevertheless, in contrast to the results for *Atgl*$^{-/-}$ mice, transgenic mice overexpressing ATGL in the heart showed a trend towards an increase of DHA-containing PC and reduced C18:0/C18:1/C18:2-containing PC. *Atgl*$^{-/-}$ mice overexpressing ATGL in the heart presented a completely restored lipid profile since fatty acid composition was the same as for fed wild type mice. The difference between knock-outs and wild types in the lipid profile was balanced out by replacing the knocked-out *Atgl*. ATGL-deficient mice showed again a decrease in DHA-containing PC versus an increase of C18:0/C18:1/C18:2(C18:3?)-containing phospholipids. KO mice that were fed the PPARα agonist WY14,643 mostly had a similar phenotype to *Atgl*$^{-/-}$ mice (but with some variations) instead of the expected restored lipid profile.

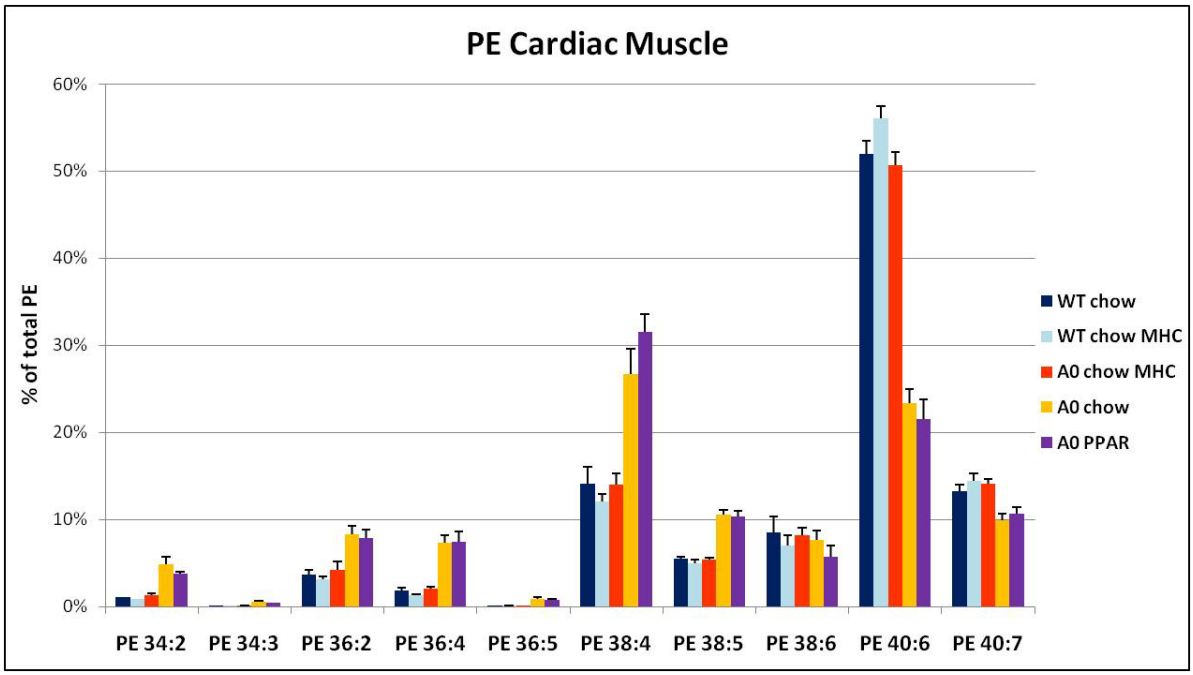

FIGURE 4.2.3. **Results from HPLC-MS/MS analysis of PE composition in mouse hearts**. Fatty acid composition of the single PE species can be seen in table 4.2.2. PE, phosphatidylethanolamine; WT, wild type; chow, fed a chow diet; MHC, myosin heavy chain (heart specific promoter for transgenic ATGL); A0, *Atgl*$^{-/-}$; PPAR, fed a chow diet supplemented with a PPARα agonist.

PE species	Fatty acid composition I	Fatty acid composition II	Possible C18:3 involvement
PE 34:2	C16:0/C18:2		
PE 34:3	C16:1/C18:2	C16:0/C18:3 (?)	
PE 36:2	C18:0/C18:2	C18:1/C18:1	
PE 36:4	C18:2/C18:2	C16:0/C20:4 (?)	C18:1/C18:3 (?)
PE 36:5	C16:1/C20:4	C16:0/C20:5 (?)	C18:2/C18:3 (?)
PE 38:4	C18:0/C20:4		
PE 38:5	C18:1/C20:4	C16:0/C22:5	
PE 38:6	C16:0/**C22:6**	C18:2/C20:4	
PE 40:6	C18:0/**C22:6**		
PE 40:7	C18:1/**C22:6**	C18:2/C22:5	

TABLE 4.2.2. **Fatty acid composition of PE species.** In column I and II the more or less common fatty acid compositions of the single PE species are indicated whereas the last column suggests possible linolenic acid incorporation.

The data obtained for fatty acid composition of phosphatidylethanolamine in mouse hearts largely resembled the PC-composition (Fig.4.2.3). Again, lipid profile was normalized to WT levels in KO mice overexpressing transgenic ATGL in the heart. Wild type mice with CM-specific expression of exogenous ATGL had again a similar lipid composition to wild type mice but with a very slight trend towards an increase of DHA-containing PL and a decrease of oleic acid/linoleic acid/linolenic acid-containing

phospholipids. ATGL-deficient mice presented opposite results, i.e. reduced DHA-containing PE and increased C18-fatty acids containing phospholipids. The lipid profile of KO mice fed WY14,643 was also very similar to the profile of "normal" KO mice. All in all, differences between genotypes were less pronounced for PE than for PC.

4.2.2.2. Liver

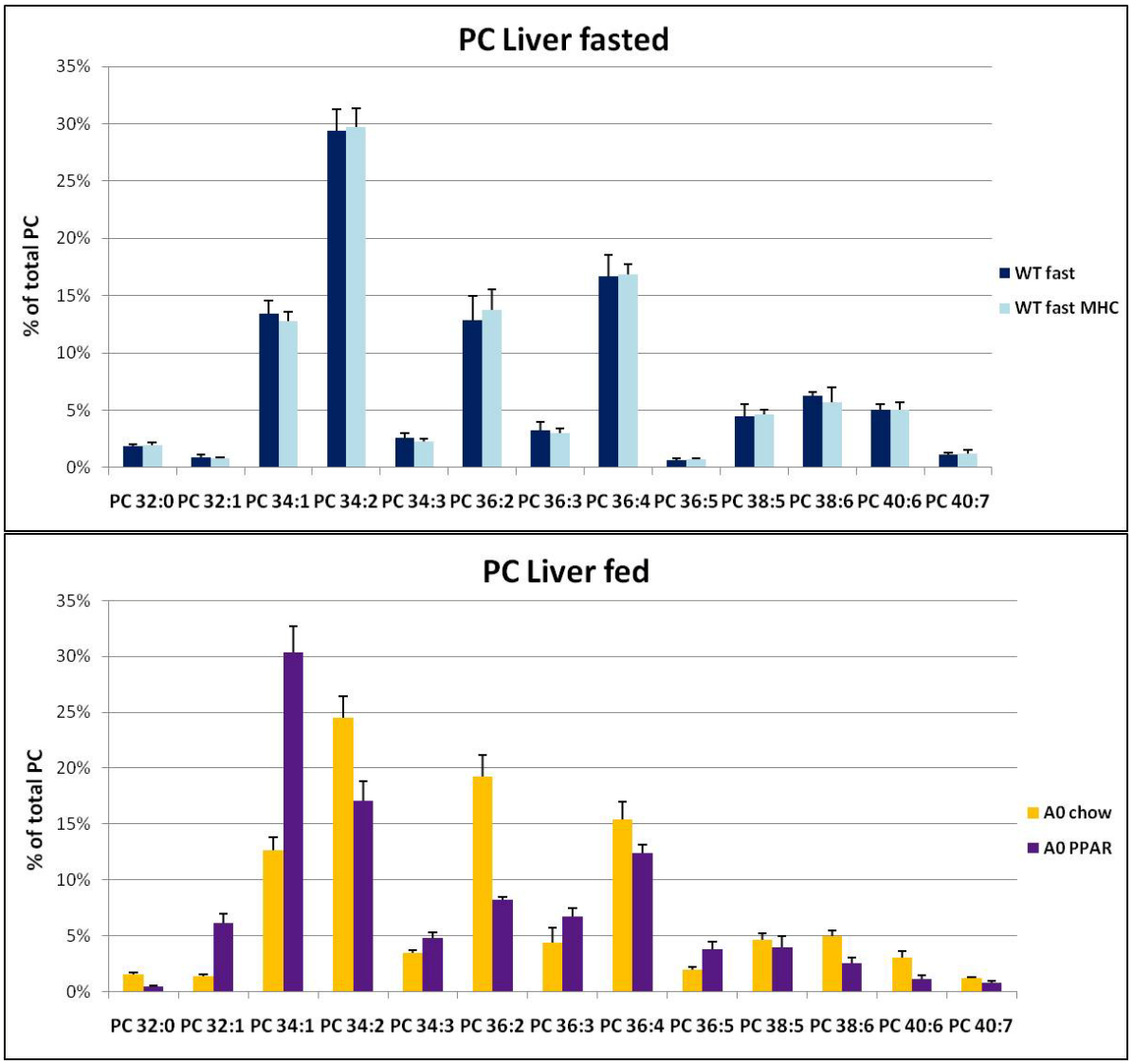

FIGURE 4.2.4. **Lipid profiling analysis in the liver of wild type and KO mice**. HPLC-MS/MS measurements were done to analyze the fatty acid composition of PC in the liver of fasted wild type mice overexpressing/not overexpressing transgenic ATGL in the liver and of knockout mice fed/not fed a PPARα agonist. Fatty acid composition of PC species in the liver is the same as in the heart (Table 4.2.1). PC, phosphatidylcholine; WT, wild type; fast, overnight (12 h) fasted mice; MHC, myosin heavy chain (heart-specific promoter); A0, *Atgl*$^{-/-}$; chow, fed a chow diet; PPAR, fed a chow diet supplemented with a PPARα agonist.

It was difficult to compare all four genotypes in the liver since wild type mice were fasted and knockout mice were fed. Therefore, the results were displayed in two separate diagrams (Fig.4.2.4). In the liver of fasted wild type mice overexpressing transgenic ATGL we observed almost the same lipid profile as for wild type mice but we did not observe this trend towards an opposite profile of ATGL-deficient mice, meaning an increase in

DHA-containing phospholipids and a decrease in C18-FA-containing lipids, that was seen in the heart (Fig.4.2.2). Contrary to the heart, the liver of ATGL-deficient mice displayed only a slight reduction in DHA-containing PC (especially PC 40:6) and a lesser increase in C18-FA-containing PC (PC 36:2) compared to the liver of fasted WT mice considering the percentage distribution (provided that lipid profiles of fed and fasted liver can be compared anyway). ATGL-deficient mice that were fed the PPARα agonist mostly had a very similar lipid profile to KO mice on a standard chow diet with very few but very pronounced differences, especially for PC 34:1 (C16:0/C18:1) which was dramatically increased and for PC 36:2 (C18:0/C18:2; C18:1/C18:1) that was significantly reduced, compared to KO mice.

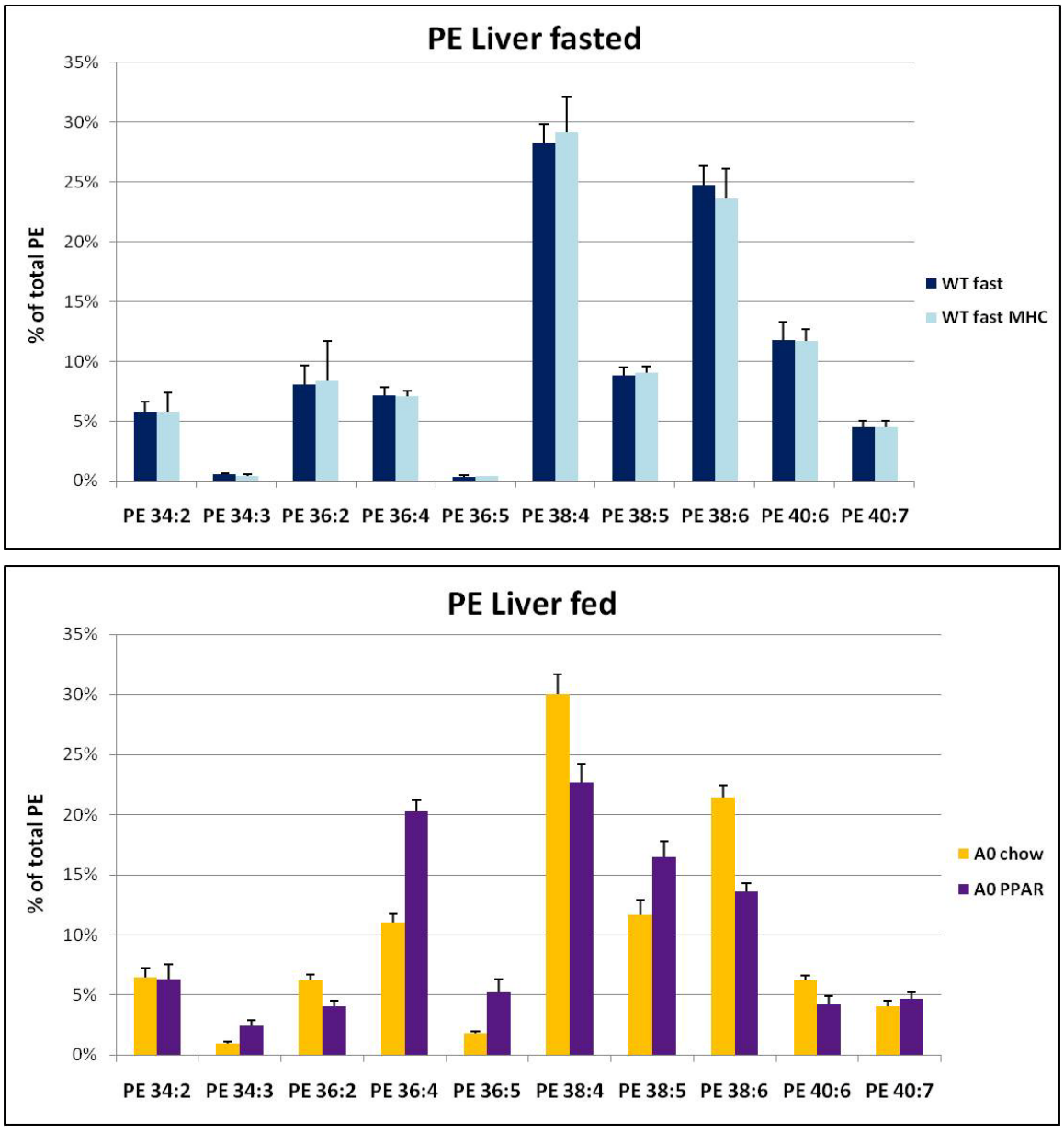

FIGURE 4.2.5. **Distribution of PE species in mouse liver analyzed by HPLC-MS/MS.** Fatty acid composition of PE species can be seen in table 4.2.2. PE, phosphatidylethanolamine; WT, wild type; fast, overnight (12 h) fasted mice; MHC, myosin heavy chain (heart-specific promoter); A0, *Atgl*$^{-/-}$; chow, fed a chow diet; PPAR, fed a chow diet supplemented with a PPARα agonist.

The PE composition in the liver of the different mice varied along the same lines as the PC composition (Fig.4.2.5). Fasted wild type mice, expressing exogenous ATGL or not, had a very similar profile. ATGL-deficient mice showed again a slight reduction in DHA-containing PE and only a slight increase in C18-FA-containing PL regarding the percentage distribution. PPARα agonist-fed KO mice principally had a similar lipid composition to ATGL-deficient mice with all differences of the KO mice profile to the profile of WT mice being more pronounced except for some phospholipids, especially PE 38:4 (C18:0/C20:4). But there were also significant differences between PE and PC lipid profile, namely regarding PE 36:4 (C18:2/C18:2; C16:0/C20:4; (C18:1/C18:3)) which was, contrary to PC 36:4 (Fig.4.2.4), increased in PPARα agonist-fed KO mice compared to ATGL-deficient mice. Looking further at the percentage distribution, PE 36:4 was increased in *Atgl*$^{-/-}$ mice compared to WT mice which was not the case for PC 36:4 (Fig.4.2.4). The PE profile thus was more in line with the trend of C18-fatty acids being increased in *Atgl*$^{-/-}$ mice.

Nevertheless, the only statement that could be made considering the phospholipid profile in the liver was that hepatic overexpression of ATGL in wild type mice did not change the distribution of PC and PE species and feeding of the PPARα agonist WY14,643 did not normalize the lipid profile to WT levels.

4.2.2.3. Brain

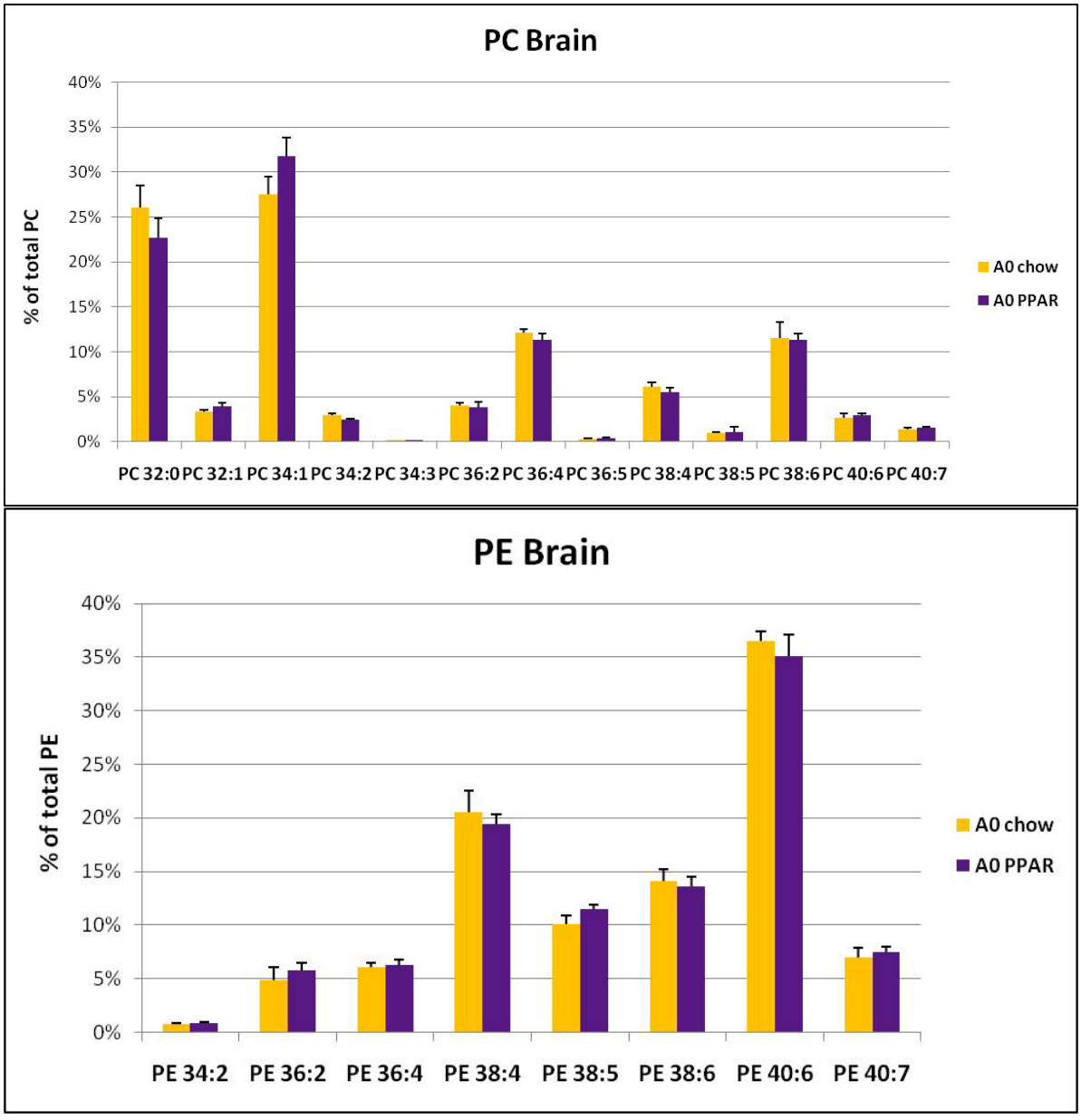

FIGURE 4.2.6. **HPLC-MS/MS analysis of fatty acid composition of PE and PC in the brain**. Lipids extracted from the brain of ATGL-deficient mice that were fed a standard chow diet supplemented/not supplemented with the PPARα agonist WY14,643 were analyzed for fatty acid composition of PE and PC by HPLC coupled to a triple-quadrupole mass spectrometer**.** Fatty acid composition of PC and PE species is depicted in table 4.2.1 and table 4.2.2. A0, *Atgl*$^{-/-}$; chow, fed a chow diet; PPAR, fed a chow diet supplemented with a PPARα agonist.

The comparison between the lipid profiles in the brains of mice fed a standard chow diet or a chow diet supplemented with the PPARα agonist WY14,643 during three weeks revealed no significant differences for fatty acid composition of PC and PE species as it was the case for relative mRNA levels of target genes.

In summary, the data of the lipid profiling analysis show that fatty acid composition in KO mice can be restored by overexpression of exogenous ATGL but cannot by feeding a PPARα agonist.

5. Discussion

The adipose triglyceride lipase, short ATGL, is a very important enzyme of the lipolytic pathway. Especially during times of high energy demand, stimulated lipolysis depends on this enzyme which fulfills the first of three steps in the breakdown of triglycerides into glycerol and free fatty acids inside lipid droplets of WAT (21, 54). These free fatty acids are the main energy sources used for mitochondrial ATP production by β-oxidation (1). When ATGL is knocked out in mice this causes a severe phenotype: Mice are obese, they accumulate triglycerides in almost every organ and finally die from cardiac insufficiency due to this lipid accumulation (31). A similar phenotype can be observed in humans suffering from NLSDM caused by autosomal recessive mutations inside the *Atgl* gene (34).

Since ATGL proved so crucial for the lipid metabolism we were interested in the lipid profile of *Atgl*$^{-/-}$ mice compared to wild type mice. At the very start we made an interesting discovery: In the cardiac muscle of mice deficient for ATGL, phospholipids - especially phosphatidylcholine (PC) and phosphatidylethanolamine (PE), but also phosphatidylserine (PS), phosphatidylinositol (PI), and cardiolipin (CL) - containing docosahexaenoic acid (DHA) were reduced. On the other hand, lipids with incorporated C18 fatty acids were increased. The same effect was observed for triglycerides.

Based on these findings we wanted to identify the link between missing ATGL activity and changes in lipid profile, especially in DHA-containing lipids. DHA is an ω-3 polyunsaturated fatty acid and can either be taken up by ingestion of fatty cold-water fish like salmon or tuna or gets synthesized from the essential fatty acid α-linolenic acid (C18:3n-3) by several elongations and desaturations (67). The first steps in DHA-biosynthesis take place in the endoplasmic reticulum where the longer-chain intermediate C24:6n-3 is produced. This intermediate is further oxidized in the peroxisomes and finally results in docosahexaenoic acid (72). The lion's share of DHA biosynthesis takes place in the liver, a minor part can be produced in the brain and only a minimal amount is synthesized in the heart (69). We decided to take a closer look at four of the seven enzymes involved in this pathway: FADS2, the Δ6-desaturase, which is the rate-limiting enzyme catalyzing the first desaturation, the Δ5-desaturase FADS1, the elongase ELOVL2 and the peroxisomal enzyme 17β-HSD4.

<u>Fed mice</u>

First, we looked into the regulation of these enzymes on transcriptional level. Liver and heart were isolated from fed wild type and ATGL-knockout mice and relative mRNA levels were compared by real-time PCR. As opposed to the heart, where relative mRNA levels of all four target genes were reduced in mice deficient for ATGL, the expression of

DHA-synthesizing enzymes in the liver was not significantly different between KO and WT mice. This would indeed be consistent with the results of the lipid profiling analysis where reduced levels of DHA-containing phospholipids were obtained only for the heart but not for the liver of fed *Atgl*$^{-/-}$ mice. However, expression of these enzymes in the heart should not have a profound effect on its lipid profile since almost all DHA is synthesized in the liver and transported to the heart (69, 70). As no effect of ATGL deficiency was detectable on the transcriptional regulation of the DHA-synthesizing pathway in the liver and based on the fact that the lack of ATGL activity has severe implications on lipid metabolism which is strongly regulated by the nutritional status and that ATGL activity itself is induced by fasting (at least in the liver) (98), expression of the enzymes was examined in fasted mice next.

Fasted mice

Contrary to the results for fed mice, the comparison of relative mRNA-levels in the liver of fasted *Atgl*$^{-/-}$ mice with those of fasted WT mice revealed interesting insights. ELOVL2 and 17β-HSD4 expression was significantly decreased in *Atgl*$^{-/-}$ mice compared to wild type mice by 73% and 69%, respectively. FADS2 levels were also reduced by 53% and FADS1 levels by 36% in knockouts, although the changes were not statistically significant. In the heart all four target genes showed significantly reduced expression in KO mice compared to wild type, as before. Thus, the effect of *Atgl* $^{-/-}$ on DHA biosynthesis in the liver could be due to missing regulation/activation of fasting induced signaling pathways whereas in the heart this regulation seems to be independent from the nutritional status. This concept was also supported by the observations that ELOVL2 and 17β-HSD4 expression was significantly increased in fasted compared to fed WT mice in the liver. FADS2 mRNA levels were also slightly upregulated in fasted WT liver whereas FADS1 expression remained almost unchanged. Thus, it was probably not a downregulation of the enzymes in the liver but rather a failed upregulation in response to the fasted state of the mice whereas the phenotype in the heart resulted only from the deficient ATGL activity and was not correlated to the nutritional status. This interpretation is substantiated by the findings of Rapoport et al. (69) which show that liver but not heart or brain DHA synthesis rates were upregulated by n-3 PUFA-deficient diets. This indicates that liver DHA synthesis is regulated by the nutritional status whereas synthesis in the heart (or brain) is not. Igarashi et al. (74) reported that diets deficient of C18:3n-3 induce the hepatic expression of desaturases and elongases involved in PUFA synthesis. The missing upregulation of FADS1 and FADS2 in fasted compared to fed WT mice and/or the lesser, insignificant downregulation in fasted compared to fed KO mice can be explained by the study of Li et al. (105). They describe that fasting did NOT induce desaturase expression in the liver of mice that were killed after 24 hours of fasting (in contrast

to the expression of β-oxidation enzymes like 17β-HSD4) since these desaturases are dually regulated by PPARα and SREBP-1c. SREBP-1c is responsible for regulating genes that are involved in fatty acid synthesis. Hence this transcription factor is important to maintain proper levels of intracellular lipids and is inhibited in the fasted state. Therefore, expression of FADS1 and FADS2 is not totally induced in wild type mice during fasting. In fasted ATGL-knockout mice, mRNA levels were further decreased as PPARα activity was possibly reduced due to ATGL deficiency. In contrast to that, FADS1 and FADS2 expression was equally induced by SREBP-1c in fed WT as well as KO mice since ATGL has probably no effect on SREBP1c-activity and/or might not be active in the liver in the fed state. But again, it was no full induction due to missing PPARα-activity this time. If expression of ELOVL2 and 17β-HSD4 is only stimulated in the fasted state, this would further explain why the presence/absence of ATGL had no effect on the relative mRNA levels of these genes in fed mice.

The results lead to the assumption that ATGL activity is needed for fasting induced regulatory mechanisms, for instance PPAR activity, and that PPARs then further stimulate the DHA/PUFA synthesis. As other PPARα target genes were shown to be downregulated in *Atgl*$^{-/-}$ mice, a regulatory function of ATGL on the activity of nuclear receptors like PPARα has already been suggested (Hämmerle et al., unpublished data). PPARα itself is further activated by fasting and regulates gene expression (mainly of genes involved in β-oxidation) depending on the nutritional status (106). ATGL could be the underlying factor for this fasting-induced activation of PPARα by releasing FFA from TG-stores during stimulated lipolysis; these FFA might further act as PPARα ligands.

PPARα agonist-fed mice

In order to verify the hypothesis exposed above, the expression of the enzymes in *Atgl*$^{-/-}$ mice was investigated under the influence of enhanced PPARα-activity. For this purpose, *Atgl*$^{-/-}$ mice were fed a chow diet supplemented with the PPARα agonist WY14,643 during three weeks. In the liver of the mice fed the PPARα agonist the expression of FADS1, FADS2, and 17β-HSD4 was significantly increased by 92%, 465%, and 289%, respectively, compared to KO mice fed the standard chow diet. For ELOVL2, no changes in expression were detected. Also In the cardiac muscle of KO mice fed the PPARα agonist WY14,643 a significant upregulation of the relative expression of FADS1, FADS2, and 17β-HSD4 was observed; in contrast to the hepatic mRNA levels, also ELOVL2 was upregulated in expression. In the brain, no changes in expression were registered upon administration of WY14,643. The expression in the brain could be regulated by other nuclear receptors/transcription factors. But most probably the PPARα agonist did not cross the blood-brain-barrier. Hence, FADS1, FADS2, and 17β-HSD4

behaved like PPARα target genes in both organs whereas ELOVL2 seemed to be differentially regulated in heart and liver.

Northern blot

For verifying purposes, the RNA isolated from PPARα agonist-fed KO mice and KO mice on a standard chow diet was used to perform a Northern blot and thereby determine actual expression levels of FADS1, FADS2, and 17β-HSD4. The blots confirmed the results obtained by real-time PCR. In the liver, the expression of FADS1 was not strongly induced in WY14,643-fed KO mice. There was still a considerable difference in expression compared to chow diet-fed KO mice. For FADS2 and 17β-HSD4 a massive induction of expression was detected in PPARα agonist-fed KO mice compared to KO mice on a standard chow diet. In these “normally” fed KO mice, labeled mRNA was barely detectable for FADS2 and 17β-HSD4. These results were in accordance with the respectively 1.9-fold, 5.7-fold, and 2.9-fold increased expression of FADS1, FADS2, and 17β-HSD4 obtained by real-time PCR measurements with the only difference that induction of expression was more pronounced for 17β-HSD4 than for FADS2 on the Northern blot. With RNA samples from cardiac myocytes one blot was prepared for labeling with a probe specific for 17β-HSD4 but no significant bands were detected although the probe worked well for labeling hepatic mRNA samples. Consequently, the expression of 17β-HSD4 in the heart had to be extremely low compared to the liver. Thus, Northern blotting confirmed that FADS1, FADS2, ELOVL2, and 17β-HSD4 are PPARα target genes, at least in the liver.

Indeed, the bifunctional enzyme (human/rat homologue to the mouse 17β-HSD4) has already been shown to be upregulated in the liver when treated with PPARα agonists (107). The expression of FADS2, the Δ6-desaturase, also was proven to be regulated by fasting in a PPARα dependant manner (108). Its expression was induced approximately 6-fold when treated with the PPARα agonist WY14,643 (109) which is in absolute concordance with our results. Furthermore, mRNA levels of ELOVL5 (elongase) and FADS1 were also increased by enhanced PPARα-activity (109) whereas ELOVL2 seems to be regulated by fasting in a PPARα-independent way since an influence of PPARα on the expression of ELOVL2 could not be detected in previous studies (109). All the more surprising were the results for the cardiac muscle (where expression of ELOVL2 was induced upon feeding of WY14,643) as ELOVL2 expression has been described not to be induced by PPARα activity. BUT this applies only to the liver. Since it has been thought for a very long time that ELOVL2 was not expressed in the heart at all, what was considered as the reason for DHA not being synthesized in the heart (69), no references about the regulation of cardiac ELOVL2 expression in the heart could be found. It might therefore be regulated in a completely different way in the heart. ELOVL2 expression in

the liver could depend on PPARβ/δ as this nuclear receptor is sensitive to changes in plasma FFA levels and there have also been identified other genes which were upregulated by fasting independently of PPARα (106). Furthermore, DHA itself has a positive regulatory effect on the binding of PPARβ/δ to DNA (80) what activates gene expression and creates a positive feedback loop. But how important is ELOVL2 activity for DHA biosynthesis after all? ELOVL2 specifically elongates C20:5 and C22:5 but these intermediates could also be elongated by Elovl5, which has a broad range of substrates (109). The missing ELOVL2 activity could consequently be compensated by ELOVL5. Nevertheless, ELOVL2 has the highest and most specific activity against 20:5n-3 (EPA) and 22:5n-3 in the liver (109) and furthermore, ELOVL5 is also a PPARα target gene and therefore most probably downregulated in *Atgl*$^{-/-}$ mice, itself (109, 110).

Overexpression of the nuclear transcription factor SREBP1c not only induced the expression of FADS1 (Δ5-desaturase) and FADS2 but also of ELOVL2 (105, 109). But for ELOVL2 the physiological importance of this induction is doubtful since in contrast to the desaturases ELOVL2 was not at all regulated by changes in insulin and glucose levels (109). Furthermore, it would not be logical if ELOVL2 was the only enzyme of DHA-biosynthesis induced exclusively by feeding and correlated regulatory mechanisms.

In conclusion it can be assumed that ATGL plays a role in regulating gene expression of several enzymes involved in the biosynthesis of DHA (and/or other PUFAs) in the liver as well as in cardiac myocytes. In the liver, this is most likely an indirect effect of ATGL which is translated by PPARα (and maybe other nuclear receptors) and has an impact only during fasting.

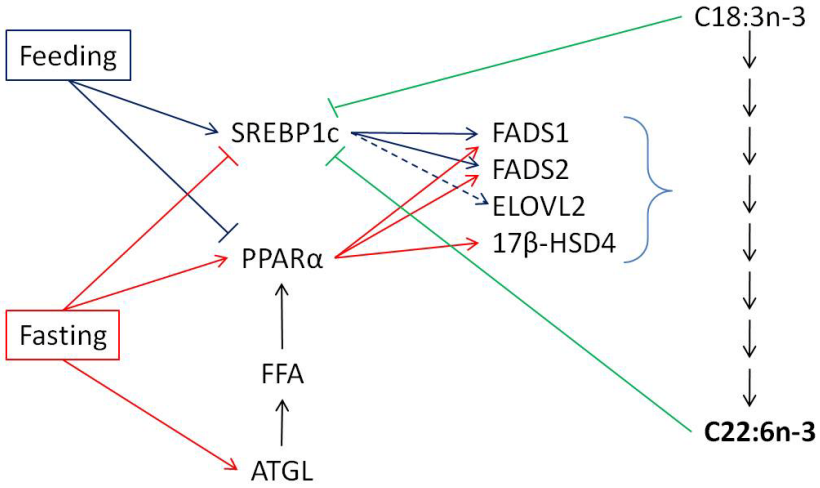

FIGURE 5.1. **Schematic representation of the hypothetical regulation of DHA biosynthesis by ATGL and the nutritional status in the liver**. The nutritional status affects the activity of nuclear receptors (PPARα, SREBP1c) which in turn induce the expression of DHA-synthesizing enzymes (FADS1, FADS2, ELOVL2, 17β-HSD4). The activation of PPARα by fasting might be mediated by ATGL which itself is activated by fasting and consequently releases FFA from triglycerides stores. On the one hand FFA act as PPARα ligands thereby inducing the expression of desaturases, on the other hand PUFA (DHA, ALA) inhibit the expression of desaturases probably via exerting a negative effect on SREBP1c (105).FFA, free fatty acids.

ATGL overexpressing transgenic mice

In order to receive a more precise impression of the role ATGL is playing in DHA biosynthesis, transcription of FADS1, FADS2, ELOVL2, and 17β-HSD4 was examined in WT and KO mice that were overexpressing exogenous ATGL. For fasted wild type mice overexpressing ATGL in the liver an increase of hepatic expression of target enzymes compared to "normal" wild type mice was expected. But, comparing their relative mRNA levels, no differences were observed. In the hearts of fed mice with cardiac muscle-specific overexpression of ATGL, however, even a decrease in expression was registered for FADS1, FADS2, and ELOVL2 compared to WT mice. This decrease was still more pronounced in ATGL-knockout mice (but in this case it was expected). Introduction of transgenic *Atgl* into their knock out genome increased the expression of all four genes again but only to the levels of WT mice overexpressing transgenic ATGL. The unchanged relative mRNA levels in the fasted liver might be due to the fact that the expression of the enzymes had already been induced as a result of fasting and had reached a maximum. Therefore, the overexpression of ATGL had no additional effect. This explanation would be consistent if the only function of ATGL in DHA biosynthesis was to transduce fasting induced upregulation of enzyme expression (via PPARs). Exogenous ATGL in both, heart and liver, might not have the same activity as endogenous ATGL and this exogenous ATGL might have suppressed endogenous ATGL production by being synthesized in such high quantities. However, protein levels and also TG-hydrolyzing activities were shown to be upregulated in transgenic mice (98, 99) what argues against a reduced/changed activity of exogenous ATGL, at least considering its TG-hydrolyzing function. Therefore, it might rather be a negative feedback mechanism as FADS1 and FADS2 have already been shown to be regulated by such inhibitory feedback pathways via PPARs (111). Thus, ATGL might activate PPARs and activated PPARs induce Δ5/Δ6-desaturase expression which in turn results in increased PUFA-levels. Since increased PUFA on the other hand negatively influence Δ5/Δ6-desaturases (74), overexpression of ATGL could in fact result in a negative feedback of the DHA-biosynthesis pathway. This would also explain the even lower cardiac expression levels in *Atgl*-transgenic mice compared to WT mice and the fact that in KO mice carrying the exogenous *Atgl* gene expression reaches only the mRNA levels of WT mice with transgenic ATGL expression. In any case, the mechanism has to be pathway-specific as MCAD expression, in contrast to FADS1, FADS2, and ELOVL2, was not downregulated by overexpressed ATGL.

In summary, the results obtained by real-time PCR measurements lead to the conclusion that there is a nuclear receptor-dependant regulation of most enzymes involved in the

expression of DHA which is influenced by negative feedback mechanisms. The activity of these nuclear receptors further seems to be regulated by ATGL, at least in the liver during times of fasting. Most likely, ATGL is necessary in the liver for providing FA as ligands for PPARα-activation since exogenous fatty acids are rare/absent during fasting. The regulatory effect of ATGL on DHA-synthesizing enzymes in the heart remains elusive; in any case there has to be a fasting-independent transcriptional regulation with ATGL-involvement. Nevertheless, DHA-synthesis rates in the heart would probably not be sufficient to cause changes in DHA-levels (69). If the effect of ATGL on DHA levels consists exclusively in its regulatory function on nuclear receptors (especially PPARα) in the liver which in turn regulate expression of some DHA synthesizing enzymes and thereby control DHA levels, the lipid profile of PPARα agonist-fed *Atgl*$^{-/-}$ mice should present increased DHA levels.

Lipid profiling

Lipid composition of phoshpatidylcholine and phosphatidylethanolamine, the PL species with the most important changes concerning DHA-incorporation, was analyzed. For PC and PE species in the cardiac muscle of *Atgl*$^{-/-}$ mice compared to WT mice we confirmed the results of previous measurements. In the cardiac muscle we saw again that levels of DHA-containing phospholipids were reduced in KO mice compared to wild type versus an increase in C18:0/C18:1/C18:2-containing phospholipids. Interestingly, mice transgenically overexpressing ATGL in the heart had a similar lipid profile to WT mice BUT with a trend towards an opposite lipid profile to KO mice. These results would further confirm the hypothesis that reduced cardiac mRNA levels in transgenic mice are the result of a negative feedback since lipid composition changed slightly into the opposite direction of KO mice but not INTO the direction of KO mice. Nevertheless, expression of the enzymes in the heart should not significantly influence DHA-levels. Still, it is conceivable that overexpressed ATGL in the heart releases FFA that are transported to the liver where they can be used as PPARα ligands and/or precursors for DHA/PUFA synthesis. This would further explain why lipid profile was restored in *Atgl*$^{-/-}$ mice with heart-specific overexpression of exogenous ATGL specifically in the heart. Proceeding to the results in PPARα agonist-fed mice, the expected normalized lipid profile was not obtained. Contrary to that, the lipid profile changed more or less into the same direction as for KO mice but this change was still more pronounced. Therefore PPARα-activation could obviously not neutralize the effect of ATGL deficiency. In the liver, the lipid profile for WT mice overexpressing ATGL was exactly the same as for “normal” WT mice. These results correspond very well to real-time PCR measurements where no changes in the relative expression of FADS1, FADS2, ELOVL2, and 17β-HSD4 were detected between these two phenotypes. *Atgl*$^{-/-}$ mice showed a similar lipid profile to WT mice in the liver. Neverthe-

less, contrary to the first measurements (where lipid profile was unchanged in the liver), now a slight decrease in DHA-containing PL and an increase in C18-fatty acid containing PL were obtained. This might be due to the fact that fasted WT mice were compared to fed KO mice and therefore differences in the lipid profile were more pronounced between these two genotypes. Thus, the reason for the apparent decrease in DHA-containing PL in knockout mice might be due to an increase in DHA-levels in WT mice during fasting. Regarding PPARα-activity, the livers from PPARα agonist-fed mice, as it was the case for PL in CM, showed a similar lipid profile to KO mice except for some single species. So, the activation of nuclear receptors cannot be the only function of ATGL in this pathway.

Summarizing the results of lipid profiling in heart and liver, ATGL was shown to operate as a regulator of LC-PUFA synthesis since levels of DHA-containing phospholipids were reduced in *Atgl*$^{-/-}$ mice and again increased to wild type levels upon transgenic expression of ATGL, at least in the cardiac muscle of knockout mice. Although PPARα was shown to induce the expression of some DHA-synthesizing enzymes during fasting and although this regulation somehow depended on ATGL, the administration of the PPARα agonist WY14,643 did not boost the production of DHA in *Atgl*$^{-/-}$ mice. Therefore, ATGL must further be crucial also for some earlier steps in DHA synthesis, most likely for releasing the precursor α-linolenic acid from triglycerides or phospholipids inside biological membranes. This would also explain why decreased levels of DHA can also be seen in fed mice although enzymes were transcriptionally downregulated only in fasted mice.

There was no difference in the brain lipid profile between KO mice on a standard chow diet and KO mice fed the PPARα agonist for both the composition of PC- as well as PE-species. This could be attributed to the fact that the agonist not crosses the blood-brain-barrier. Furthermore, the brain has specific mechanisms to retain DHA for much longer than any other organ. In a study, rats fed an α-linolenic acid-deficient diet showed a 3-fold prolonged half-life of DHA (from 33 to 90 days) in the brain compared to rats fed a normal diet due to a downregulated expression of DHA-metabolizing enzymes (69). These observations are consistent with the findings of Igarashi et al. (74). Although DHA is especially incorporated into brain and retinal phospholipids, no significantly higher levels of DHA-containing PC and PE were obtained in the brain compared to liver and heart. ATGL deficiency should have no effect because mice were still able to retain DHA in the brain as described above. But DHA is found at very high levels especially inside PS and this lipid was not further investigated.

Conclusion and outlook

In summary, our study assigns an essential role to ATGL in DHA biosynthesis. At present we can conclude from all these results that ATGL has an effect on the expres-

sion of DHA-synthesizing enzymes and that there has to be an impact of ATGL on nuclear receptors. Whether ATGL just regulates PPAR activity by providing free fatty acids as ligands or whether there is another possible interaction remains elusive. The (reduced) expression of several selected enzymes of the DHA-biosynthesis pathway in KO mice was induced by administration of a PPARα agonist. Consequently FADS1, FADS2, and 17β-HSD4 (and maybe ELOVL2 in the heart) were identified as PPARα target genes and the regulation by PPARα was shown to depend on ATGL. Still, the induced expression of DHA-synthesizing enzymes did not increase DHA levels. This could be due to the fact that not all enzymes, especially ELOVL2, were restored in their function by administration of the PPAR agonist. But if that was the case, EPA (C20:5n-3) (or other intermediates) should have accumulated which did not happen. Therefore, any other dysregulation or negative feedback mechanism has to block DHA synthesis at the very beginning. It is conceivable that ATGL plays a role in releasing the precursor for DHA biosynthesis from biological membranes. C18:3n-3, which is taken up by nutrition and then incorporated into chylomicrons and lipoproteins, might only be available for DHA synthesis if released by the hydrolyzing activity of ATGL. This would be all the more probable if the liver also stored some of the dietary α-linolenic acid (C18:3n-3; ALA) and was not immediately using up the available ALA for DHA synthesis because in that case α-linolenic acid would need to be released again from its stores. This conclusion is in accordance with a paper which describes that with time the labeling of liver lipids shifted from C18:3n-3 in TG to C22:6n-3 in PL, what suggests that the liver initially stored at least part of the C18:3n-3 as TG and only then converted it to DHA (62). Some very recently published results (2010) also match our findings that elevated gene expression does not increase DHA levels: this research group reports that n-3 PUFA levels seem to be regulated exclusively **by substrate supply** and not by alterations in gene expression (112). It remains unclear why the effect on the lipid profile only occurs and/or is more pronounced in the heart as DHA is almost exclusively synthesized in the liver. DHA-levels might principally be low in the liver (since DHA exerts its functions mainly in brain and retina (62, 63) but also in the cardiovascular system (85, 90)) and DHA might always be very rapidly transported to other organs so that the reduced levels have no effect in the liver. Indeed, 60 minutes after infusion of [U-^{13}C]α-LA, ^{13}C-DHA already appears in the arterial plasma (70). Another explanation could be that the liver does no longer distribute any DHA in case hepatic production levels are low which causes reduced levels in other organs that depend on the liver for DHA supply. The brain that requires DHA the most is less dependent on liver synthesis since it produces higher amounts of DHA itself compared to the heart (69) and retains DHA if the liver is no longer providing this FA (62). Furthermore it is not yet clear why PPARα agonist-feeding even worsens the phenotype. Induction of

PPARα-activity might only increase β-oxidation (111) so that the precursors and also DHA are degraded instead of being converted and/or produced. Additionally, if ATGL has a PPARα-independent action on DHA-biosynthesis, the logical consequence would be that PPARα cannot reverse the *Atgl*$^{-/-}$ phenotype (but this would also not worsen the phenotype).

A closer look still needs to be taken at C18:3n-3 (ALA) levels, especially in triglycerides of serum and liver, to determine if in knockout mice the precursor accumulates instead of being converted. If this is not the case, C18:3n-3 has to be consumed in some other way since it is implicated in the standard chow diet and consequently taken up by nutrition. The accumulation of C18:3n-3-levels already could have been detected in the first lipid-profiling analyses but these measurements were done by Ingo Streith in St. Louis, US, with a method that required the fatty acids of interest to be selected PRIOR to the measurement. The problem was that usually in WT mice C18:3n-3 levels are so low that they cannot be measured at all. Therefore, C18:3n-3 was not selected and consequently not measured. The difficulty with the following (our) measurements was that only total amount of C-atoms and H-atoms was recorded and not the exact FA-composition. Usually the major compositions of the various TG-species are known. But for ATGL-knockout mice it might have been helpful to carry out an additional step and measure the exact composition as an accumulation of C18:3n-3 could have been detected in case one of the C18-FA in some of the PC/PE-species was C18:3n-3. However, it is more likely that C18:3n-3 accumulates in triglycerides in any case (62). The measurement of triglycerides hasn't worked so far though, because the measuring method (HPLC-qTOF) is still being established.

In conclusion, it may be said that further research will be necessary in order to fully comprehend the function of ATGL in the DHA/PUFA synthesizing pathway.

This lipase is not only the main enzyme for hydrolysis of triglyceride stores but also further regulates innumerable signaling and gene expression pathways by providing free fatty acids and other intermediates of the lipolytic process.

ATGL is in any case crucial for the smooth functioning of the lipid metabolism and will remain an exciting research question still for some time to come.

6. References

1. **Nelson, D.L., and Cox, M.M.** *Lehninger Principles of Biochemistry.* 5th edition. W.H. Freeman, 2008. ISBN 1429208929.

2. **Kolman, J., and Röhm, K.H.** *Taschenatlas der Biochemie.* 3. Edition. Thieme, 2002. ISBN-10: 3137594030.

3. **McNaught, A.D., and Wilkinson, A.** *IUPAC. Compendium of Chemical Terminology.* Oxford : Blackwell Scientific Publications, 1997. ISBN: 052151150X.

4. **Christophe, A.B., and DeVriese, S.** *Fat digestion and absorption.* AOCS (Amer Oil Chemists Society) Press, 2000. ISBN: 189399712X.

5. WKU Bio113 - Lipids. *WKU Biology Department.* [Online] [Cited: 09 10, 2010.] http://bioweb.wku.edu/courses/biol115/wyatt/biochem/lipid/lipid1.htm.

6. **Alberts, B., Johnson, A., Lewis, J., Raff, M., Roberts, K., and Walter, P.** *Molecular biology of the cell.* 4th edition. New York : Garland Science, 2002. ISBN: 0815340729.

7. **Werner, A., Kuipers, F. and Verkade, H.J.** Fat Absorption and Lipid Metabolism in Cholestasis -- Madame Curie Bioscience Database -- NCBI Bookshelf. *NCBI Bookshelf.* [Online] [Cited: 08 23, 2010.] http://www.ncbi.nlm.nih.gov/bookshelf/br.fcgi?book=eurekah&part=A20519#A20542.

8. **Löffler, G., and Petrides, P.E.** *Biochemie und Pathobiochemie.* 7. Auflage. Springer-Verlag GmbH, 2002. ISBN 3540422951.

9. **Carlier, H., Bernard, A., and Caselli, C.** Digestion and absorption of polyunsaturated fatty acids. *Reprod Nutr Dev.* 1991, **31**, 475-500.

10. **Thomson, A.B., Keelan, M., Garg, M.L., and Clandinin, M.T.** Intestinal aspects of lipid absorption: in review. *Can J Physiol Pharmacol.* 1989, **67**, 179-191.

11. **Coleman, R.A., and Lee, D.P.** Enzymes of triacylglycerol synthesis and their regulation. *Prog Lipid Res.* 2004, **43**, 134-176.

12. **Thomson, A.B., Schoeller, C., Keelan, M., Smith, L.C., and Clandinin, M.T.** Lipid absorption: passing through the unstirred layers, brush-border membrane, and beyond. *Can J Physiol Pharmacol.* 1993, **71**, 531-555.

13. **Shi, Y. and Burn, P.** Lipid metabolic enzymes: Emerging drug targets for the treatment of obesity. *Nature Reviews.* 2004, **3**, 695-710.

14. **Karlson, P., Doenecke, D., and Koolman, J.** *Kurzes Lehrbuch der Biochemie für Mediziner und Naturwissenschaftler.* 14. Auflage. Stuttgart : Thieme Verlag, 2005. ISBN: 3133578146.

15. **Goldberg, I.J.** Lipoprotein lipase and lipolysis: central roles in lipoprotein metabolism and atherogenesis. *J Lip Res.* 1996, **37**, 693-707.

16. **Kostner, G.M., Scharnagl, H., Kostner, K., and März, W.** Zusammensetzung und Stoffwechsel der Lipoproteine. [Hrsg.] Peter Schwandt. *Handbuch der Fettstoffwechselstörungen: Dyslipoproteinämien und Atherosklerose: Diagnostik, Therapie und Prävention.* 3. Auflage. Schattauer Verlag, 2006, 2-65.

17. **Porter, C.J.H., Trevaskis, N.L., and Charman, W.N.** Lipids and lipid-based formulations: optimizing the oral delivery of lipophilic drugs. *Nat Rev Drug Discov.* 2007, 6, 231-248.

18. **Shi, Y., and Burn, P.** Lipid metabolic enzymes: emerging drug targets for the treatment of obesity. *Nat Rev Drug Discov.* 2004, **3**, 695-710.

19. **Ahmadian, M., Wang, Y., and Sul, H.S.** Lipolysis in adipocytes. *Int J Biochem Cell Biol.* 2010, **42**, 555-559.

20. **Zechner, R., and Madeo, F.** Another way to get rid of fat. *Nature.* 2009, **458**, 1118-1119.

21. **Zechner, R., Kienesberger, P.C., Haemmerle, G., Zimmermann, R., and Lass, A.** Adipose triglyceride lipase and the lipolytic catabolism of cellular fat stores. *J Lipid Res.* 2009, **50**, 3-21.

22. **Zimmermann, R., Lass, A., Haemmerle, G., and Zechner, R.** Fate of fat: The role of adipose triglyceride lipase in lipolysis. *Biochim Biophys Acta.* 2008, **1791**, 494-500.

23. **Gibbons, G.F., Islam, K., and Pease, R.J.** Mobilisation of triacylglycerol stores. *Biochim Biophys Acta.* 2000, **1483**, 37-57.

24. **Schweiger, M., Schreiber, R., Haemmerle, G., Lass, A., Fledelius, C., Jacobsen, P., Tornqvist, H., Zechner, R., and Zimmermann, R.** Adipose triglyceride lipase and hormone-sensitive lipase are the major enzymes in adipose tissue triacylglycerol catabolism. *J Biol Chem.* 2006, **281**, 40236-40241.

25. **Ducharme, N.A., and Bickel, P.E.** Minireview: Lipid Droplets in Lipogenesis and Lipolysis. *Endocrinology.* 2008, **149**, 942-949.

26. **Lafontan, M., and Berlan, M.** Fat cell adrenergic receptors and the control of white and brown fat cell function. *J Lipid Res.* 1993, **34**, 1057-1081.

27. **Rosen, E.D., and Spiegelman, B.M.** Molecular regulation of adipogenesis. *Annu Rev Cell Dev Biol.* 2000, **16**, 145-171.

28. **Zimmermann, R., Strauss, J.G., Haemmerle, G., Schoiswohl, G., Birner-Gruenberger, R., Riederer, M., Lass, A., Neuberger, G., Eisenhaber, F., Hermetter, A., and Zechner, R.** Fat Mobilization in Adipose Tissue is promoted by Adipose Triglyceride Lipase. *Science.* 2004, **306**, 1383-1386.

29. **Villena, J.A., Roy, S., Sarkadi-Nagy, E., Kim, K.-H., and Sul, H.S.** Desnutrin, an adipocyte gene encoding a novel patatin domain-containing protein, is induced by fasting and glucocorticoids: ectopic expression of desnutrin increases triglyceride hydrolysis. *J Biol Chem.* 2004, **279**, 47066-47075.

30. **Jenkins, C.M., Mancuso, D.J., Yan, W., Sims, H.F., Gibson, B., and Gross, R.W.** Identification, cloning, expression, and purification of three novel human calcium-independent phospholipase A2 family members possessing triacylglycerol lipase and acylglycerol transacylase activities. *J Biol Chem.* 2004, **279**, 48968-75.

31. **Haemmerle, G., Lass, A., Zimmermann, R., Gorkiewicz, G., Meyer, C., Rozman, J., Heldmaier, G., Maier, R., Theussl, C., Eder, S., Kratky, D., Wagner, E.F., Klingenspor, M., Hoefler, G., and Zechner, R.** Defective lipolysis and altered engery metabolism in mice lacking adipose triglyceride lipase. *Science.* 2006, **312**, 734-737.

32. **Raben, D.M., and Baldassare, J.J.** A new lipase in regulating lipid mobilization: hormone-sensitive lipase is not alone. *Trends Endocrinol Metab.* 2005, **16**, 35-36.

33. **Zechner, R., Strauss, J.G., Haemmerle, G., Lass, A., and Zimmermann, R.** Lipolysis: pathway under construction. *Curr Opin Lipidol.* 2005, **16**, 333-340.

34. **Schweiger, M., Lass, A., Zimmermann, R., Eichmann, T.O., and Zechner, R.** Neutral lipid storage disease: genetic disorders caused by mutations in adipose triglyceride lipase/PNPLA2 or CGI-58/ABHD5. *Am J Endocrinol Metab.* 2009, **297**, 289-296.

35. **Kim, J.Y., Tillison, K., Lee, J.-H., Rearick, D.A., and Smas, C.A.** The adipose tissue triglyceride lipase ATGL/PNPLA2 is downregulated by insulin and TNFα in 3T3-L1 adipocytes and is a target for transactivation by PPARγ. *Am J Physiol Endocrinol Metab.* 2006, **291**, 115-127.

36. **Rydel, T.J., Williams, J.M., Krieger, E., Moshiri, F., Stallings, W.C., Brown, S.M., Pershing, J.C., Purcell, J.P., and Murtaza, F.A.** The Crystal Structure, Mutagenesis, and Activity Studies reveal that Patatin is a Lipid Acyl Hydrolase with a Ser-Asp Catatlytic Dyad. *Biochem.* 2003, **42**, 6696-6708.

37. **Neuberger, G., and Eisenhaber, F.** *REPORT 2 Sequence analysis of NM 025802, NM 054088 XP, 128189.* Dr. Bohrgasse 7 A-1030 Wien : Bioinformatics Group Research Institute of Molecular Pathology.

38. **Schweiger, M., Schoiswohl, G., Lass, A., Radner, F.P.W., Haemmerle, G., Malli, R., Graier, W., Cornaciu, I., Oberer, M., Salvayre, R., Fischer, J., Zechner, R., and Zimmermann, R.** The C-terminal Region of Human Adipose Triglyceride Lipase Affects Enzyme Activity and Lipid Droplet Binding. *J Biol Chem.* 2008, **283**, 17211-17220.

39. **Fischer, J., Lefèvre, C., Morava, E., Mussini, J.M., Laforêt, P., Negre-Salvayre, A., Lathrop, M., and Salvayre, R.** The gene encoding adipose triglyceride lipase (PNPLA2) is mutated in neutral lipid storage disease with myopathy. *Nat Genet.* 2007, **39**, 28-30.

40. **Gruber, A., Cornaciu, I., Lass, A., Schweiger, M., Poeschl, M., Eder, C., Kumari, M., Schoiswohl, G., Wollinski, H., Kohlwein, S.D., Zechner, R., Zimmermann, R., and Oberer, M.** The N-terminal Region of Comparative Gene Identification-58 (CGI-58) is Important for Lipid Droplet Binding and Activation of Adipose Triglyceride Lipase. *J Biol Chem.* 2010, **285**, 12289-12298.

41. **Lass, A., Zimmermann, R., Haemmerle, G., Riederer, M., Schoiswohl, G., Schweiger, M., Kienesberger, P., Strauss, J.G., Gorkiewicz, G., and Zechner, R.** Adipose triglyceride lipase-mediated lipolysis of cellular fat stores is activated by CGI-58 and defective in Chanarian-Dorfman Syndrome. *Cell Metab.* 2006, **3**, 309-319.

42. **Lefèvre, C., Jobard, F., Caux, F., Bouadjar, B., Karaduman, A., Heilig, R., Lakhdar, H., Wollenberg, A., Verret, J.L., Weissenbach, J., Ozguc, M., Lathrop, M., Prud'homme, J.F., and Fischer, J.** Mutations in CGI-58, the gene encoding a new protein of the esterase/lipase/thioesterase subfamily, in Chanarian-Dorfman syndrome. *Am J Hum Genet.* 2001, **69**, 1002-1012.

43. **Granneman, J.G., Moore, H.P., Krishnamoorthy, R., and Rathod, M.** Perilipin controls lipolysis by regulating the interactions of AB-hydrolase containing 5 (Abhd5) and adipose triglyceride lipase (Atgl). *J Biol Chem.* 2009, **284**, 34538-34544.

44. **Granneman, J.G., Moore, H.P., Granneman, R.L., Greenberg, A.S., Obin, M.S., and Zhu, Z.** Analysis of lipolytic protein trafficking and interactions in adipocytes. *J Biol Chem.* 2007, **282**, 5726-5735.

45. **Langin, D.** Control of fatty acid and glycerol release in adipose tissue lipolysis. *C R Biol.* 2006, **329**, 598-607; discussion 653-655.

46. **Miyoshi, H., Perfield, J.W. 2nd, Souza, S.C., Shen, W.J., Zhang, H.H., Stancheva, Z.S., Kraemer, F.B., Obin, M.S., and Greenberg, A.S.** Control of adipose triglyceride lipase action by serine 517 of perilipin A globally regulates protein kinase A-stimulated lipolysis in adipocytes. *J Biol Chem.* 2007, **282**, 996-1002.

47. **Brasaemle, D.L., Subramanian, V., Garcia, A., Marcinkiewicz, A., and Rothenberg, A.** Perilipin A and the control of triacylglycerol metabolism. *Mol Cell Biochem.* **326**, 15-21.

48. **Yang, X., Lu, X., Lombès, M., Rha, G.B., Chi, Y.-I., Guerin, T.M., Smart, E.J., and Liu, J.** The G0/G1 Switch Gene 2 Regulates Adipose Lipolysis through Association with Adipose Triglyceride Lipase. *Cell Metab.* 2010, **11**, 194-205.

49. **Subramanian, V., Rothenberg, A., Gomez, C., Cohen, A.W., Garcia, A., Bhattacharyya, S., Shapiro, L., Dolios, G., Wang, R., Lisanti, M.P., and Brasaemle, D.L.** Perilipin A mediates the reversible binding of CGI-58 to lipid droplets in 3T3-L1 adipocytes. *J Biol Chem.* 2004, **279**, 42062-42071.

50. **Yamaguchi, T., Omatsu, N., Matsushita, S., and Osumi, T.** CGI-58 interacts with perilipin and is localized to lipid droplets. Possible involvement of CGI-58 mislocalization in Chanarian-Dorfman syndrome. *J Biol Chem.* 2004, **279**, 30490-30497.

51. **Karlsson, M., Contreras, J.A., Hellman, U., Tronqvist, H., and Holm, C.** cDNA cloning, tissue distribution, and identification of the catalytic triad of monoglyceride lipase. *J Biol Chem.* 1997, **272**, 27218-27233.

52. **Kienesberger, P., Lee, D., Pulinilkunnil, T., Brenner, D.S., Cai, L., Magnes, C., Koefeler, H.C., Streith, I.E., Rechberger, G.E., Haemmerle, G., Flier, J.S., Zechner, R., Kim, Y.-B., and Kershaw, E.E.** Adipose triglyceride lipase (ATGL) deficiency causes tissue-specific changes in insulin signaling. *J Biol Chem.* 2009, **284**, 30218-30229.

53. **Peyot, M.L., Guay, C., Latour, M.G., Lamontagne, J., Lussier, R., Pineda, M., Ruderman, N.B., Haemmerle, G., Zechner, R., Joly, E., Madiraju, S.R.M., Poitout, V., and Prentki, M.** Adipose triglyceride lipase is implicated in fuel- and non-fuel-stimulated insulin secretion. *J biol chem.* 2009, **284**, 16848-16859.

54. **Huijsman, E., van de Par, C., Economou, C., van der Poel, C., Lynch, G., Schoiswohl, G., Haemmerle, G., Zechner, R., and Watt, M.J.** Adipose triglyceride lipase deletion alters whole body energy metabolism and impairs exercise performance in mice. *Am J Endocrinol Metab.* 2009, **297**, 505-513.

55. **Alsted, T.J., Nybo, L., Schweiger, M., Fledelius, C., Jacobsen, P., Zimmermann, R., Zechner, R., and Kiens, B.** Adipose triglyceride lipase in human skeletal muscle is upregulated by exercise training. *Am J Physiol Endocrinol Metab.* 2008, **296**, E445-E453.

56. **Radner, F.P.W., Streith, I.E., Schoiswohl, G., Schweiger, M., Kumari, M., Eichmann, T.O., Rechberger, G., Koefeler, H.C., Eder, S., Schauer, S., Theussl, H.C., Preiss-Landl, K., Lass, A., Zimmermann, R., Hoefler, G., Zechner, R., and Haemmerle, G.** Growth retardation, impaired triacylglycerol catabolism, hepatic steatosis, and lethal skin barrier defect in mice lacking comparative gene identification-58 (CGI-58). *J Biol Chem.* 2010, **285**, 7300-7311.

57. **Jordans, G.H.** The familial occurence of fat containing vacuoles in the leukocytes diagnosed in two brothers suffering from dystrophia musculorum progressiva (ERB). *Acta Med Scand.* 1953, **145**, 419-423.

58. **Langin, D., Dicker, A., Tavernier, G., Hoffstedt, J., Mairal, A., Ryden, M., Arner, E., Sicard, A., Jenkins, C.M., Viguerie, N., van Harmelen, V., Gross, R.W., Holm, C., and Arner, P.** Adipocyte lipases and defect of lipolysis in human obesity. *Diabetes.* 2005, **54**, 3190-3197.

59. **Ryden, M., Jocken, J., van Harmelen, V., Dicker, A., Hoffstedt, J., Wiren, M., Blomqvist, L., Mairal, A., Langin, D., Blaak, E., and Arner, P.** Comparative studies of the role of hormone-sensitive lipase and adipose triglyceride lipase in human fat cell lipolysis. *Am J Physiol Endocrinol Metab.* 2007, **292**, E1847-E1855.

60. **Steinberg, G.R., Kemp, B.E., and Watt, M.J.** Adipose triglyceride lipase expression in human obesity. *Am J Physiol Endocrinol Metab.* 2007, **293**, E958-E964.

61. **Kobayashi, K., Inoguchi, T., Maeda, Y., Nakashima, N., Kuwano, A., Eto, E., Ueno, N., Sasaki, S., Sawada, F., Fujii, M., et al.** The lack of the C-terminal domain of adipsoe triglyceride lipase causes neutral lipid storage disease through impaired interactions with lipid droplets. *J Clin Endocrinol Metab.* 2008, **93**, 2877-2884.

62. **Scott, B.L., and Bazan, N.G,.** Membrane docosahexaenoate is supplied to the developing brain and retina by the liver. *Proc Natl Acad Sci.* 1989, **86**, 2903-2907.

63. **Kim, H.-Y., Akbar, M., Lau, A., and Edsall, L.** Inhibition of Neuronal Apoptosis by Docosahexaenoic Acid (22:6n-3). *J Biol Chem.* 2000, **275**, 35215-35223.

64. **Su, H.-M., Moser, A.B., Moser, H.W., and Watkins, P.A.** Peroxisomal Straight-chain Acyl-CoA Oxidase and D-bifunctional Protein Are Essential for the Retroconversion Step in Docosahexaenoic Acid Synthesis. *J Biol Chem.* 2001, **276**, 38115-38120.

65. **Guesnet, P., and Alesandri, J.-M.** Docosahexaenoicacid (DHA) and the developing central nervous system - Implications for dietary recommendations. *Biochimie.* 2010 (Epub ahead of print).

66. Doconexent - PubChem Public Chemical Database. *PubChem Public Chemical Database.* [Online] [Cited: 09 10, 2010.] http://pubchem.ncbi.nlm.nih.gov/summary/summary.cgi?cid=445580;.

67. **Ferdinandusse, S., Denis, S., Mooijer, P.A.W., Zhang, Z., Reddy, J.K., Spector, A.A., and Wanders, R.J.A.** Identification of the peroxismal β-oxidation enzymes involved in the biosynthesis of docosahexaenoic acid. *J Lipid Res.* 2001, **42**, 1987-1995.

68. **Tang, C., Cho, H.P., Nakamura, M.T., and Clarke, S.D.** Regulation of human delta-6 desaturase gene transcription: identification of a functional direct repeat-1 element. *J Lipid Res.* 2003, **44**, 686-695.

69. **Rapoport, S.I., Igarashi, M., and Gao, F.** Quantitative contributions of diet and liver synthesis to docosahexaenoic acid homeostasis. *Prostaglandins Leukot Essent Fatty Acids.* 2010, **82**, 273-276.

70. **Gao, F., Kiesewetter, D., Chang, L., Kaizong, M., Bell, J.B., Rapoport, S.I., and Igarashi, M.** Whole-body synthesis-secretion rated of long-chain n-3 PUFAs from circulating unesterified alpha-linolenic acid in unanesthetized rats. *J Lipid Res.* 2009, **50**, 749-758.

71. **Qiu, X.** Biosynthesis of docosahexaenoic acid (DHA, 22:6-4,7,10,13,16,19): two distinct pathways. *Prostaglandins Leukot Essent Fatty Acids.* 2002, **68**, 181-186.

72. **Sprecher, H., Luthria, D.L., Mohammed, B.S., and Baykousheva, S.P.** Reevaluation of the pathways for the biosynthesis of polyunsaturated fatty acids. *J Lipid Res.* 1995, **36**, 2472-2477.

73. **Leonard, A.E., Kelder, B., Bobik, E.G., Chuang, L.-T., Lewis, C.J., Kopchick, J.J., Mukerji, P., and Huang, Y.-S.** Identification and Expression of Mammalian Long-Chain PUFA Elongation Enzymes. *Lipids.* 2002, **37**, 733-740.

74. **Igarashi, M., Kaizong, M., Chang, L., Bell, J.M., and Rapoport, S.I.** Dietary n-3 PUFA deprivation for 15 weeks upregulates elongase and desaturase expression in rat liver but not brain. *J Lipid Res.* 2007, **48**, 2463-2470.

75. **Kitson, A.P., Stroud, C.K., and Stark, K.D.** Elevated Production of Docosahexaenoic Acid in Females: Potential Molecular Mechanisms. *Lipids.* 2010, **45**, 209-224.

76. **Calder, P.C.** Polyunsaturated fatty acids and inflammatory processes: New twists in an old tale. *Biochimie.* 2009, **91**, 791-795.

77. **Simoens, C.M., Deckelbaum, R.J., Massant, J.J., and Carpentier, Y.A.** Inclusion of 10% fish oil in mixed medium-chain triacylglycerol - long-chain triacylglycerol emulsions increases plasma triacylglycerol clearance and induces rapid eicosapentaenoic acid (20:5n-3) incorporation into blood cell phospholipids. *Am J Clin Nutr.* 2008, **88**, 282-289.

78. **Chapkin, R.S., Kim, W., Lupton, J.R., and McMurray, D.N.** Dietary docosahexaenoic and eicosapentaenoic acid: emerging mediators of inflammation. *Prostaglandins Leukot Essent Fatty Acids.* 2009, **81**, 187-191.

79. **Niemoller, T.D., and Bazan, N.G.** Docosahexaenoic acid neurolipidomics. *Prostaglandins Other Lipid Mediat.* 2010, **91**, 85-89.

80. **Di Nunzio, M., Danesi, F., and Bordoni, A.** n-3 PUFA as regulators of cardiac gene transcription: a new link between PPAR activation and fatty acid composition. *Lipids.* 2009, **44**, 1073-1079.

81. **Xie, L., and Innis, S.M.** Genetic Variants of the FADS1 FADS2 Gene Cluster Are Associated with the Altered (n-6) and (n-3) Essential Fatty Acids in Plasma and Erythrocyte Phospholipids in Women during Pregnancy and in Breast Milk during Lactation. *J Nutr.* 2008, **138**, 2222-2228.

82. **Katakura, M., Hashimoto, M., Shahdat, H.M., Gamoh, S., Okui, T., Matsuzaki, K., and Shido, O.** Docosahexaenoic acid promotes neuronal differentiation by regulating basic helix-loop-helix transcription factors and cell cycle in neural stem cells. *Neuroscience.* 2009, **160**, 651-660.

83. **Eriksson, P.S., Perfilieva, E., Björk-Eriksson, T., Alborn, A.M., Nordborg, C., Peterson, D.A., and Gage, F.H.** Neurogenesis in the adult human hippocampus. *Nat Med.* 1998, **4**, 1313-1317.

84. **Stoffel, W., Holz, B., Jenke, B., Binczek, E., Günter, R.H., Kiss, C., Karakesisoglou, I., Thevis, M., Weber, A.-A., Arnhold, S., and Addicks, K.** Δ6-Desaturase (FADS2) deficiency unveils the role of ω3- and ω6-polyunsaturated fatty acids. *EMBO J.* 2008, **27**, 2281-2292.

85. **Hiratsuka, S., Koizumi, K., Ooba, T., and Yokogoshi, H.** Effects of Dietary Docosahexaenoic Acid Connecting Phospholipids on the Learning Ability and Fatty Acid Composition of the Brain. *J Nutr Sci Vitaminol.* 2008, **55**, 374-380.

86. **al., Wheeler et.** Improvement of memory and learning abilities. 1957.

87. **Martinez, M., Vàzquez, E., García-Silva, M.T., Manzanares, J., Bertran, J.M., Castelló, F., and Mougan, I.** Therapeutic effects of docosahexaenoic acid ethyl ester in patients with generalized peroxisomal disorders. *Am J Clin Nutr.* 2000, **71**, 376S-385S.

88. **Rotstein, N.P., Politi, L.E., and Aveldano, M.I.** Docosahexaenoic acid promotes differentiation of developing photoreceptors in culture. *Invest Ophthalmol Vis Sci.* 1998, **39**, 2750-2758.

89. **Muntané, G., Janué, A., Fernandez, N., Odena, M.A., Oliveira, E., Boluda, S., Portero-Otin, M., Naudí, A., Boada, J., Pamplona, R., and Ferrer, I.** Modification of brain lipids but not phenotype in alpha-synucleinopathy transgenic mice by long-term dietary n-3 fatty acids. *Neurochem Int.* 2010, **56**, 318-328.

90. **Schacky, Clemens von.** Cardiovascular disease prevention and treatment. *Prostaglandins Leukot Essent Fatty Acids.* 2009, **81**, 193-198.

91. **Grimsgaard, S., Bønaa, K.H., Hansen, J.-B., and Nordøy, A.** Highly purified eicosapentaenoic acid and docosahexaenoic acid in humans have similar triacylglycerol-lowering effects but divergent effects on serum fatty acids. *Am J Clin Nutr.* 1997, **66**, 649-659.

92. **Madsen, L., Rustan, A.C., Vaagenes, H., Berge, K., Dyroy, E., and Berge, R.K.** Eicosapentaenoic and Docosahexaenoic Acid Affect Mitochondrial and Peroxisomal Fatty Acid Oxidation in Relation to Substrate Preference. *Lipids.* 1999, **34**, 951-963.

93. **Tuller, E.R., Beavers, C.T., Lou, J.R., Ihnat, M.A., Benbrock, D.M., and Ding, W.-Q.** Docosahexaenoic Acid Inhibits Superoxide Dismutase 1 Gene Transcription in Human Cancer Cells: The Involvement of Peroxisome Proliferator-Activated Receptor alpha and Hypocia-Inducible Factor 2alpha Signaling. *Mol Pharmacol.* 2009, **76**, 588-595.

94. **Cho, H.P, Nakamura, M., and Clarke, S.** Cloning, Expression, and Fatty Acid Regulation of the Human Δ5-Desaturase. *J Biol Chem.* 1999, **274**, 37335-37339.

95. **Spandidos, A., Wang, X., Wang, H., and Seed, B.** PrimerBank: a resource of human and mouse PCR primer pairs for gene expression detection and quantification. *Nucleic Acids Res.* 2010, **38**, D792-D799.

96. **Spandidos, A., Wang, X., Wang, H., Dragnev, S., Thurber, T., and Seed, B.** A comprehensive collection of experimentally validated primers for Polymerase Chain Reaction quantitation of murine transcript abundance. *BMC Genomics.* 2008, **9**, 633.

97. **Wang, X., and Seed, B.** A PCR primer bank for quantitative gene expression analysis. *Nucleic Acids Res.* 2003, **31**, e154.

98. **Schoiswohl, G., Schweiger, M., Schreiber, R., Gorkiewicz, G., Preiss-Landl, K., Taschler, U., Zierler, K.A., Radner, F.P., Eichmann, T.O., Kienesberger, P.C., Eder, S., Lass, A., Haemmerle, G., Alsted, T.J., Kiens B, Hoefler G, Zechner, R., Zimmermann, R.** Adipose triglyceride lipase plays a key role in the supply of the working muscle with fatty acids. *J Lipid Res.* 2010, **51**, 490-491.

99. **Reid, B.N., Ables, G.P., Otlivanchik, O.A., Schoiswohl, G., Zechner, R., Blaner, W.S., Goldberg, I.J., Schwabe, R.F., Chua, S.C. Jr, Huang, L.S.** Hepatic overexpression of hormone-sensitive lipase and adipose triglyceride lipase promotes fatty acid oxidation, stimulates direct release of free fatty acids, and ameliorates steatosis. *J Biol Chem.* 2008, **283**, 13087-13099.

100. FlyChip: The UK Drosophila Microarray Facility - RNA quality control. *FlyChip: The UK Drosophila Microarray Facility.* [Online] [Cited: 09 10, 2010.] http://www.flychip.org.uk/protocols/gene_expression/rna_qc.php.

101. **Shendure, J., and Hanlee, J.** Next-generation DNA sequencing. *Nature Biotechnology.* 2008, **26**, 1135-1145.

102. **Port, M., Schmelz, H.U., Stassen, T., Müeller, K., Stockinger, M., Obermair, R., Abend, M.** Correcting false gene expression measurements from degraded RNA using RTQ-PCR. *Diagn Mol Pathol.* 2007, **16**, 38-49.

103. School of Chemistry - Bristol University - UK. *University of Bristol - Mass spectrometric resources - Tandem MS.* [Online] [Cited: 09 10, 2010.] www.chm.bris.ac.uk/ms/theory/tandem-ms.html.

104. **Wittmann, C.** Fluxome analysis using GC-MS. *Microb Cell Fact.* 2007, **6**, 6.

105. **Li, Y., Nara, T.Y., and Nakamura, M.T.** Peroxisome proliferator-activated receptor α is required for feedback regulation of highly unsaturated fatty acid synthesis. *J Lipid Res.* 2005, **46**, 2432-2440.

106. **Sanderson, L.M., Degenhardt, T., Koppen, A., Kalkhoven, E., Desvergne, B., Müller, M., and Kersten, S.** Peroxisome Proliferator-Activated Receptor β/δ (PPARβ/δ) but Not PPARα Serves as Plasma Free Fatty Acid Sensor in Liver. *Mol Cell Biol.* 2009, **29**, 6257-6267.

107. **Frederiksen, K.S., Wulff, E.M., Sauerberg, P., Mogensen, J.P., Jeppesen, L., and Fleckner, J.** Prediction of PPARα ligand-mediated physiological changes using gene expression profiles. *J Lipid Res.* 2004, **45**, 592-601.

108. **Blavy, P., Gondret, F., Guillou, H., Lagarrigue, S., Martin, P.G.P., van Milgen, J., Radulescu, O., and Siegel, A.** A minimal model for hepatic fatty acid balance during fasting: application to PPARα-deficient mice. *J Theor Biol.* 2009, **261**, 266-278.

109. **Wang, Y., Botolin, D., Xu, J., Christian, B., Mitchell, E., Jayaprakasam, B., Nair, M., Peters, J.M., Busik, J., Olson, L.K., and Jump, D.B.** Regulation of hepatic fatty acid elongase and desaturase expression in diabetes and obesity. *J Lipid Res.* 2006, **47**, 2028-2041.

110. **Wang, Y., Gonzalez-Torres, M., Tripathy, S., Botolin, D., Christian, B., and Jump, D.B.** Elevated heptaic fatty acid elongase-5 affects multiple pathways controlling hepatic lipid and carbohydrate composition. *J Lipid Res.* 2008, **49**, 1538-1552.

111. **Matsuzaka, T., Shimano, H., Yahagi, N., Amemiya-Kudo, M., Yoshikawa, T., Hasty, A.H., Tamura, Y., Osuga, J., Okazaki, H., Iizuka, Y., Takahashi, A., Sone, H., Gotoda, T., Ishibashi, S., and Yamada, N.** Dual regulation of Δ5- and Δ6-desaturase gene expression by SREBP-1 and PPARα. *J Lipid Res.* 2002, **43**, 107-114.

112. **Tu, W.C., Cook-Johnson, R.J., James, M.J., Mühlhäusler, B.S., and Gibson, R.A.** Omega-3 long chain fatty acid synthesis is regulated more by substrate levels than gene expression. *Prostaglandins Leukot Essent Fatty Acids.* 2010, **83**, 61-68.

Common abbreviations

AA	arachidonic acid
ALA	α-linolenic acid
ATGL	adipose (tissue) triglyceride lipase
Atgl$^{-/-}$	homozygous deficiency for ATGL
ATP	adenosine triphosphate
BAT	brown adipose tissue
BCA	bicinchoninic acid
Bp	base pairs
BR	brain
BSA	bovine serum albumin
BSTFA	N,O-Bis(trimethylsilyl)trifluoroacetamide
CDS	Chanarian-Dorfman syndrome
CGI-58	comparative gene identification-58
CIP	calf intestinal phosphatase
CL	cardiolipin
CM	cardiac muscle/myocytes
Ct	cycle threshold
DAG	diacylglycerol(s)
(k)Da	(kilo)Dalton
(d)dATP	(di)deoxyadenosine triphosphate
(d)dCTP	(di)deoxycytidine triphosphate
(d)dGTP	(di)deoxyguanosine triphosphate
(d)dTTP	(di)deoxythymidine triphosphate
DEPC	diethylpyrocarbonate
DG	diglyceride(s)
DGAT	diacylglycerol/diglyceride acyltransferase
DHA	docosahexaenoic acid
(c)DNA	(complementary) desoxyribonucleic acid
dNTPs	deoxynucleoside triphosphates
EDTA	ethylenediaminetetraacetic acid
ELOVL	elongation of very long-chain (fatty acids)
FADS	Fatty acid desaturase
fast	fasted
(F)FA	(free) fatty acid(s)
G0S2	G0/G1 switch gene 2
GC	gas chromatography
HDL	high density lipoprotein
HPLC	high pressure liquid chromatography

HSD	hydroxysteroid dehydrogenase
HSL	hormone sensitive lipase
KO	knockout
LB	lysogeny broth
MAG	monoacylglycerol
MCAD	medium-chain specific acyl-CoA dehydrogenase
MG	monoglyceride
MGAT	monoacylglycerol/monoglyceride acyltransferase
MGL	monoacylglycerol/monoglyceride lipase
MM	mastermix
MOPS	3-(N-morpholino)propanesulfonic acid
MS	mass spectrometry
NEFA	non-esterified fatty acid(s)
NLSD(M/I)	neutral lipid storage myopathy/ichthyosis
p	probability
PC	phosphatidylcholine
PCR	polymerase chain reaction
PE	phosphatidylethanolamine
PI	phosphatidylinositol
PKA	protein kinase A
PL	phospholipid(s)
PP	polypropylene
PPAR	peroxisome proliferator activated receptor
PS	phosphatidylserine
(LC)PUFA	long-chain polyunsaturated fatty acid(s)
“qRT-PCR”	“quantitative real-time polymerase chain reaction”, correct →
real-time qRT-PCR	real-time quantitative reverse-transcriptase polymerase chain reaction
(r/m)RNA	(ribosomal/messenger) ribonucleic acid
RT	room temperature or reverse transcriptase
SDS	sodium dodecyl sulfate
SSC	saline-sodium citrate
TAE	Tris, acetic acid, EDTA
TAG	triacylgylcerol
TE	Tris, EDTA
TG	triglyceride(s)
TNFα	tumor necrosis factor α
V	volt
WAT	white adipose tissue
WT	wild type

Curriculum Vitae

Name:	Teresa Sara Lindinger
Residence Place:	8010 Graz
	1080 Wien
Date of Birth:	February 18th, 1985
Place of Birth	Eberstalzell, Upper Austria
Nationality:	Austria

Education:

1988 – 1991	Kindergarten, Vorchdorf
1991 – 1996	Primary school, Vorchdorf
1996 – 2003	Secondary school, BRG/WKBRG Schloss Traunsee, Gmunden
June 2003	Matura
2003 - 2004	Translation studies of French and Spanish, University of Vienna
2004 - 2005	Study of Pharmacy, University of Vienna
2005 - 2010	Study of Molecular Biology, University of Vienna
Nov. 2009 – Oct. 2010	Diploma thesis in the laboratory of Rudolf Zechner, PhD, at the Institute of Molecular Biosciences, Karl Franzens University, Graz

Conference Attendance

18 – 20 March 2010	3rd International Graz Symposium on Lipid and Membrane Biology, Graz, Austria
28 May – 2 June 2010	9th Conference of the International Society for the Study of Fatty Acids and Lipids, Maastricht, Netherlands

Skills

Languages:	German native speaker. Fluent in English and French. Basic Spanish.
Computer skills:	Comprehensive knowledge of Office applications.